Spring 4-25-2013

Capacity Fade Analysis and Model Based Optimization of Lithium-ion Batteries

Venkatasailanathan Ramadesigan
Washington University in St. Louis

WASHINGTON UNIVERSITY IN ST. LOUIS

School of Engineering and Applied Science

Department of Energy, Environmental and Chemical Engineering

Dissertation Examination Committee:

Venkat Subramanian, Chair
Richard Axelbaum
Pratim Biswas
Richard Braatz
Hiro Mukai
Palghat Ramachandran

Capacity Fade Analysis and Model Based Optimization of Lithium-ion Batteries

by

Venkatasailanathan Ramadesigan

A dissertation presented to the
Graduate School of Arts and Sciences
of Washington University in
partial fulfillment of the
requirements for the degree
of Doctor of Philosophy

May 2013

St. Louis, Missouri

Table of Contents

List of Figures

List of Tables

Acknowledgements

I would like to express my sincere gratitude and appreciation to Prof. Venkat R. Subramanian for giving me the opportunity to be a part of his research group. I thank him for his guidance and support throughout the course of my PhD. He has been extremely patient with me while I explored my way through various research topics. I have benefited immensely from various discussions and interactions with him and I thank him for his encouragement and advice and for supporting my abilities throughout my stay here. I would like to thank the members of my dissertation committee, Prof. Richard Axelbaum, Prof. Pratim Biswas, Prof. Hiro Mukai and Prof. Palghat Ramachandran for their valuable suggestions, critical comments and support during different stages of this work throughout my PhD. I would like to specially thank Prof. Richard Braatz, at MIT for serving in my dissertation committee and his guidance through his innumerable suggestions, edits and comments to my manuscripts and conference presentations.

I acknowledge the financial support provided by the National Reconnaissance Office (DII), National Science Foundation under contract numbers CBET-0828002 and CBET-1008692, Washington University in St. Louis, and the U.S. government for performing various tasks in this work.

Special thanks are due the postdocs both in the M.A.P.L.E. group both from the past and present: Dr. Vijay Boovaragavan, Dr. Ravi Methekar, and Dr. Carl Pirkle for their input, suggestions and innumerable discussions during my stay. I also would like to thank the external collaborators: Dr. Shriram Santhanagopalan, Kejia Chen and Folarin Latinwo for their valuable contributions as co-authors in my manuscripts. I thank all my colleagues at WashU, past and present members of the M.A.P.L.E group: Vinten, Mounika, Mandy, Sumitava, Paul, Bharat and Matt for their input and suggestions and contributions during the course of my PhD. My sincere

thanks are due to all the administrative and IT staff in the department of EECE: Rose, Kim, Jim, Tim, Beth, Lesley, Trisha and Lynn for making my life easier by taking care of all the official business, setting up of projectors, software and hardware needs with little involvement from my part.

I am indebted to all my friends (the list is too long) both here in the US and back home in India for their support and encouragement. Special thanks to my roommates Vivek and Phani and all my friends at WashU for making my stay in St. Louis memorable and enjoyable. This work would never have been possible but for my parents' constant support, encouragement, and understanding. I am extremely grateful and express my deepest gratitude and love to them. Above all, I would like to thank God, the Almighty, for having made everything possible by giving me strength and courage to get this done.

॥ श्रीः ॥

ABSTRACT OF THE DISSERTATION

Capacity Fade Analysis and Model Based Optimization of Lithium-ion Batteries

by

Venkatasailanathan Ramadesigan

Doctor of Philosophy in Energy, Environmental and Chemical Engineering

Washington University in St. Louis, 2013

Professor Venkat Subramanian, Chair

Electrochemical power sources have had significant improvements in design, economy, and operating range and are expected to play a vital role in the future in a wide range of applications. The lithium-ion battery is an ideal candidate for a wide variety of applications due to its high energy/power density and operating voltage. Some limitations of existing lithium-ion battery technology include underutilization, stress-induced material damage, capacity fade, and the potential for thermal runaway. This dissertation contributes to the efforts in the modeling, simulation and optimization of lithium-ion batteries and their use in the design of better batteries for the future. While physics-based models have been widely developed and studied for these systems, the rigorous models have not been employed for parameter estimation or dynamic optimization of operating conditions. The first chapter discusses a systems engineering based approach to illustrate different critical issues possible ways to overcome them using modeling, simulation and optimization of lithium-ion batteries. The chapters 2-5, explain some of these ways to facilitate (i) capacity fade analysis of Li-ion batteries using different approaches for modeling capacity fade in lithium-ion batteries, (ii) model based optimal design in Li-ion batteries and (iii) optimum operating conditions (current profile) for lithium-ion batteries based on dynamic optimization techniques. The major outcomes of this thesis will be, (i) comparison of different types of modeling efforts that will help predict and understand capacity fade in lithium-

ion batteries that will help design better batteries for the future, (ii) a methodology for the optimal design of next-generation porous electrodes for lithium-ion batteries, with spatially graded porosity distributions with improved energy efficiency and battery lifetime and (iii) optimized operating conditions of batteries for high energy and utilization efficiency, safer operation without thermal runaway and longer life.

Chapter 1 : Introduction to modeling lithium-ion batteries from a systems engineering perspective

This chapter is reproduced with permission from *J. Electrochem. Soc.*, **159** (3), R31 (2012). The author is grateful to the co-authors for their significant contributions under sections 1.2.3, 1.2.4, 1.3.2, 1.3.4, 1.4.2 and 1.4.4.

1.1. Introduction

Lithium-ion batteries are becoming increasingly popular for energy storage in portable electronic devices. Compared to alternative battery technologies, Li-ion batteries provide one of the best energy-to-weight ratios, exhibit no memory effect, and have low self-discharge when not in use. These beneficial properties, as well as decreasing costs, have established Li-ion battery as a leading candidate for the next generation of automotive and aerospace applications.[1,2] Li-ion battery are also a good candidate for green technology. Electrochemical power sources have had significant improvements in design, economy, and operating range and are expected to play a vital role in the future in automobiles, power storage, military, mobile-station, and space applications. Lithium-ion chemistry has been identified as a good candidate for high-power/high-energy secondary batteries and commercial batteries of up to 75 Ah have been manufactured. Applications for batteries range from implantable cardiovascular defibrillators operating at 10 μA, to hybrid vehicles requiring pulses of up to 100 A. Today the design of these systems have been primarily based on (1) matching the capacity of anode and cathode materials, (2) trial-and-error investigation of thicknesses, porosities, active material, and additive loading, (3) manufacturing convenience and cost, (4) ideal expected thermal behavior at the system level to handle high currents, etc., and (5) detailed microscopic models to understand, optimize, and

design these systems by changing one or few parameters at a time. The term 'lithium-ion battery' is now used to represent a wide variety of chemistries and cell designs. As a result, there is a lot of misinformation about the failure modes for this device as cells of different chemistries follow different paths of degradation. Also, cells of the same chemistry designed by various manufacturers often do not provide comparable performance, and quite often the performance observed at the component or cell level does not translate to that observed at the system level.

Problems that persist with existing lithium-ion battery technology include underutilization, stress-induced material damage, capacity fade, and the potential for thermal runaway.[3] Current issues with lithium-ion batteries can be broadly classified at three different levels as shown schematically in Figure 1-1: market level, system level, and single cell sandwich level (a *sandwich* refers to the smallest entity consisting of two electrodes and a separator). At the market level, where the end-users or the consumers are the major target, the basic issues include cost, safety, and life. When a battery is examined at the system level, researchers and industries face issues such as underutilization, capacity fade, thermal runaways, and low energy density. These issues can be understood further at the sandwich level, at the electrodes, electrolyte, separator, and their interfaces. Battery researchers attribute these shortcomings to major issues associated with Solid-Electrolyte Interface (SEI)-layer growth, unwanted side reactions, mechanical degradation, loss of active materials, and the increase of various internal resistances such as ohmic and mass transfer resistance. This dissertation analyses and contributes to the application of modeling, simulation, and systems engineering to address the issues at the sandwich level for improved performance at the system level resulting in improved commercial marketability.

Systems engineering can be defined as a robust approach to the design, development, and operation of systems. The approach consists of the identification and quantification of system

goals, creation of alternative system design concepts, analysis of design tradeoffs, selection and implementation of the best design, verification that the design is properly manufactured and integrated, and post-implementation assessment of how well the system meets (or met) the goals.[4] Process systems engineering has been successfully employed for designing, operating, and controlling various engineering processes and many efforts are currently being attempted for Li-ion batteries. The development of new materials (including choice of molecular constituents and material nano- and macro-scale structure), electrolytes, binders, and electrode architecture are likely to contribute towards improving the performance of batteries. For a given chemistry, the systems engineering approach can be used to optimize the electrode architecture, operational strategies, cycle life, and device performance by maximizing the efficiency and minimizing the potential problems mentioned above.

The schematic in Figure 1-2 shows four systems engineering tasks and the interactions between these tasks. Ideally, the eventual goal of the systems engineering approach applied to Li-ion batteries would develop a detailed multiscale and multiphysics model formulated so that its equations can be simulated in the most efficient manner and platform, which would be employed in robust optimal design. The first-principles model would be developed iteratively with the model predictions compared with experimental data at each iteration, which would be used to refine the detailed model until its predictions became highly accurate when validated against experimental data not used in the generation of the model. This dissertation make an effort to present a brief contribution in each of the four systems engineering tasks listed above to enable better understanding and use of lithium-ion batteries in the future.

Systems engineering approaches have been used in the battery literature in the past, but not necessarily with all of the tasks and their interactions in Figure 1-2 implemented to the highest

level of fidelity. Such a systems engineering approach can address a wide range of issues in batteries, such as

1. Identification of base transport and kinetic parameters
2. Capacity fade modeling (continuous or discontinuous)
3. Identification of unknown mechanisms
4. Improved life by changing operating conditions
5. Improved life by changing material properties
6. Improved energy density by manipulating design parameters
7. Improved energy density by changing operating protocols
8. Electrolyte design for improved performance
9. State estimation in packs
10. Model predictive control that incorporates real-time estimation of State-of-Charge (SOC) and State-of-Health (SOH).

The next section reviews the status of the literature in terms of modeling, simulation, and optimization of lithium-ion batteries, which is followed by a discussion of the critical issues in the field (Section 1.3), and methods for addressing these issues and expected future directions (Section 1.4).

1.2. Background

In Figure 1-2, model development forms the core of the systems engineering approach for the optimal design of lithium-ion batteries. Generally, the cost of developing a detailed multiscale and multiphysics model with high predictive ability is very expensive, so model development efforts start with a simple model and then add complexity until the model predictions are

sufficiently accurate. That is, the simplest fundamentally strong model is developed that produces accurate enough predictions to address the objectives. The best possible physics-based model can depend on the type of issue being addressed, the systems engineering objective, and on the available computational resources. This section describes various types of models available in the literature, the modeling efforts being undertaken so far, and the difficulties in using the most comprehensive models in all scenarios.

An important task is to experimentally validate the chosen model to ensure that the model predicts the experimental data to the required precision with a reasonable confidence. This task is typically performed in part for experiments designed to evaluate the descriptions of physicochemical phenomena in the model whose validity is less well established. However, in a materials system such as a lithium-ion battery, most variables in the system are not directly measurable during charge-discharge cycles, and hence are not available for comparison to the corresponding variables in the model, to fully verify the accuracy of all of the physicochemical assumptions made in the derivation of the model. Also, model parameters that cannot be directly measured experimentally typically have to be obtained by comparing the experimental data with the model predictions.

A trial-and-error determination of battery design parameters and operating conditions is inefficient, which has motivated the use of battery models to numerically optimize battery designs. This numerical optimization can be made more efficient by use of reformulated or reduced order models.[5,6] Simulation time plays a role in determining the use of these models in various applications, and high simulation times have limited the application of battery optimization based on physics-based models. Efficient ways of simulating battery models is an active area of research and many researchers have published various mathematical techniques

and methods to simulate physics-based battery models faster.[5-8] This has enabled greater use of optimization and systems engineering based on physics-based models.[9-11]

Once an efficient method of simulating the battery models is devised, the next step is to formulate optimization problems to address the real-world challenges described in the previous section. The objective function can be chosen based on the required performance objectives at the system level. Optimization of operating conditions, control variables, and material design (architecture) can be performed based on specific performance objectives described in more detail in Section 1.2.4. After obtaining either an optimal operating protocol or electrode architecture for a specific performance objective, the results should be verified using experiments.

Mathematical models for lithium-ion batteries vary widely in terms of complexity, computational requirements, and reliability of their predictions (see Figure 1-3). Including more detailed physicochemical phenomena in a battery model can improve its predictions but at a cost of increased computational requirements, so simplified battery models continue to be applied in the literature, when appropriate for the particular needs of the application. This section summarizes the literature on model development for lithium-ion batteries, and the application of these models in systems engineering. Models for the prediction of battery performance can be roughly grouped into four categories: empirical models, electrochemical engineering models, multiphysics models, and molecular/atomistic models.

1.2.1. Empirical Models

Empirical models employ past experimental data to predict the future behavior of lithium-ion batteries without consideration of physicochemical principles. Polynomial, exponential, power law, logarithmic, and trigonometric functions are commonly used as empirical models. The

computational simplicity of empirical models enables very fast computations, but since these models are based on fitting experimental data for a specific set of operating conditions, predictions can be very poor for other battery operating conditions. Such battery models are also useless for the design of new battery chemistries or materials.

1.2.2. Electrochemical Engineering Models

The electrochemical engineering field has long employed continuum models that incorporate chemical/ electrochemical kinetics and transport phenomena to produce more accurate predictions than empirical models. Electrochemical engineering models of lithium-ion batteries have appeared in the literature for more than twenty years.[12] Below is a summary of electrochemical engineering models, presented in order of increasing complexity.

1.2.2.a. Single-Particle Model

The single-particle model (SPM) incorporates the effects of transport phenomena in a simple manner. Zhang et al.[13] developed a model of diffusion and intercalation within a single electrode particle, which was expanded to a sandwich by considering the anode and cathode each as a single particle with the same surface area as the electrode.[14] In this model, diffusion and intercalation are considered within the particle, but the concentration and potential effects in the solution phase between the particles are neglected.[14,15] The following typical reactions are considered in each of the particle in the SPM (*MO* refers to metal oxide):

Cathode: $MO_y + Li^+ + e^- \underset{\text{Charge}}{\overset{\text{Discharge}}{\rightleftharpoons}} LiMO_y$; Anode: $LiC_6 \underset{\text{Charge}}{\overset{\text{Discharge}}{\rightleftharpoons}} Li^+ + e^- + C_6$

Due to these simplifications, this model can be quickly simulated, but is only valid for limited conditions, such as low rates and thin electrodes.[15] Greater efficiency can be obtained by including a parabolic profile approximation for the lithium concentration within the particle.[14,16]

1.2.2.b. Ohmic Porous-Electrode Models

The next level of complexity is a porous-electrode model that accounts for the solid- and electrolyte-phase potentials and current while neglecting the spatial variation in the concentrations. The model assumes either linear, Tafel, or exponential kinetics for the electrochemical reactions and incorporates some additional phenomena, such as the dependency of conductivities as a function of porosity. Optimization studies have been performed using this model to design the separator and electrode thicknesses[17-19] and ideal spatial variations of porosity within electrodes.[11]

1.2.2.c. Pseudo-Two-Dimensional Models

The pseudo-two-dimensional (P2D) model expands on the ohmic porous-electrode model by including diffusion in the electrolyte and solid phases, as well as Butler-Volmer kinetics (see Figure 1-4). Doyle et al.[12] developed a P2D model based on concentrated solution theory to describe the internal behavior of a lithium-ion sandwich consisting of positive and negative porous electrodes, a separator, and a current collector. This model was generic enough to incorporate further advancements in battery systems understanding, leading to the development of a number of similar models.[14,20-30] This physics-based model is by far the most used by battery researchers, and solves for the electrolyte concentration, electrolyte potential, solid-state potential, and solid-state concentration within the porous electrodes and the electrolyte concentration and electrolyte potential within the separator. This model based on the principles of transport phenomena, electrochemistry, and thermodynamics is represented by coupled nonlinear partial differential equations (PDEs) in x, r, and t that can take seconds to minutes to simulate. The inclusion of many internal variables allow for improved predictive capability, although at a greater computational cost than the aforementioned models.

1.2.3. Multiphysics Models

Multiscale, multidimensional, and multiphysics electrochemical-thermal coupled models are necessary to accurately describe all of the important phenomena that occur during the operation of lithium-ion batteries for high power/energy applications such as in electric/hybrid vehicles.

1.2.3.a. Thermal Models

Including temperature effects into the P2D model adds to the complexity, but also to the validity, of the model, especially in high power/energy applications. Due to the added computational load required to perform thermal calculations, many researchers have decoupled the thermal equations from the electrochemical equations by using a global energy balance, which makes it impossible to capture the effects on the performance of the cells due to temperature changes.[31-35] Other researchers have similarly decoupled the thermal simulation of the battery stack from the thermal/electrochemical simulation of a single cell sandwich.[36,37] Other thermal models have been reported that are coupled with first-principles electrochemical models both for single cells and cell stacks.[38-40] The global energy balance is only valid when the reaction distribution is uniform all over the cell; for accurate estimation of heat generation in a cell, the local variations in the reaction current and SOC must be incorporated.[41] Recently, Guo et al.[15] published a simplified thermal model applied to a single particle. Some papers have presented 2D thermal-electrochemical coupled models for lithium-ion cells that take into account the effects of local heat generation.[42,43] Similar studies predict battery discharging performance at different operating temperatures.[44] Additionally, the coupling of a 1D electrochemical model with a lumped thermal model by means of an Arrhenius form of temperature dependence for the physicochemical properties has been reported.[45-47] Recently, researchers have begun considering 3D thermal models to better understand the dynamic operation and control of lithium-ion batteries for large-scale applications. Since such models are quite computationally expensive,

several approximations are made, resulting in various shortcomings. Some models cannot monitor the thermal effect of electrochemical parameters,[33,48] while other models require empirical input from experiments or other simulations,[49,50] (or use volume-averaged equations for the solid-phase intercalation). Another approach assumes a linear current-potential relationship and neglects spatial concentration variations and is therefore only valid for low power operations.[51] A Multi-Scale Multi-Dimensional (MSMD) model[52] and a model derived from a grid of 1D electrochemical/thermal models[53] have also been implemented for 3D thermal simulation of batteries.

1.2.3.b. Stress-Strain and Particle Size/Shape Distributions

Intercalation of lithium causes an expansion of the active material, such as graphite or manganese oxide, while lithium extraction leads to contraction. The diffusion of lithium in graphite is not well understood, but some work has been done to model the diffusion and intercalation of lithium into the electrode material.[25,54,55] Since lithium diffuses within the particle, the expansion and contraction of the material will not happen uniformly across the particle (i.e., the outer regions of the particle will expand first due to lithium intercalating there first). This spatial nonuniformity causes stress to be induced in the particle and may lead to fracture and loss of active material,[56,57] which is one of the mechanisms for capacity fade. Various models have been developed to examine the volume change and stress induced by lithium-ion intercalation for single particles.[58-60] A two-dimensional microstructure model was developed[61] to extend the stress-strain analysis from single particles and was eventually incorporated into the full P2D model.[62] These models show that high rates of charging result in increased stress and increased chance of fracture, which can be somewhat mitigated by using smaller particles, or ellipsoidal particles. Additionally during battery cycling, some particles are

lost or agglomerate to form larger sized particles, which results in performance degradation. In addition, porous materials rarely have uniform particle size and shape. Some continuum models have accounted for the distribution of particle sizes and its effect on the battery performance,[63,64] for example, through the equation[63]

$$\frac{\partial \tilde{i}_2}{\partial x} = \left(4\pi \int_0^{\infty} N(r) Y(r) r^2 dr \right) \left(\tilde{\Phi}_1 - \tilde{\Phi}_2 \right) \qquad [1.1]$$

where $\tilde{i}_2$ is the fraction of total current flowing in solution, $N(r)$ is the number of particles per unit volume of composite electrode with a radius between size r and $r + dr$ in the porous electrode, $Y(r)$ is a function that relates the outward normal current density per unit surface area of a particle to the potential difference, and $\tilde{\Phi}_1 - \tilde{\Phi}_2$ is the potential difference between the solid particle and the adjacent solution. A promising future direction would be to extend such models to include variations in particle size and shape distribution by (1) writing f in terms of the multiple independent particle coordinates that define the particle shape (typically 3), and (2) replacing the single integral with a more complicated volume integral.

The time-dependent change in the particle size distribution due to breakage and agglomeration can be modeled by a spatially-varying multi-coordinate population balance equation:

$$\frac{\partial f(l,x,t)}{\partial t} + \sum_i \frac{\partial (G_i f)}{\partial l_i} = h(l,x,t,f) \qquad [1.2]$$

where $f(l,x,t)$ is the particle size and shape distribution function, x is the spatial coordinate, l_i is the i^{th} independent size coordinate, l is the vector with elements l_i (typically of dimension three), $G_i(l,t) = dl_i/dt$ is the growth rate along the i^{th} independent size coordinate (which is

negative for shrinkage), $h(l,x,t,f)$ is the generation/disappearance rate of particle formation (e.g., due to breakage and agglomeration), and t is time.[65-68] The expression for $h(l,x,t,f)$ for breakage and agglomeration contains integrals over the $f(l,x,t)$, and the h and G_i have dependencies on additional states such as local lithium-ion concentrations. This model to capture the effects of morphology within a material, called a *mesoscale model*,[69,70] would enable the material degradation due to spatially-varying and time-varying changes in the particle size and shape distribution to be explicitly addressed.

1.2.3.c. Stack Models

In order to simulate battery operations more accurately, battery models are improved by considering multiple cells arranged in a stack configuration. Simulation of the entire stack is important when thermal or other effects cause the individual cells to operate differently from each other. Since it is often not practical or possible to measure each cell individually in a stack, these differences can lead to potentially dangerous or damaging conditions such as overcharging or deep-discharging certain cells within the battery, which can cause thermal runaway or explosions. The ability to efficiently simulate battery stacks would facilitate the health monitoring of individual cell behavior during charging and discharging operations and thereby increasing safety by reducing the chances of temperature buildup causing thermal runaway. The significant increase in computational requirements to simulate a stack model has slowed its development and most examples of stack modeling perform some approximation or decoupling to facilitate efficient simulation.[34,37,71] Researchers have also published simplified coupled thermal electrochemical models applied to a single particle for stacks in parallel and series configurations.[72] Fully coupled battery stack simulations have been performed for a limited number of cells by using reformulation techniques to simplify simulation.[73]

1.2.4. Molecular/Atomistic Models

1.2.4.a. Kinetic Monte Carlo Method

The Kinetic Monte Carlo (KMC) method is a stochastic approach that has been used to model the discharge behavior of lithium ions during intercalation. Such models[74-77] have been used to simulate diffusion of lithium from site to site within an active particle to aid in understanding on how different crystal structures affect lithium mobility[73] and how the activation barrier varies with lithium-ion concentration.[76,77] Additionally, Monte Carlo methods have been used to predict thermodynamic properties.[78] KMC has also been applied to simulate the growth of the passive SEI-layer across the surface of the electrode particle, to simulate one of the mechanisms for capacity fade.[79]

1.2.4.b. Molecular Dynamics

Molecular dynamics has been used to gain insight into several molecular-scale phenomena that arise during the operation of lithium-ion batteries. One of the applications has been to the simulation of the initial growth of the passivating SEI film at the interface of the solvent and graphite anode. The application of a large negative potential during initial charging decomposes ethylene carbonate (EC) in the solvent, to produce the passivating SEI film containing lithium ethylene dicarbonate and salt decomposition products. Although molecular dynamics is too computationally too expensive for simulation of more than tens of picoseconds of battery operation, the method was demonstrated to be fast enough for simulation of the initial stage of SEI layer formation.[80] The simulations were able to predict the formation of carbon monoxide, which has been detected in experiments, and predicted that the initial SEI layer formation occurs is initiated at highly oxidized graphite edge regions of the anode.

Another application of molecular dynamics to lithium-ion batteries has been the simulation of the initial transport of lithium ions through a polycrystalline cathode.[81] Between each crystal grain is an amorphous intergranular film (IGF), and the motivation for the study was the conjecture that lithium ions diffuse much faster through the IGF than through the crystal grains. Although the simulations employed a particular lithium silicate glass as a solid electrolyte and vanadia with an amorphous V_2O_5 IGF separating the crystal grains, the results are expected to have more general applicability. The simulations were feasible with molecular dynamics because the conclusions only required that the lithium ion diffuse far enough into the cathode to quantify the differences in diffusion rates through the IGF and crystal grains. The simulation of effective diffusivities is one of the most common applications of molecular dynamics.[82]

1.2.4.c. Density Functional Theory

Density functional theory (DFT) calculations can be used to provide predictive insight into the structure and function of candidate electrode materials. The ground-state energy is given as a unique functional of the electron density, which can be calculated by self-consistently solving for the atomic orbitals. Geometry optimizations are used to determine structures, energetics, and reaction mechanisms. In the area of sustainable energy storage, DFT calculations have been used to predict and rationalize the structural changes that occur upon cycling of electrode materials, for example, in the calculation of activation barriers and thermodynamic driving forces for Ni ions in layered lithium nickel manganese oxides. Similar calculations have been used to determine the lattice properties and electronic structure of graphite and LiC_6.[83] Additionally, DFT calculations can be used to examine the effect of lithium intercalation on the mechanical properties of a graphite electrode, including Young's modulus, expansion of the unit cell, and the resulting stress effects,[84] as well as to compare the stability of $LiPF_6$ (a common electrolyte) in

various solvents.[85] DFT calculations have also been used to examine the mechanisms affecting the stability and function of the organic electrolytes separating the electrode materials, as in the reductive decompositions of organic propylene carbonate and ethylene carbonate to build up a solid-electrolyte interface that affects cycle-life, lifetime, power capability, and safety of lithium-ion batteries.

1.2.5. Simulation

Multiple numerical methods are available for the simulation of any particular battery model. For empirical models, analytical solutions are usually possible and can be easily solved in Microsoft® Excel or Matlab®.[86] Analytical solutions can be implemented in a symbolic language such as Mathematica®,[87] or Maple®,[88] or Mathcad®,[89] or in a compiled language such as FORTRAN or C++. Analytical solutions based on linear model equations often involve eigenvalues, which might have to be determined numerically. For nonlinear model equations, sometimes analytical series solutions using perturbation methods[90] or other symbolic techniques[91] can be derived. Numerical simulation methods are more flexible, with multiple methods available for any particular battery model. The best numerical methods tend to be more sophisticated when moving towards the upper right of the battery models shown in Figure 1-3.

For SPMs for a single electrode, analytical solutions have been derived for constant-current operation and cannot be obtained directly for the constant-potential operation, due to the fact that the boundary flux is implicitly determined by the nonlinear Butler-Volmer equation particularly when the open circuit voltage changes with state of charge. At this scale, especially for AC impedance data, analytical solutions are easily obtained and have been heavily used even for estimating unknown diffusion coefficients.[92]

When two electrodes are included in an SPM, an analytical solution is available for constant-current operation but not for constant-potential operation, for reasons as stated above, or when film formation for the SEI layer is modeled. Beyond SPM and porous electrode ohmic resistance models, analytical solutions are not possible for simulating charge-discharge curves. A SPM with two electrodes consists of a single partial differential equation for each electrode. Conversely, a finite-difference scheme discretized with 50 node points in the radial direction generates 50×2 + 50×2 = 200 differential algebraic equations (DAEs). Recall that the SPM is computationally efficient but is not accurate, especially for high rates. For P2D models[12] typically the finite-difference approach has been used. A P2D model with polynomial approximation[16] for the solid phase, when discretized with 50 node points in the spatial direction for each variable, results in a system of 250 DAEs for each electrode and 100 DAEs for the separator. Thus, the total number of DAEs to be solved for the P2D model across the entire cell is 250 + 250 + 100 = 600 DAEs. The addition of temperature effects to this model results in 750 DAEs to be solved simultaneously. Stack models are much more computationally expensive, as the number of DAEs is equal to the number of cells in the stack (N) times the number of equations coming from each sandwich. Using the finite-difference discretization of spatial variables in x, y, and r with 50 node points along each direction in a pseudo-3D thermal-electrochemical coupled model would generate 15,000 + 7500 + 15,000 = 37,500 DAEs to be solved simultaneously for a single sandwich.

The speed and accuracy of a numerical method depends upon the complexity of the model equations, including operating and boundary conditions, and the numerical algorithm. The most common numerical methods for simulation of lithium-ion batteries are the finite-difference method (FDM), finite-volume method (FVM, or sometimes called the control volume

formulation), and finite-element method (FEM). The main continuum simulation methods reported in the literature for the simulation of batteries can be classified as

(1) DUALFOIL.[24] This software employs Newman's BAND subroutine,[93] which is a finite-difference method used to simulate electrochemical systems for more than four decades. Symbolic software such as Mathematica® [87] and Maple® [88] can be used for determining analytical expressions for the Jacobians and for generating the associated FORTRAN code for use with the BANDJ subroutine.[21]

(2) FVM with various time-discretization schemes,[94] which has been applied to P2D models.

(3) COMSOL® [95]/BATTERY DESIGN STUDIO® [96], which implements the FEM/FDM in a user-friendly interface and includes a module that implements the P2D battery model.

(4) Finite-difference or reformulation schemes in spatial coordinates with adaptive solvers such as DASSL in time.[21]

Each approach has its advantages and disadvantages. DUALFOIL is a freely available FORTRAN code. The FDM has been used extensively in battery simulation[21] as it is easy to implement and modify. The FVM is closely related to the FDM but more easily handles irregular geometries. The FEM handles both irregular geometries and heterogeneous compositions, but is much harder to implement by hand, and so is usually only applied to batteries using commercial FEM software such as COMSOL. An advantage of commercial software like COMSOL is ease of use and that the numerical implementation is invisible to the user and results from COMSOL can be directly integrated to MATLAB environment, which is a widely used tool for control and optimization. However, a disadvantage is that COMSOL's numerical implementations cannot be modified by the user to (1) increase computational efficiency by exploiting additional mathematical structure in the model equations or (2) integrate such efficient simulation results

into advanced systems engineering algorithms for optimal design, operation, or control in a computationally efficient manner.

When optimization fails while using COMSOL-like codes, detective work is required to determine whether the numerical simulation was robust enough to provide accurate numerical Jacobians. Also, as of today, global optimization methods are readily available only for algebraic equations. Algebraic optimization schemes can be formulated by discretization of all the variables and parameters including the control variables,[97,98] but these optimization schemes typically have too high complexity to be solvable using existing global optimization software. Many groups are working on the development of optimization software that is more computationally efficient at computing local optima for dynamic optimizations or on ensuring convergence to a global optimum.[99,100]

BATTERY DESIGN STUDIO® [96] has a module for the simulation of P2D lithium-ion battery models. Adaptive solvers provide advantages in speed compared to fixed time-discretization schemes. Researchers have used DASSL for solving battery models.[21] DASSL/DASPK use backward differentiation schemes in time, which are numerically stable and efficient. For the same set of equations, these adaptive schemes can provide an order of magnitude savings in time. Battery models more advanced than the P2D model are usually solved offline in the literature (an exception is the P2D thermal model from Gu et al.[42,46] and the stress-strain model from Renganathan et al.[61]).

To understand the importance of capacity fade in a lithium-ion secondary battery system, significant efforts have been devoted to the development of mathematical models that describe the discharge behavior and formation of the active and passive SEI layers. The majority of these models are empirical or semi-empirical.[101,102] Other works have attempted to simulate capacity

fade by considering the lithium deposition as a side reaction and the resulting increased resistance.[29,103-107] Others have simulated capacity fade by modeling the active material loss, or change of internal parameter with cycling.[29,104-109] Other researchers have used KMC methods to examine the SEI layer formation at the microscale level.[79] Such a model, however, is computationally expensive, which makes online simulation difficult. Further work is needed to couple such fundamental models to the popular continuum models in use.

1.2.6. Optimization Applied to Li-ion Batteries

Several researchers have applied optimization to design more efficient electrochemical power sources. Newman and co-workers obtained optimal values of battery design parameters such as electrode thickness and porosity.[19,22,24,110-113] To simplify the optimization, many of these papers employed models with analytical solutions, which are only available in limiting cases. Battery design optimization using a full order model has been demonstrated by several researchers.[22,24,111,112] Newman and co-workers report the use of Ragone plots for studies regarding the optimization of design parameters, changing one design parameter at a time, such as electrode thickness, while keeping other parameters constant, Ragone plots for different configurations can be obtained. Hundreds of simulations are required when applied current is varied to generate a single curve in a Ragone plot, which is tedious and computationally expensive. An alternative is to simultaneously optimize the battery design parameters and operating conditions such as the charging profile.[9] Parameters have been simultaneously optimized for different models and goodness of fits compared based on statistical analysis.[114] Parameter estimation has also been used in a discrete approach to analyze and predict capacity fade using a full-order P2D model.[106,107] Golmon et al.[115] attempted a multiscale design optimization for improving electrochemical and mechanical performance of the battery by

manipulating both micro- and macro-scale design variables such as local porosities, particle radii, and electrode thickness to minimize internal stresses and maximize capacity of the battery. A surrogate-based framework using global sensitivity analysis has been used to optimize electrode properties.[116] Simulation results from P2D models have been used to generate approximate reduced-order models for use in global sensitivity analysis and optimization. Rahimian et al.[10] used a single-particle model when computing the optimum charging profile for maximizing the life of battery during cycling. Below is a description of the systems engineering tasks of (1) parameter estimation, (2) model-based optimal design, and (3) state estimation that have been applied to lithium-ion batteries.

Parameter estimation is typically formulated as the minimization of the sum-of-squared differences between the model outputs and their experimentally measured values for each cycle *i*, for example,[117-119]

$$\min_{\theta_i} \sum_{j=1}^{n_i} \left[y_i(t_j) - y_{model,i}(t_j;\theta_i) \right]^2 \qquad [1.3]$$

where $y_i(t_j)$ is the measured voltage at time t_j for cycle *i*, $y_{model,i}(t_j;\theta_i)$ is the voltage computed from the battery model at time t_j for cycle *i* for the vector of model parameters θ_i (the parameters being estimated from the experimental data), and n_i is the number of time points in cycle *i*. Solving the optimization [1.3] is known in the literature as *least-squares estimation*.[117-119] Many numerical algorithms are available for solving the nonlinear optimization [1.3], such as the steepest descent, Gauss-Newton, and Levenberg-Marquardt methods.[118] These iterative methods reduce the sum-of-squared differences between the model outputs and the experimental data points until the error is no longer significantly reduced. More sophisticated Bayesian estimation

methods employ the same numerical algorithms but use optimization objectives that take into account prior information on the model parameters.[120]

Battery design parameters such as cell thickness and electrode porosity and operating profiles can be optimized using the same numerical algorithms, for objectives such as maximization of performance (e.g., energy density, life) or minimization of capacity fade and mechanical degradation. These optimizations are solved subject to the model equations and any physical constraints. The optimal estimation of unmeasured states in lithium-ion batteries can also be formulated in terms of a constrained model-based optimization. The optimization objectives, models, and constraints differ for different systems engineering tasks, but can all be written in terms of one general formulation:[121]

$$\min_{\mathbf{z}(x),\mathbf{u}(x),\mathbf{p}} \Psi \qquad [1.4]$$

$$\text{such that } \frac{d}{dx}\mathbf{z} = \mathbf{f}(\mathbf{z}(x),\mathbf{y}(x),\mathbf{u}(x),\mathbf{p}), \qquad \mathbf{f}(\mathbf{z}(0)) = 0, \qquad \mathbf{g}(\mathbf{z}(1)) = 0, \qquad [1.5]$$

$$\mathbf{g}(\mathbf{z}(x),\mathbf{y}(x),\mathbf{u}(x),\mathbf{p}) = 0, \qquad [1.6]$$

$$\mathbf{u}_L \le \mathbf{u}(x) \le \mathbf{u}_U, \qquad \mathbf{y}_L \le \mathbf{y}(x) \le \mathbf{y}_U, \qquad \mathbf{z}_L \le \mathbf{z}(x) \le \mathbf{z}_U, \qquad [1.7]$$

where Ψ is the optimization objective,[122] $\mathbf{z}(x)$ is the vector of differential state variables, $\mathbf{y}(x)$ is the vector of algebraic variables, $\mathbf{u}(x)$ is the vector of control variables, and $\mathbf{p}$ is the vector of design parameters. Although there are many numerical methods for solving constrained optimization problems,[123-125] this chapter summarizes only control vector parameterization (CVP) as this is the method that is easiest to implement and most commonly used in industrial applications. The CVP method parameterizes the optimization variables, by employing basis functions or discretization, in terms of a finite number of parameters to produce a nonlinear

program that can be solved using standard software. First-principles models for lithium-ion batteries tend to be highly stiff, requiring adaptive time-stepping for reasonable computational efficiency.[100] CVP is well suited for optimizations over such models, as CVP incorporates the model equations by calling a user-specified subroutine for simulating the model equations. Any speedup obtained by an adaptive time-stepping for the model equations directly translates into a speedup on the CVP calculations.

More specifically, the control variable $\mathbf{u}(x)$ in CVP is parameterized by a finite number of parameters, typically as a polynomial or piecewise-linear function or by partitioning its values over space, and the resulting nonlinear program is solved numerically. Most numerical optimization algorithms utilize an analytically or numerically determined gradient of the optimization objective and constraints to march towards improved values for the optimization variables in the search space. In CVP, as the number of intervals increases, the number of equations increases and makes optimization more computationally expensive. Hence the fastest and most efficient battery model and code for the desired level of accuracy is recommended when applying CVP or any alternative optimization methods.

A discussion of simulating lithium-ion batteries at the systems-level is incomplete without addressing issues pertaining to the estimation of state-of-charge and health of the battery. Designing a tool to predict the life or performance of a battery is an interesting optimization problem with implications on material modifications during the initial battery formulation for a particular application, allowance for making a specific maintenance plan during the course of the life of the battery, and, most importantly, on the cost of the battery. Precise estimations of SOC and SOH are also essential to ensure the safe operation of batteries, that is, preventing the battery from overcharging and thermal runaway.

Some commonly used methods in the industry to monitor the SOC of the battery include monitoring of the cell impedance,[126-129] equivalent circuit analyses,[130,131] techniques based on fuzzy logic,[132,133] or pattern recognition.[134] Optical and eddy current methods[135,136] are being devised to monitor available capacity in battery systems with flat response surfaces. Based on the algorithm used for estimation, the models used to estimate SOC and SOH can be classified broadly into two categories. Some utilities such as the battery packs used in on-board satellites during the lack of solar energy or cells used in watches follow a routine or pre-programmed load. In such instances, it is possible to develop a degradation model based on *a priori* testing, knowing the operating conditions and the design parameters of the cell. Such a model does not require frequent updates for the parameters, unless there is a significant change in the operating conditions. In some other applications, such as battery packs used in vehicles, the battery is subjected to a dynamic load that changes as frequently as every few milliseconds. In these cases, the degradation mechanism and hence state of charge or the state of health of the power system depends on the load conditions imposed in the immediate past and it is necessary to monitor the cell on a regular basis. There are some differences between the algorithms used to make life-estimates for the case with the known operating parameters compared to the dynamic-load case. The latter situation is less forgiving in terms of the calculation time, for example. SOC and SOH estimators have been an integral part of battery controllers; however, the estimations have been primarily based on empirical circuit-based models that can fail under abusive or non-ideal operating conditions. Precise estimations of SOC and SOH are very essential for the safe operation of the batteries, in order to prevent them from overcharging and thermal runaway. Santhanagopalan et al.[137] reviewed past efforts on the monitoring and estimation of SOC in the literature, and reported an online Kalman filter-based SOC estimation for lithium-ion batteries

based on a single-particle model. Klein et al.[7] recently published state estimation using a reduced order model for a lithium-ion battery. Smith et al.'s[8] analysis of a 1D electrochemical model for a lithium-ion battery indicated that the electrode surface concentration was more easily estimated from the real-time measurements than the electrode bulk concentration. Domenico et al.[138] designed an extended Kalman filter for SOC estimation based on an electrochemical model coupling the average solid active material concentration with the average values of the chemical potentials, electrolyte concentration, and the current density.

1.3. Critical Issues in the Field

This section describes the challenges that arise when building predictive models for lithium-ion batteries and employing these models for systems engineering.

1.3.1. Sparsity of Manipulated Variables

Once the battery is manufactured and closed in a sealed case, the battery is discharged (used) according to the requirements of the application. The only variables that can be manipulated during battery operation to make best use of the battery is the charging current profile and operating temperature, which can affect transport and electrochemical rates resulting in modified performance.

Before the battery is sealed, the design variables such as the electrode dimensions, the type of materials, and materials properties such as porosity, active surface area, and microstructure can be selected so as to provide the best possible performance. The resulting battery design can be verified at small scale (e.g., few milli- or micro-Ah batteries) relatively easily in the laboratory, but scaling up to the large-scale batteries required for some industrial applications is challenging.

1.3.2. Need for Better Fundamental Models to Understand SEI-layer, Structure

The physicochemical understanding is incomplete for much of the phenomena that occur inside a battery, such as capacity fade, stress-strain effects, mechanical degradation, and mechanisms for failure due to shocks, defects, and shorts. Much progress has been made in the last twenty years on failure mechanisms, stress-strain models, capacity fade mechanisms involving side reactions, SEI-layer formation, and other phenomena, and studies have been published with the objective of understanding battery operation at the molecular scale, using kinetic Monte Carlo simulations, molecular dynamics, and density functional theory calculations, and at the mesoscale using population balance models. The molecular-scale models are simulated off-line (that is, not in real-time) and their predictions have been fed to continuum-scale models. A potential future application of molecular- and mesoscale models would be in the real-time prediction of the states of the battery at the small length scales for use in more accurate prediction of the whole battery performance in real time.

1.3.3. Robustness and Computational Cost in Simulation and Optimization

Battery models result in multiple DAEs to be simulated with unknown initial conditions while operating for multiple cycles of charge and discharge. For these models adaptive time steppers are usually more than an order of magnitude faster than uniform time-discretization. Several adaptive solvers are available for solutions of DAE models.[139-142] Recently, many easy-to-use ODE solvers have been made available (ode15s, ode15i, etc.) from MATLAB®,[86] "NDsolve" from MATHEMATICA®,[87] and "dsolve" from MAPLE®[88] to solve non-stiff, stiff and moderately stiff DAE models of index-1.

In spite of recent advancements, many of these DAE solvers and initialization routines can fail due to numerical convergence problems during Newton iteration to solve nonlinear equations

and singular/ill-conditioned Jacobian matrices resulting from small integration steps. The complexity in battery model simulation is increased by steep variations of the dependent variables (concentrations and potentials) between charging and discharging.

Battery simulations for extended operations, such as during switching from constant-current to constant-potential operations, typically require some form of event detection. The DAEs for battery models increase in complexity and also in number as the accuracy and predictability of models increase. Simulation times for battery models range from milliseconds for empirical circuit-based models to minutes for P2D/P3D models and even days for a multiscale model such as a P2D model coupled with KMC simulation, limiting the options for real-time simulations.

1.3.4. Uncertainties in Physicochemical Mechanisms

Although much literature exists for capacity fade, SEI-layer formation, and other phenomena, no existing model simulates all of the mechanisms for capacity fade or battery failure. More detailed information is required to sufficiently specify a hypothesized mechanism for a phenomenon before it can implemented in a simulation model, such as

- Which chemical species are formed and consumed in each phase and at the interface between phases?

- What is the physical configuration of each chemical species at the interface between phases (e.g., is a molecule on an electrode surface sticking out into the electrolyte or flat against the surface)?

- How many sites does each molecule on a solid surface cover?

Substantial experimental design efforts are required to answer such questions so the answers can be incorporated into first-principles lithium-ion battery models. Also, most applications

using batteries for long-term requirements depend on projections made from model predictions coupled with limited test data; however, the relationship between failure modes during the test conditions and those during actual operating scenarios have not been clearly established – necessitating the tools used in SOC and SOH predictions to be independent of the operating or manufacturing conditions. Quite often in such scenarios, the use of look-up tables limits the confidence in the predictive capabilities of the models.

Conventional degradation models based on extensive testing of batteries under various operating conditions and loads have in general attributed the degradation of battery performance to loss of the active material and loss of lithium that can be cycled. Several detailed models to quantify the signature of these parameters on the aging profile of lithium ion batteries have been presented.[29,143] Other approaches include the use of arbitrary empirical parameters obtained by regressing test data. These models usually interpolate the SOC and the health of the battery based on pre-stored database of information. Such models are widely employed in the industry when sufficient information on the physics of the materials in the batteries is not available – this problem is commonplace among module and pack manufacturers, who assemble the units from cells manufactured by a third-party. It is standard industrial practice to calibrate such models[144,145] since monitoring the evolution of all of the physical parameters such as transport coefficients and the reaction rates within each cell inside the pack is expensive, if not impossible. Network models have also been used to address non-uniform degradation in large format cells.[146]

1.4. Addressing the Critical Issues, Opportunities, and Future Work

This section describes some approaches for addressing the critical issues raised in the previous section, looking towards likely future research directions in the modeling and systems engineering of lithium-ion batteries.

1.4.1. Sparsity of Manipulated Variables

Currently, batteries are charged at constant current until a cut-off potential is reached or a time limit followed by charging at constant potential. However, these charging protocols may result in thermal runaway, leading to under-utilization and possibly even explosions. Given the limited variables that are available for manipulation, it is especially important to make the best utilization of these variables during battery operations. A first-principles battery model can be employed in a dynamic optimization framework to compute a time-varying charging profile that maximizes life, minimizes capacity fade, and improves battery performance.

The determination of an optimized charging profile requires a first-principles model that has high predictive accuracy for a wide range of operating conditions, since charge transfer, reaction kinetics, and diffusion rates may be quite different than in the experiments used in the model development. A first-principles model that describes the battery behavior at the meso- and microscale models would be able to take these effects into account during the dynamic optimization. The application of dynamic optimization to compute an optimal charging profile is illustrated here for a P2D model[9] for lithium-ion batteries. The dynamic optimization for a cell was formulated as:

$$\max_{i_{applied}(t)} E(t_f)$$
$$s.t.\ \frac{dE}{dt} = V(t) i_{applied}(t) \qquad [1.8]$$
$$V(t) \le 4.05 \text{ V}$$
$$t_f \le 1 \text{ hour}$$

where the optimization objective E is the total energy stored in the cell, V is the voltage obtained from the cell as computed from the first-principles model, $i_{applied}$ is the applied current to the cell, the charging time t_f was restricted to 1 hr, the maximum allowed voltage was 4.05 V, and the value for V as a function of time. The implementation of dynamic optimization is facilitated by the use of a reformulated model[6] to compute the optimization objective. The time profiles for the electrolyte concentration at the cathode/current collector interface in Figure 1-6 are for three different charging scenarios: (1) conventional charging at constant-current followed by constant-potential charging, (2) constant-current charging at an optimized value obtained by solving the dynamic optimization for a fixed value, and (3) the time-varying charging profile given by Eq. 5. The electrolyte concentration at $X = 0$ (the cathode/current collector interface) has the highest peak value during dynamically optimized charging, due to its higher initial current. For the chosen chemistry, mass transfer limitations in the electrolyte occur at higher currents. This protocol indicates that, to increase the energy density, store more energy at shorter time albeit causing mass transfer limitations in the electrolyte and let the concentration equilibrate at longer times to ensure longer operability of the battery. During dynamically optimized charging, the electrolyte concentration decreases in the latter part of charging, as lithium-ion transfer slows while more lithium ions are packed into the carbon matrix in the negative electrode. In contrast, after the first 10 minutes the electrolyte concentration is nearly constant during optimized constant-current charging. When a meaningful global objective function was chosen at the

system level and robust optimization tool and meaningful models are used, improvements in 'local' battery behavior are observed.

The above approach can be considered as a top-down approach, where operating conditions or charging protocols are determined at the system level (battery as a whole), and the system-level behavior is affected by the local mass/charge transfer and reaction effects (Figure 1-1) and indirectly manipulates non-measurable internal variables such as the electrolyte concentration or potential or also the solid-phase concentrations as shown schematically in Figure 1-6. Physics-based models are required in the dynamic optimization to correctly relate the local effects to the system-level behavior as quantified by the optimization objective. The more detailed and accurate the model, the more optimal 'local' behavior can be determined using the few manipulated variables at the system level.

Note that the SPM model lacks sufficient information on the behavior in the cell to be of much usefulness in the above optimizations. If the first-principles model employed in the optimization includes a high fidelity thermal model, then the localized temperatures in the cell can be included as a constraint in the optimization. A more detailed multiscale model that includes more of the physicochemical phenomena would be needed for optimization of battery operations for very quick charging generally involving rates of 2C or higher.

Another approach that can be used to address the sparsity of manipulated variables is to have the limited number of material properties (manipulated variables) vary spatially. If the electrode architecture is designed to minimize and address every possible local nonideality at the sandwich level, then the system level performance will improve. This can be viewed as the bottom-up approach, where the material properties or electrode architecture, etc. are determined at the electrode level (micro-scale), to produce improved performance at the system level (Figure 1-1).

Physics-based models are required in the optimization framework to correctly relate the local effects to the system-level behavior as quantified by the optimization objective. For example, consider the minimization of the ohmic resistance at the sandwich level (Figure 1-1). Chapter 4 considers the design of spatially-varying porosity profiles in next-generation electrodes based on simultaneous optimization of a porous electrode model. Model-based optimal design (not including the solid-phase intercalation mechanism) is applied to a porous positive electrode made of lithium cobalt oxide, which is commonly used in lithium-ion batteries for various applications. For a fixed amount of active material, optimal grading of the porosity across the electrode was found to decrease the ohmic resistance by 15-33%, which in turn increases the electrode capacity to hold and deliver energy. The optimal porosity grading was predicted to have 40% lower variation in the ohmic resistance to variations in model parameters due to manufacturing imprecision or capacity fade. The results suggest the potential for the simultaneous model-based design of electrode material properties that employ more detailed physics-based first-principles electrochemical engineering models to determine optimal design values for manufacture and experimental evaluation. Optimization of spatially-uniform porosity reduced the ohmic resistance by 20%, whereas optimization for a spatially-varying profile results in a reduction of 33% (Figure 1-7).[11] Physics-based models are required in the optimization framework to correctly relate the local effects to the system-level behavior as quantified by the optimization objective. Note that improved performance for both solid-phase potential and current are obtained locally, which leads to reduced ohmic resistance across the sandwich, which then relates to improved performance for charge-discharge curves at the system level.

To address all the issues in Figure 1-1, a more detailed model is required (i.e., moving right along the diagonal in Figure 1-3). Possible material properties that can be varied as a function of

distance are given in Figure 1-2. Note that for particle radius, optimization with the P2D model would yield only the smallest possible radius, but stress-strain models would suggest a different size for mechanical stability.[115]

The more sophisticated the battery model, more computationally intensive the simulations and optimization. While the value of adding more physicochemical phenomena into battery models is clear, and discussed in more detail below, there is also a need to improve the computationally efficiency in the simulation of these models by reformulation or order reduction.

1.4.2. Need for Better Fundamental Models to Understand SEI-layer, Structure

Different simulation methods are effective at different scales (see Figure 1-5), which has motivated efforts to combine multiple methods to simulate multiscale systems. Battery models that dynamically couple the molecular- through macro-scale phenomena could have a big impact in understanding and designing lithium-ion batteries. The above continuum models could be coupled with stress-strain models and population balance models to describe the time evolution of the size and shape distribution of particles. Probably the first step would be to couple molecular models with P2D models, to thoroughly validate the coupled simulation algorithms before moving to more computationally expensive 3D continuum models. KMC methods could be combined with P2D models to analyze surface phenomena such as growth of the SEI layer in a detailed manner, similarly as has been applied to other electrochemical systems.[70,147-156] For a 125×125 mesh, 2D KMC coupled with P2D model with time steps ranging from nanoseconds to seconds would require simulation times ranging from minutes to hours and even days for a single cycle. Another multiscale coupling that could be useful is to occasionally employ molecular dynamics to update transport parameters in a P2D or 3D model. Molecular dynamics can provide information that cannot be predicted using a P2D or 3D continuum model, but long times cannot

be simulated using molecular dynamics, so the combination of the two approaches has the potential to increase fidelity while being computationally feasible.

The current literature review suggests that typical researchers have expertise and skills in one or two of the models/methods reported in Fig 6. If researchers with expertise in different fields collaborate, the task of multiscale model development becomes easier and faster progress can be expected. While black-box approaches are available for some of the methods in Figure 1-5, it is strongly recommended that, at least for case studies, hard-coded direct numerical simulation is carried out to enable better understanding of coupling between models at different length and time scales.

1.4.3. Robustness and Computational Cost in Simulation and Optimization

The complexities of battery systems have made efficient simulation challenging. The most popular model, the P2D model, is often used because it is derived from well understood kinetic and transport phenomena, but the model results in a large number of highly nonlinear partial differential equations that must be solved numerically. For this reason, researchers have worked to simplify the model though reformulation or reduced order methods to facilitate effective simulation. One method of simplification is to eliminate the radial dependence of the solid phase concentration using a polynomial profile approximation,[16] by representing it using the particle surface concentration and the particle average concentration, both of which are functions of the linear spatial coordinate and time only. This type of volume-averaging[157,158] combined with the polynomial approximation[159,160] has been shown to be accurate for low to medium rates of discharge.[16,161-164] At larger discharge rates, other approaches have been developed to eliminate the radial dependence while maintaining accuracy.[102,161-164]

One of the major difficulties in simulating Li-ion battery models is the need for simulating solid phase diffusion in a second dimension *r*. It increases the complexity of the model as well as the computational time/cost to a great extent. Traditional approach towards solid phase diffusion leads to more difficulties, with the use of emerging cathode materials, which involve phase changes and thus moving boundaries. A computationally efficient representation for solid-phase diffusion is proposed in this chapter. The operating condition has a significant effect on the validity, accuracy and efficiency of various approximations for the solid-phase diffusion. Chapter 2 compares approaches available today for solid phase reformulation and provides two efficient forms for constant and varying diffusivities in the solid phase. This chapter introduces an efficient method of Eigen function based Galerkin Collocation and a mixed order finite difference method for approximating/representing solid-phase concentration variations within the active materials of porous electrodes for a pseudo-2D model for lithium-ion batteries.

Recently, discretization in space alone has been used by researchers to reduce the model to a system of DAEs with time as the sole independent variable in order to take advantage of the speed gained by time-adaptive solvers such as DASSL/DASPK.[5,6,140] Such solvers also have the advantage of being capable of detecting events, such as a specific potential cutoff, and running the simulation only to that point.

Complications arise when determining consistent initial conditions for the algebraic equations. Consequently, many good solvers fail to solve DAE models resulting from simulation of battery models.[165] As a result, it is necessary to develop initialization techniques to simulate battery models. Many such methods can be found in the literature for a large number of engineering problems. Recently, a perturbation approach has been used to efficiently solve for consistent initial conditions for battery models.[166]

Proper orthogonal decomposition (POD) has been used to reduce the computational cost in various sets of model equations, by fitting a reduced set of eigenvalues and nodes to obtain a reduced number of equations.[5] Alternatively, model reformulation techniques have been used to analytically eliminate a number of equations before solving the system.[6] Other researchers have used orthogonal collocation and finite elements, rather than finite differences, in order to streamline simulations.[167,168]

For stack and/or thermal modeling of certain battery systems, many attempts have decoupled equations within the developed model.[31-40] This approach breaks up a single large system into multiple, more manageable systems that can be solved independently. This allows the model to be solved quickly, but at the expense of accuracy. For this reason, efficient models that maintain the dynamic online coupling between the thermal and electrochemical behavior, as well as between individual cells in the stack are preferred.

Numerical algorithms for optimization can get stuck in local optima, which can be nontrivial to troubleshoot when the number of optimization parameters is large. This problem can at least be partly addressed using a sequential step-by-step approach (see Figure 1-8). For illustration purposes, consider the maximization of the energy density with l_p, l_n, l_s, ε_p, and ε_n, where l is the thickness of each region and ε the porosity (p – positive electrode, s – separator, and n – negative electrode).

(1) Choose a battery model that can predict the optimization objective and is sensitive to the manipulated variables (e.g., a P2D model).

(2) Reformulate or reduce the order of the model for efficient simulation. This step has to be judiciously made to ensure that the reduced order model is valid in the range of manipulated variables for optimization.

(3) Maximize energy density with l_p,

(4) Using the solution from Step 3 as an initial guess, find optimal values for the two parameters (l_p, ε_p).

(5) Add parameters one by one, in the same manner as in Step 4.

(6) Arrive at optimal performance with multiple parameters.

(7) If needed before Step 3, find results with a simpler and less accurate model for a good initial guess.

(8) After convergence, feed in more sophisticated models (for example, including stress effects) to make sure mechanical stability is not compromised.

A similar approach can be used for CVP for dynamic optimization with the total time interval divided as 2, 4, 8, etc. for subsequent optimizations until convergence.

The above algorithm will tend to have better convergence if the parameters in Steps 3-5 are rank ordered from having the largest to the lowest effect on the optimization objective. While advances have been made in the computation of global optima for dynamic optimizations,[100,169] it will be at least a decade before such methods are computationally efficient enough for application to the optimal design of lithium-ion batteries using nontrivial physics-based models.

Figure 1-9 shows improved performance at each step of an optimization while successively adding manipulated variables. Capacity matching was used a constraint for the thickness of the negative electrode.

1.4.4. Uncertainties in Physicochemical Mechanisms

Uncertainty quantification methods have been applied to hundreds of different kinds of systems to assess the progress of the development of first-principles models and to assess the confidence in model predictions.[120,170,171] The Monte Carlo method and its many variants for uncertainty quantification are computationally expensive and have become less used over time compared to power series and polynomial chaos expansions. These expansion-based approaches avoid the high computational cost associated with applying the Monte Carlo method or parameter gridding by first computing an approximation to the full simulation model, followed by application of robustness analysis to the approximate model. These expansion-based methods are computationally efficient enough for application to lithium-ion batteries.

For example, consider the discrete estimation of model parameters as a way to track the effects of capacity fade. As of today, capacity fade is attributed to many reasons. This depends upon the chemistry, mode of operation, and size. A wide range of reasons can be linked to transport and kinetic parameters as published elsewhere.[106,107,172] Five effective transport and kinetic parameters were estimated by applying least-squares estimation to the 250 mAh button cells experimental voltage-discharge data. The estimated parameters were the effective diffusion coefficient of lithium ion in the solution phase (D_1), effective diffusion coefficient of lithium in the solid phase for the negative and positive electrodes (D_{sn} and D_{sp}), and electrochemical reaction rate constants for the negative and positive electrodes (k_n and k_p).

The effective negative-electrode solid-phase diffusion coefficient and reaction rate constant (D_{sn} and k_n) were found to decrease monotonically with cycle #, whereas the other three parameters did not follow any particular trend. This suggested that the voltage-discharge curves may not contain sufficient information to accurately estimate the effective values of D_1, D_{sp}, and k_p, and that the change in the voltage-discharge curves with cycle # could be captured by estimation of only the effective solid-phase diffusion coefficient D_{sn} and reaction rate constant k_n for the negative electrode. A more detailed analysis suggested that the voltage-discharge curves were very sensitive to the value of the effective solid-phase diffusion coefficient D_{sn} but weakly sensitive to deviations in the model parameters D_1, D_{sp}, k_p, and k_n from their nominal values, resulting in large uncertainties in their values when fit to experimental voltage-discharge curves. That the voltage-discharge curves were much sensitive to a negative-electrode parameter (D_{sn}) suggests that mechanisms for capacity fade in the negative electrode, rather than the electrolyte or positive electrode, were the most important for this battery under these operating conditions.[107]

The overall trend in the variation of model parameters is more reliably assessed by plotting nominal estimates over many cycles. A discrete approach was adopted for the prediction of capacity fade by tracking the change in effective transport and kinetic parameters with cycle number (N). The model parameters D_{sn} and k_n fit to the experimental data for cycles 25, 100, 200, 300, 400, and 500 were used to predict the remaining battery life based on voltage-discharge curves measured in past cycles. To characterize the degradation in the model parameters, a power law was fit to the estimated parameter values from cycles 25 to 500 as shown in Figure 1-10. By implicitly assuming that the changes in the parameter values are the result of the same mechanism in later cycles, the parameter values for the subsequent cycles were

predicted using the power-law expressions. The voltage-discharge curve predicted by this model was in very good agreement with the experimental data at cycle 1000, indicating that the model was able to predict capacity fade as shown in Figure 1-10. It is likely that when more detailed multiscale models become available, there will not be a need to perform fitting and tracking of transport and kinetic parameters with cycles. Chapter 3 describes in detail how this discrete approach was used to predict the life of a battery with real experimental data.

A rapid update of the parameters usually involves some form of a moving horizon algorithm that estimates the parameters used in the model using an initial set of data points (for example between from the start of the experiment to some interval of time t). These values for the parameters (θ_t) are then used to predict the cell performance for the next few data points (e.g., between times t and $t + \Delta t$). The error between the model predictions and the actual data points collected between t and $t + \Delta t$ is then used to calculate the updated set of parameters $\theta_{t+\Delta t}$. This process is repeated at periodic intervals of time or the load. Filtering techniques are commonly employed for on-line estimation;[137,173,174] in most of these algorithms, the measured change in the response is divided between the actual battery response and system noise, based on pre-determined weights assigned to the functions calculating the noise and the battery models. The predicted response for the voltage is compared at the next time step and a correction term is introduced to the weights. More elaborate moving horizon estimates include the influence from several sets of parameters from the past on the current estimates. One example is the use of exponential forgetting functions.[175,176] In this example, the effect of the parameter values θ_t, $\theta_{t+\Delta t}$, $\theta_{t+2\Delta t}$, etc. on the current estimate $\theta_{t+k\Delta t}$ is assumed to decay exponentially. The steps are summarized below:

Step 1: Choose a subset of data points N_0 that end when the parameters need to be updated. Calculate the initial value for the SOC.

Step 2: Calculate the value of the exponential forgetting function at the end of N_0.

Step 3: Use the next set of data points N_0+1 to N_1, to calculate the updated values for the parameters in the model equations.

Step 4: Update the SOC for the next set of data points using the parameter values from the previous step.

Step 5: Update the exponential forgetting function, based on the data points N_0+1 to N_1, new values for the parameters, and the current value of the SOC.

Step 6: Repeat Steps 1 to 5 until the end of the data set. This procedure produces a set of values for the SOC updated whenever the error between the model and the experimental data is significant.

The use of such online-tracking algorithms, together with reliable models requiring modest computational effort, greatly reduces the uncertainty associated with assessing the failure mode of the batteries, and can be implemented for a variety of operating conditions. The states of interest are tracked as and when the system operates; the advantages offered by this approach are two-fold: (1) any mitigation scheme can be implemented fairly quickly since the operator does not wait until performing the scheduled capacity checks on the batteries and (2) the proposed methodology does not rely solely on a characterization chart made under lab-scale testing environment, and captures the wear-and-tear imposed by the system on the batteries.

1.5. References

1. M. Armand and J. M. Tarascon, *Nature*, **451**, 652 (2008).
2. J. M. Tarascon and M. Armand, *Nature*, **414**, 359 (2001).
3. J. Newman, K. E. Thomas, H. Hafezi and D. R. Wheeler, *J Power Sources*, **119**, 838 (2003).
4. R. Shishko and R. Aster, *NASA Special Publication*, **6105** (1995).
5. L. Cai and R. E. White, *J Electrochem Soc*, **156**, A154 (2009).
6. V. R. Subramanian, V. Boovaragavan, V. Ramadesigan and M. Arabandi, *J Electrochem Soc*, **156**, A260 (2009).
7. R. Klein, N. A. Chaturvedi, J. Christensen, J. Ahmed, R. Findeisen and A. Kojic, in *Proceedings of the American Control Conference*, p. 6618 (2010).
8. K. A. Smith, C. D. Rahn and C. Y. Wang, *Energ Convers Manage*, **48**, 2565 (2007).
9. R. Methekar, V. Ramadesigan, R. D. Braatz and V. R. Subramanian, *ECS Trans*, **25**, 139 (2010).
10. S. K. Rahimian, S. C. Rayman and R. E. White, *J Electrochem Soc*, **157**, A1302 (2010).
11. V. Ramadesigan, R. N. Methekar, F. Latinwo, R. D. Braatz and V. R. Subramanian, *J Electrochem Soc*, **157**, A1328 (2010).
12. M. Doyle, T. F. Fuller and J. Newman, *J Electrochem Soc*, **140**, 1526 (1993).
13. D. Zhang, B. N. Popov and R. E. White, *J Electrochem Soc*, **147**, 831 (2000).
14. S. Santhanagopalan, Q. Z. Guo, P. Ramadass and R. E. White, *J Power Sources*, **156**, 620 (2006).
15. M. Guo, G. Sikha and R. E. White, *J Electrochem Soc*, **158**, A122 (2011).
16. V. R. Subramanian, V. D. Diwakar and D. Tapriyal, *J Electrochem Soc*, **152**, A2002 (2005).
17. M. Doyle and J. Newman, *Electrochim Acta*, **40**, 2191 (1995).
18. M. Doyle and J. Newman, *J Power Sources*, **54**, 46 (1995).
19. J. Newman, *J Electrochem Soc*, **142**, 97 (1995).
20. P. Arora, M. Doyle, A. S. Gozdz, R. E. White and J. Newman, *J Power Sources*, **88**, 219 (2000).
21. G. G. Botte, V. R. Subramanian and R. E. White, *Electrochim Acta*, **45**, 2595 (2000).
22. M. Doyle, J. Newman, A. S. Gozdz, C. N. Schmutz and J. M. Tarascon, *J Electrochem Soc*, **143**, 1890 (1996).
23. T. F. Fuller, M. Doyle and J. Newman, *J Electrochem Soc*, **141**, 982 (1994).
24. T. F. Fuller, M. Doyle and J. Newman, *J Electrochem Soc*, **141**, 1 (1994).
25. P. M. Gomadam, J. W. Weidner, R. A. Dougal and R. E. White, *J Power Sources*, **110**, 267 (2002).
26. J. Newman and W. Tiedemann, *AIChE J*, **21**, 25 (1975).
27. G. Ning, R. E. White and B. N. Popov, *Electrochim Acta*, **51**, 2012 (2006).
28. P. Ramadass, B. Haran, P. M. Gomadam, R. White and B. N. Popov, *J Electrochem Soc*, **151**, A196 (2004).
29. P. Ramadass, B. Haran, R. White and B. N. Popov, *J Power Sources*, **123**, 230 (2003).
30. K. E. Thomas and J. Newman, *J Electrochem Soc*, **150**, A176 (2003).
31. S. Al Hallaj, H. Maleki, J. S. Hong and J. R. Selman, *J Power Sources*, **83**, 1 (1999).
32. D. Bernardi, E. Pawlikowski and J. Newman, *J Electrochem Soc*, **132**, 5 (1985).
33. Y. Chen and J. W. Evans, *J Electrochem Soc*, **140**, 1833 (1993).
34. Y. F. Chen and J. W. Evans, *J Electrochem Soc*, **141**, 2947 (1994).

35. T. I. Evans and R. E. White, *J Electrochem Soc*, **136**, 2145 (1989).
36. C. R. Pals and J. Newman, *J Electrochem Soc*, **142**, 3274 (1995).
37. C. R. Pals and J. Newman, *J Electrochem Soc*, **142**, 3282 (1995).
38. D. R. Baker and M. W. Verbrugge, *J Electrochem Soc*, **146**, 2413 (1999).
39. G. G. Botte, B. A. Johnson and R. E. White, *J Electrochem Soc*, **146**, 914 (1999).
40. L. Song and J. W. Evans, *J Electrochem Soc*, **147**, 2086 (2000).
41. L. Rao and J. Newman, *J Electrochem Soc*, **144**, 2697 (1997).
42. W. B. Gu and C. Y. Wang, in *Lithium Batteries, The Electrochemical Society Proceedings Series*, S. Surampudi, R. A. Marsh, Z. Ogumi and J. Prakash, Editors, p. 748, Pennington, NJ (2000).
43. V. Srinivasan and C. Y. Wang, *J Electrochem Soc*, **150**, A98 (2003).
44. K. Kumaresan, G. Sikha and R. E. White, *J Electrochem Soc*, **155**, A164 (2008).
45. W. F. Fang, O. J. Kwon and C. Y. Wang, *Int J Energ Res*, **34**, 107 (2010).
46. W. B. Gu and C. Y. Wang, *J Electrochem Soc*, **147**, 2910 (2000).
47. K. Smith and C. Y. Wang, *J Power Sources*, **160**, 662 (2006).
48. J. Newman and W. Tiedemann, *J Electrochem Soc*, **142**, 1054 (1995).
49. S. C. Chen, C. C. Wan and Y. Y. Wang, *J Power Sources*, **140**, 111 (2005).
50. J. Lee, K. W. Choi, N. P. Yao and C. C. Christianson, *J Electrochem Soc*, **133**, 1286 (1986).
51. M. W. Verbrugge, *AIChE J*, **41**, 1550 (1995).
52. G.-H. Kim and K. Smith, *Meet Abstr - Electrochem Soc*, **802**, 1295 (2008).
53. R. E. Gerver, *3D Thermal-Electrochemical Lithium-ion Battery Computational Modeling*, Masters Thesis, The University of Texas at Austin, Austin, TX, (2009).
54. K. Persson, V. A. Sethuraman, L. J. Hardwick, Y. Hinuma, Y. S. Meng, A. van der Ven, V. Srinivasan, R. Kostecki and G. Ceder, *J Phys Chem Lett*, **1**, 1176 (2010).
55. G. K. Singh, G. Ceder and M. Z. Bazant, *Electrochim Acta*, **53**, 7599 (2008).
56. M. C. Tucker, J. A. Reimer and E. J. Cairns, *Electrochem Solid St*, **3**, 463 (2000).
57. H. F. Wang, Y. I. Jang, B. Y. Huang, D. R. Sadoway and Y. T. Chiang, *J Electrochem Soc*, **146**, 473 (1999).
58. J. Christensen and J. Newman, *J Solid State Electr*, **10**, 293 (2006).
59. J. Christensen and J. Newman, *J Electrochem Soc*, **153**, A1019 (2006).
60. X. C. Zhang, W. Shyy and A. M. Sastry, *J Electrochem Soc*, **154**, A910 (2007).
61. S. Renganathan, G. Sikha, S. Santhanagopalan and R. E. White, *J Electrochem Soc*, **157**, A155 (2010).
62. R. E. Garcia, Y. M. Chiang, W. C. Carter, P. Limthongkul and C. M. Bishop, *J Electrochem Soc*, **152**, A255 (2005).
63. J. P. Meyers, M. Doyle, R. M. Darling and J. Newman, *J Electrochem Soc*, **147**, 2930 (2000).
64. D. E. Stephenson, E. M. Hartman, J. N. Harb and D. R. Wheeler, *J Electrochem Soc*, **154**, A1146 (2007).
65. D. L. Ma, R. D. Braatz and D. K. Tafti, *Int J Mod Phys B*, **16**, 383 (2002).
66. X. Y. Woo, R. B. H. Tan and R. D. Braatz, *Cryst Growth Des*, **9**, 156 (2009).
67. X. Y. Woo, R. B. H. Tan, P. S. Chow and R. D. Braatz, *Cryst Growth Des*, **6**, 1291 (2006).
68. H. M. Hulburt and S. Katz, *Chem Eng Sci*, **19**, 555 (1964).
69. R. D. Braatz, E. G. Seebauer and R. C. Alkire, in *Electrochemical Surface Modification - Thin Films, Functionalization and Characterization, Advances in Electrochemical Science and Engineering* R. C. Alkire, D. M. Kolb, J. Lipkowski and P. N. Ross, Editors, Wiley-VCH Verlag GmbH & Co., Weinheim, Germany, **10,** Chapter 4, 289 (2008).

70. T. O. Drews, E. G. Webb, D. L. Ma, J. Alameda, R. D. Braatz and R. C. Alkire, *AIChE J*, **50**, 226 (2004).
71. Y. F. Chen and J. W. Evans, *J Electrochem Soc*, **143**, 2708 (1996).
72. M. Guo and R. E. White, *J Electrochem Soc*, **158**, A1166 (2011).
73. P. W. C. Northrop, V. Ramadesigan, S. De and V. R. Subramanian, *J Electrochem Soc*, **158** (12), A1461 (2011).
74. J. Bhattacharya and A. Van der Ven, *Phys Rev B*, **81** (2010).
75. A. B. Bortz, M. H. Kalos and J. L. Lebowitz, *J Comput Phys*, **17**, 10 (1975).
76. A. Van der Ven and G. Ceder, *Electrochem Solid St*, **3**, 301 (2000).
77. A. Van der Ven, J. C. Thomas, Q. C. Xu, B. Swoboda and D. Morgan, *Phys Rev B*, **78** (2008).
78. M. Wagemaker, A. Van Der Ven, D. Morgan, G. Ceder, F. M. Mulder and G. J. Kearley, *Chem Phys*, **317**, 130 (2005).
79. R. N. Methekar, P. W. C. Northrop, K. J. Chen, R. D. Braatz and V. R. Subramanian, *J Electrochem Soc*, **158**, A363 (2011).
80. K. Leung and J. L. Budzien, *Phys Chem Chem Phys*, **12**, 6583 (2010).
81. S. H. Garofalini, *J Power Sources*, **110**, 412 (2002).
82. W. Q. Li and S. H. Garofalini, *Solid State Ionics*, **166**, 365 (2004).
83. K. R. Kganyago and P. E. Ngoepe, *Phys Rev B*, **68** (2003).
84. Y. Qi, H. Guo, J. L. G. Hector and A. Timmons, *J Electrochem Soc*, **157**, A558 (2010).
85. K. Tasaki, K. Kanda, S. Nakamura and M. Ue, *J Electrochem Soc*, **150**, A1628 (2003).
86. Mathworks website, [http://www.mathworks.com, last accessed November, 2011]
87. Wolfram website, [http://www.wolfram.com, last accessed November, 2011]
88. Maplesoft website, [http://www.maplesoft.com/Products/Maple, last accessed Novermber, 2011]
89. Mathcad website, [http://www.ptc.com/products/mathcad, last accessed November, 2011]
90. A. Varma and M. Morbidelli, *Mathematical Methods in Chemical Engineering*, Oxford Univ. Press, New York, NY [u.a.] (1997).
91. V. R. Subramanian, B. S. Haran and R. E. White, *Comput Chem Eng*, **23**, 287 (1999).
92. S. Motupally, C. C. Streinz and J. W. Weidner, *J Electrochem Soc*, **142**, 1401 (1995).
93. J. S. Newman and K. E. Thomas-Alyea, *Electrochemical Systems*, Wiley-Interscience, Hoboken, N.J. (2004).
94. I. Bloom, B. W. Cole, J. J. Sohn, S. A. Jones, E. G. Polzin, V. S. Battaglia, G. L. Henriksen, C. Motloch, R. Richardson, T. Unkelhaeuser, D. Ingersoll and H. L. Case, *J Power Sources*, **101**, 238 (2001).
95. COMSOL website, [http://www.comsol.com, last accessed November, 2011]
96. Battery Design LLC. website, [http://www.batdesign.com/batterydesign.html, last accessed November, 2011]
97. L. T. Biegler and V. M. Zavala, *Comput Chem Eng*, **33**, 575 (2009).
98. M. Tawarmalani and N. V. Sahinidis, *Math Program*, **103**, 225 (2005).
99. B. Houska, H. J. Ferreau and M. Diehl, *Optim Contr Appl Met*, **32**, 298 (2011).
100. A. B. Singer and P. I. Barton, *J Global Optim*, **34**, 159 (2006).
101. B. Y. Liaw, R. G. Jungst, G. Nagasubramanian, H. L. Case and D. H. Doughty, *J Power Sources*, **140**, 157 (2005).
102. C. Y. Wang, W. B. Gu and B. Y. Liaw, *J Electrochem Soc*, **145**, 3407 (1998).

103. P. Arora, B. N. Popov, B. Haran, M. Ramasubramanian, S. Popova and R. E. White, *Corros Sci*, **39**, 739 (1997).
104. H. J. Ploehn, P. Ramadass and R. E. White, *J Electrochem Soc*, **151**, A456 (2004).
105. P. Ramadass, A. Durairajan, B. Haran, R. White and B. Popov, *J Electrochem Soc*, **149**, A54 (2002).
106. V. Ramadesigan, V. Boovaragavan, M. Arabandi, K. Chen, H. Tsukamoto, R. Braatz and V. Subramanian, *ECS Trans*, **19**, 11 (2009).
107. V. Ramadesigan, K. J. Chen, N. A. Burns, V. Boovaragavan, R. D. Braatz and V. R. Subramanian, *J Electrochem Soc*, **158**, A1048 (2011).
108. A. T. Stamps, C. E. Holland, R. E. White and E. P. Gatzke, *J Power Sources*, **150**, 229 (2005).
109. Q. Zhang and R. E. White, *J Power Sources*, **179**, 793 (2008).
110. J. Christensen, V. Srinivasan and J. Newman, *J Electrochem Soc*, **153**, A560 (2006).
111. M. Doyle, *Design and Simulation of Lithium Rechargeable Batteries*, Ph. D. Dissertation, University of California, Berkeley, CA, (1995).
112. V. Srinivasan and J. Newman, *J Electrochem Soc*, **151**, A1530 (2004).
113. S. Stewart, P. Albertus, V. Srinivasan, I. Plitz, N. Pereira, G. Amatucci and J. Newman, *J Electrochem Soc*, **155**, A253 (2008).
114. S. Santhanagopalan, Q. Z. Guo and R. E. White, *J Electrochem Soc*, **154**, A198 (2007).
115. S. Golmon, K. Maute and M. L. Dunn, *Meet Abstr - Electrochem Soc*, **1101**, 513 (2011).
116. W. Du, A. Gupta, X. Zhang, A. M. Sastry and W. Shyy, *Meet Abstr - Electrochem Soc*, **1101**, 1623 (2011).
117. J. V. Beck and K. J. Arnold, *Parameter Estimation in Engineering and Science*, Wiley, New York (1977).
118. Å. Björck, *Numerical Methods for Least Squares Problems*, SIAM Press, Philadelphia, PA (1996).
119. R. Gunawan, M. Y. L. Jung, E. G. Seebauer and R. D. Braatz, *AIChE J*, **49**, 2114 (2003).
120. M. W. Hermanto, N. C. Kee, R. B. H. Tan, M. S. Chiu and R. D. Braatz, *AIChE J*, **54**, 3248 (2008).
121. D. Marquardt, *SIAM J App Math*, **11**, 431 (1963).
122. Any maximization can be written as a minimization by multiplication of the objective by minus one.
123. L. T. Biegler, *Comput Chem Eng*, **8**, 243 (1984).
124. M. D. Canon, C. D. Cullum, Jr. and E. Polak, *Theory of Optimal Control and Mathematical Programming*, McGraw-Hill, New York (1970).
125. S. Strand, *Dynamic Optimization in State-space Predictive Control Schemes*, University of Trondheim, Norwegian Institute of Technology, (1991).
126. H. Blanke, O. Bohlen, S. Buller, R. W. De Doncker, B. Fricke, A. Harnmouche, D. Linzen, M. Thele and D. U. Sauer, *J Power Sources*, **144**, 418 (2005).
127. F. Huet, *J Power Sources*, **70**, 59 (1998).
128. A. Hammouche, E. Karden and R. W. De Doncker, *J Power Sources*, **127**, 105 (2004).
129. P. Mauracher and E. Karden, *J Power Sources*, **67**, 69 (1997).
130. A. J. Salkind, C. Fennie, P. Singh, T. Atwater and D. E. Reisner, *J Power Sources*, **80**, 293 (1999).
131. M. W. Verbrugge and R. S. Conell, *J Electrochem Soc*, **149**, A45 (2002).
132. K. S. Jeong, W. Y. Lee and C. S. Kim, *J Power Sources*, **145**, 319 (2005).

133. P. Singh, C. Fennie and D. Reisner, *J Power Sources*, **136**, 322 (2004).
134. T. Hansen and C. J. Wang, *J Power Sources*, **141**, 351 (2005).
135. V. Mancier, A. Metrot and P. Willmann, *J Power Sources*, **117**, 223 (2003).
136. J. D. Weiss, Optical state-of-charge monitor for batteries, US Patent No. 5,949,219 (1999).
137. S. Santhanagopalan and R. E. White, *J Power Sources*, **161**, 1346 (2006).
138. D. Di Domenico, G. Fiengo and A. Stefanopoulou, in *Proceedings of the IEEE International Conference on Control Applications*, p. 702 (2008).
139. Nuclear Energy Agency website, [http://www.nea.fr/abs/html/uscd1224.html, last accessed November, 2011]
140. K. E. Brenan, S. L. V. Campbell and L. R. Petzold, *Numerical Solution of Initial-Value Problems in Differential-Algebraic Equations*, SIAM Press, Philadelphia, PA (1996).
141. P. Deuflhard, E. Hairer and J. Zugck, *Numer Math*, **51**, 501 (1987).
142. E. Hairer and G. Wanner, *Solving Ordinary Differential Equations II Stiff and Differential-Algebraic Problems*, Springer, Berlin; Heidelberg; New York (1996).
143. S. Santhanagopalan, Q. Zhang, K. Kumaresan and R. E. White, *J Electrochem Soc*, **155**, A345 (2008).
144. R. G. Jungst, G. Nagasubramanian, H. L. Case, B. Y. Liaw, A. Urbina, T. L. Paez and D. H. Doughty, *J Power Sources*, **119**, 870 (2003).
145. J. Wang, P. Liu, J. Hicks-Garner, E. Sherman, S. Soukiazian, M. Verbrugge, H. Tataria, J. Musser and P. Finamore, *J Power Sources*, **196**, 3942 (2011).
146. K. Smith, G.-H. Kim and A. Pesaran, Modeling of Nonuniform Degradation in Large-Format Li-ion Batteries, in *Advanced Automotive Battery and EC Capacitor Conference*, Long Beach, CA (2009).
147. R. D. Braatz, R. C. Alkire, E. Seebauer, E. Rusli, R. Gunawan, T. O. Drews, X. Li and Y. He, *J Process Contr*, **16**, 193 (2006).
148. R. D. Braatz, R. C. Alkire, E. G. Seebauer, T. O. Drews, E. Rusli, M. Karulkar, F. Xue, Y. Qin, M. Y. L. Jung and R. Gunawan, *Comput Chem Eng*, **30**, 1643 (2006).
149. T. O. Drews, R. D. Braatz and R. C. Alkire, *J Electrochem Soc*, **150**, C807 (2003).
150. T. O. Drews, R. D. Braatz and R. C. Alkire, *Int. J. Multiscale Comput. Eng*, **2**, 313 (2004).
151. T. O. Drews, S. Krishnan, J. C. Alameda, D. Gannon, R. D. Braatz and R. C. Alkire, *Ibm Journal of Research and Development*, **49**, 49 (2005).
152. X. H. Li, T. O. Drews, E. Rusli, F. Xue, Y. He, R. Braatz and R. Alkire, *J Electrochem Soc*, **154**, D230 (2007).
153. X. H. Li, T. O. Drews, E. Rusli, F. Xue, Y. He, R. Braatz and R. Alkire, *J Electrochem Soc*, **154**, S15 (2007).
154. Y. Qin, X. H. Li, F. Xue, P. M. Vereecken, P. Andricacos, H. Deligianni, R. D. Braatz and R. C. Alkire, *J Electrochem Soc*, **155**, D223 (2008).
155. E. Rusli, T. O. Drews, D. L. Ma, R. C. Alkire and R. D. Braatz, *J Process Contr*, **16**, 409 (2006).
156. E. Rusli, F. Xue, T. O. Drews, P. M. Vereecken, P. Andricacos, H. Deligianni, R. D. Braatz and R. C. Alkire, *J Electrochem Soc*, **154**, D584 (2007).
157. V. Balakotaiah and S. Chakraborty, *Chem Eng Sci*, **58**, 4769 (2003).
158. V. Balakotaiah and H. C. Chang, *SIAM J App Math*, **63**, 1231 (2003).
159. M. Golubitsky, D. G. Schaeffer and I. Stewart, *Singularities and Groups in Bifurcation Theory*, Springer Verlag, Berlin, Germany (1988).
160. F. A. Howes and S. Whitaker, *Chem Eng Sci*, **40**, 1387 (1985).

161. V. Ramadesigan, V. Boovaragavan, J. C. Pirkle and V. R. Subramanian, *J Electrochem Soc*, **157**, A854 (2010).
162. S. Liu, *Solid State Ionics*, **177**, 53 (2006).
163. K. Smith and C. Y. Wang, *J Power Sources*, **161**, 628 (2006).
164. Q. Zhang and R. E. White, *J Power Sources*, **165**, 880 (2007).
165. B. Wu and R. E. White, *Comput Chem Eng*, **25**, 301 (2001).
166. R. N. Methekar, V. Ramadesigan, J. C. Pirkle Jr and V. R. Subramanian, *Comput Chem Eng*, **35**, 2227 (2011).
167. L. Cai and R. E. White, *Meet Abstr - Electrochem Soc*, **1002**, 1126 (2010).
168. S. I. Lee, Y. S. Kim and H. S. Chun, *Electrochim Acta*, **47**, 1055 (2002).
169. B. Chachuat, A. B. Singer and P. I. Barton, *Ind Eng Chem Res*, **45**, 8373 (2006).
170. D. L. Ma and R. D. Braatz, *IEEE T Contr Syst T*, **9**, 766 (2001).
171. Z. K. Nagy and R. D. Braatz, *J Process Contr*, **17**, 229 (2007).
172. Z. K. Nagy and R. D. Braatz, *IEEE T Contr Syst T*, **11**, 694 (2003).
173. G. L. Plett, *J Power Sources*, **134**, 252 (2004).
174. G. L. Plett, *J Power Sources*, **161**, 1356 (2006).
175. M. Verbrugge and B. Koch, *J Electrochem Soc*, **153**, A187 (2006).
176. M. Verbrugge and E. Tate, *J Power Sources*, **126**, 236 (2004).
177. J. Dahn, *219th ECS Meeting* (2011).
178. S. J. Harris, A. Timmons, D. R. Baker and C. Monroe, *Chem Phys Lett*, **485**, 265 (2010).
179. Y. Luo, W. B. Cai and D. A. Scherson, *J Electrochem Soc*, **149**, A1100 (2002).

1.6. Figures

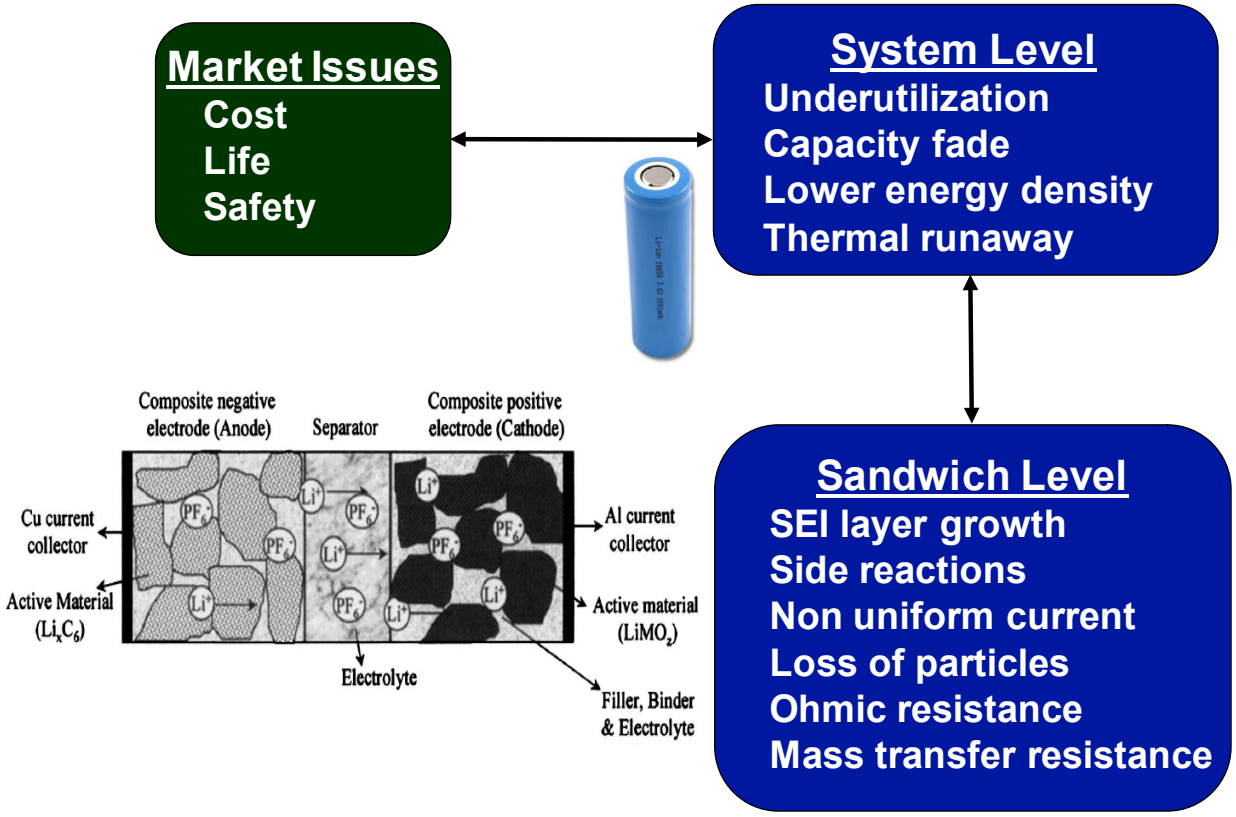

Figure 1-1: Current issues with Li-ion batteries at the market level and the related performance failures observed at the system level, which are affected by multiple physical and chemical phenomena at the sandwich level.

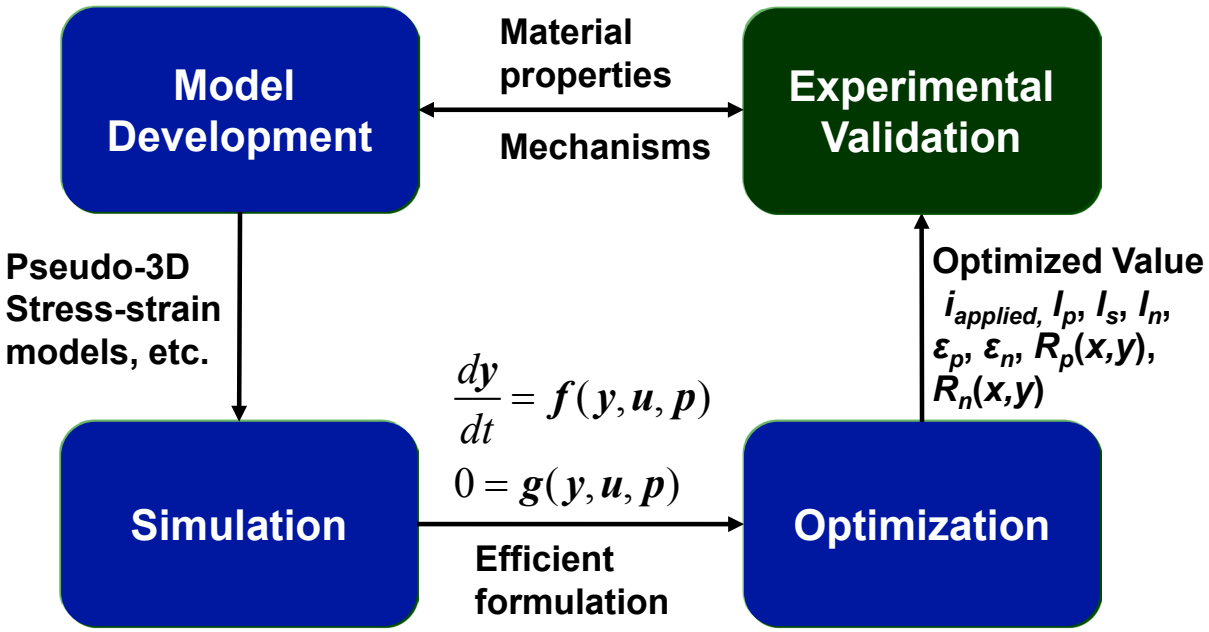

Figure 1-2: Schematic of systems engineering tasks and the interplay between them: In the figure, u, y, and p are vectors of algebraic variables, differential variables, and design parameters, respectively.

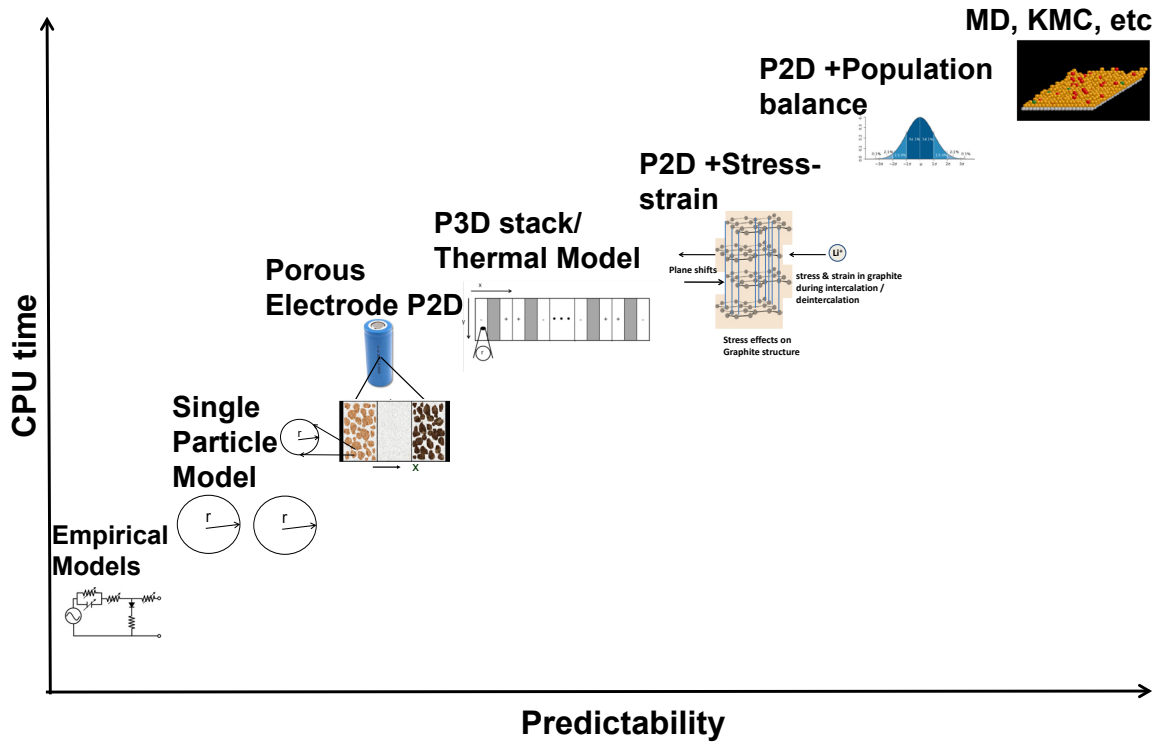

Figure 1-3: Wide range of physical phenomena dictates different computational demands (images taken from various sources on the internet and literature).

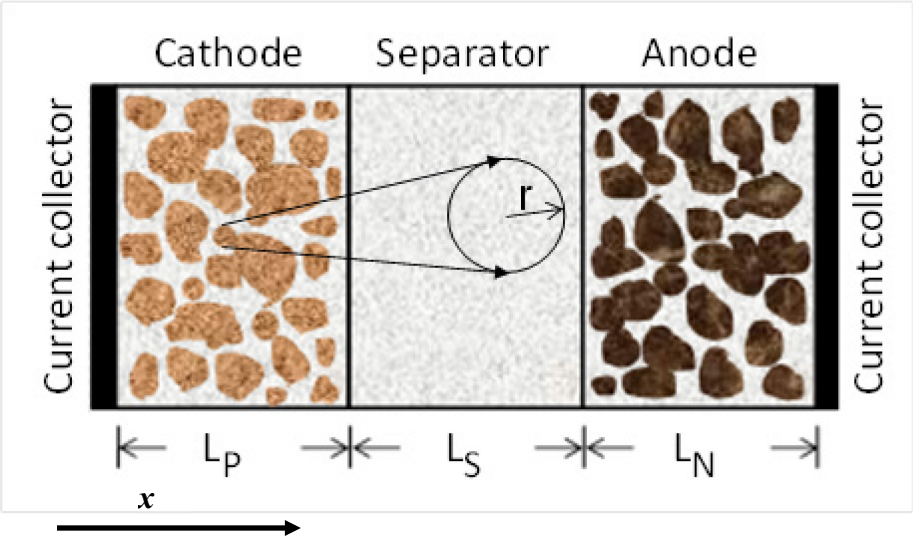

Figure 1-4: P2D model with schematic of the sandwich with the cathode, anode, and separator also showing the spherical particles in the pseudo-second dimension.

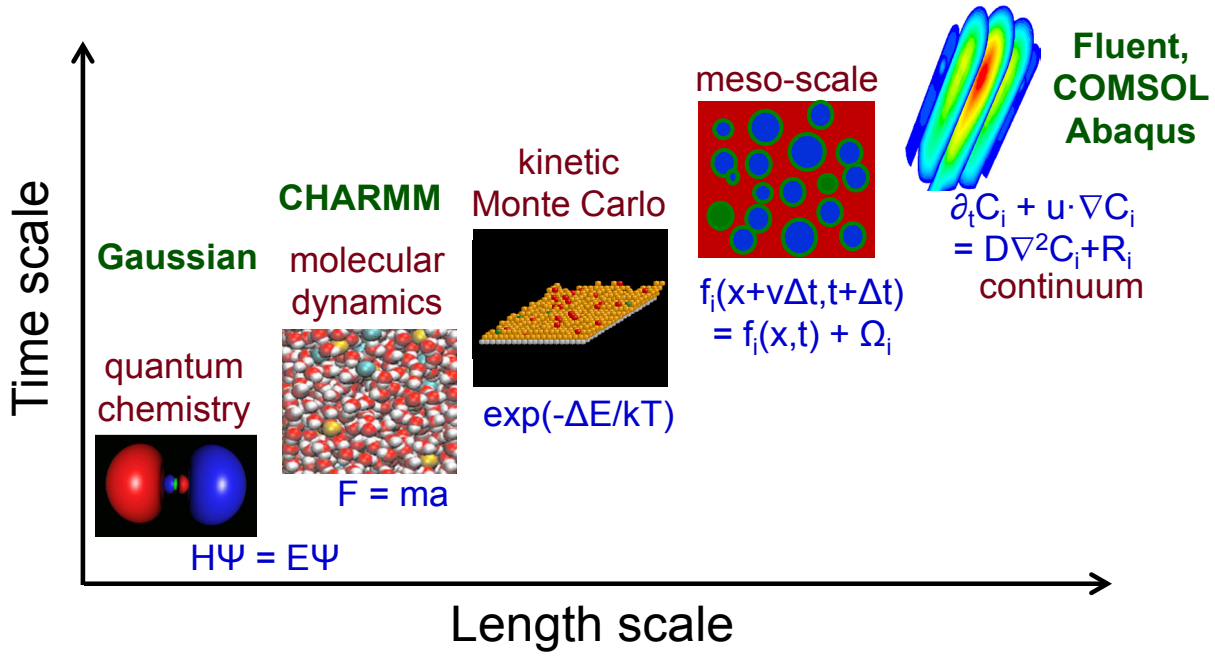

Figure 1-5: Approximate ranking of methods appropriate for the simulation of different time and length scales.

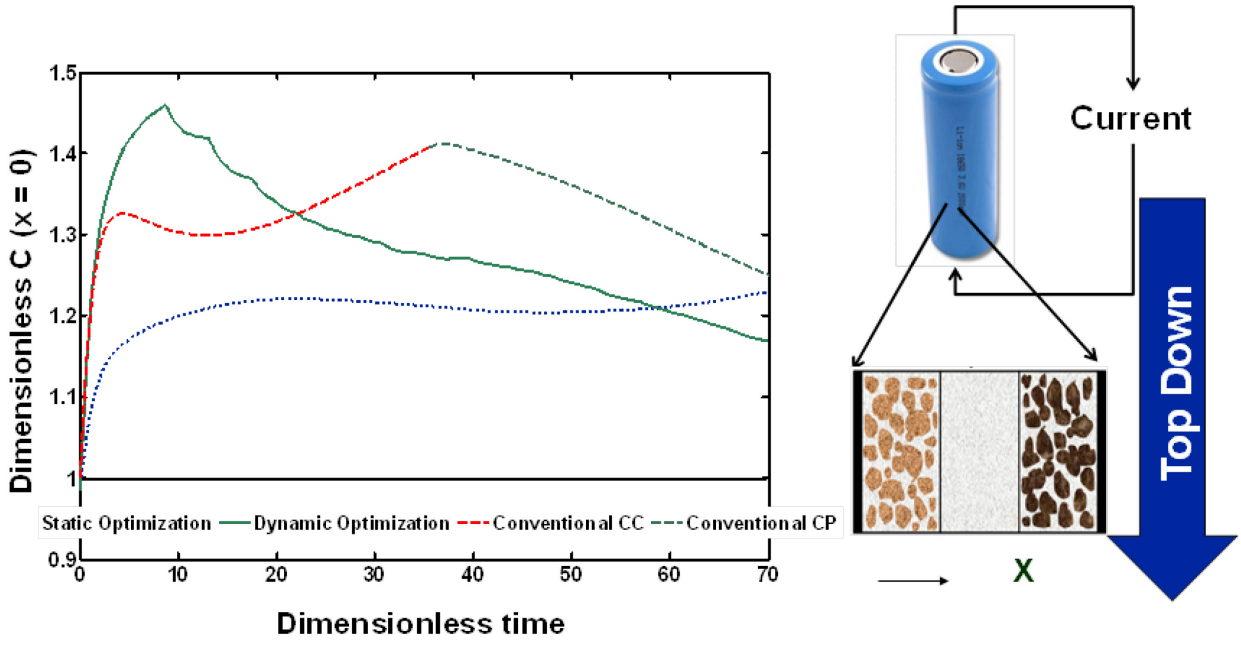

Figure 1-6: Dynamic analysis of electrolyte concentration at the positive electrode for the three charging protocols. The solid line at C = 1 represents the equilibrium concentration.

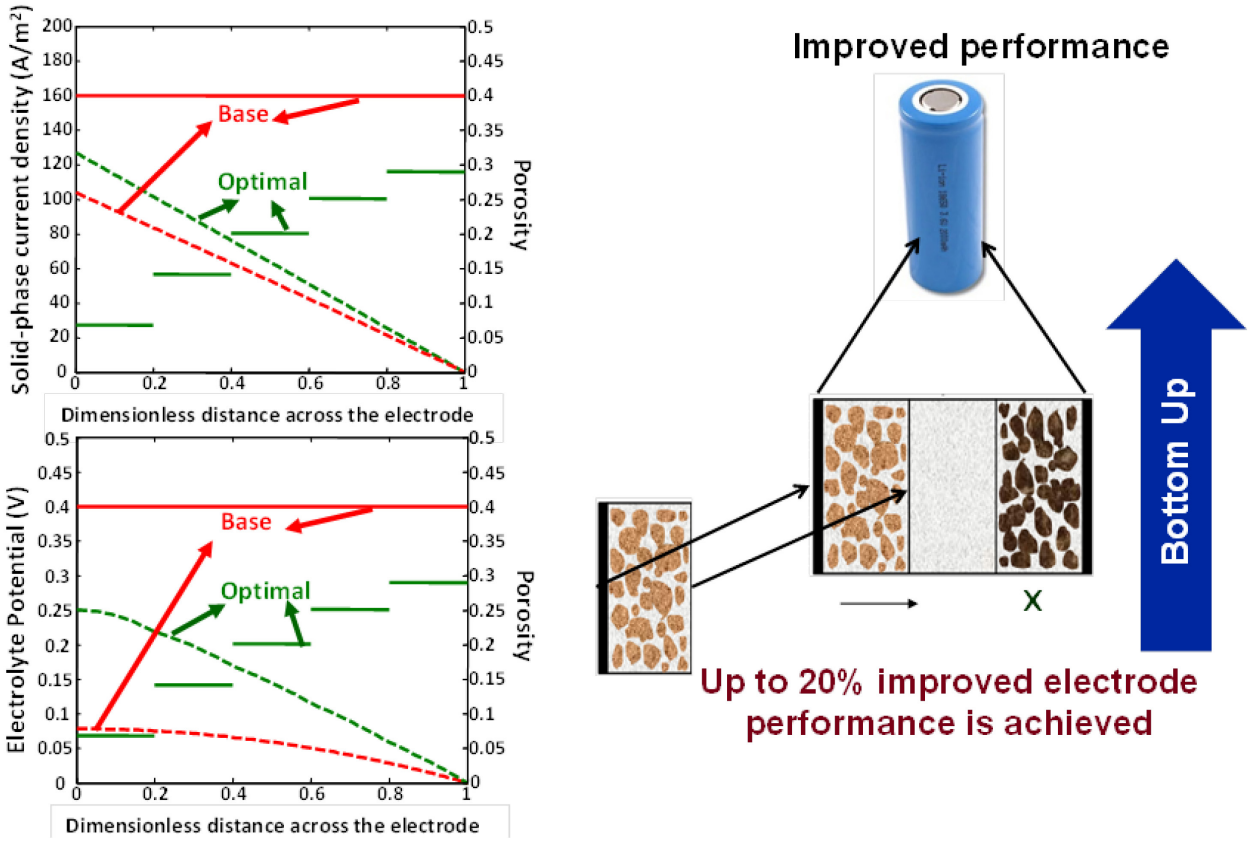

Figure 1-7: Model-based optimal battery design based on a porous electrode model. Solid lines are for porosity, and dashed lines represent solid-phase current density (A/m2)/ Electrolyte potential (V).

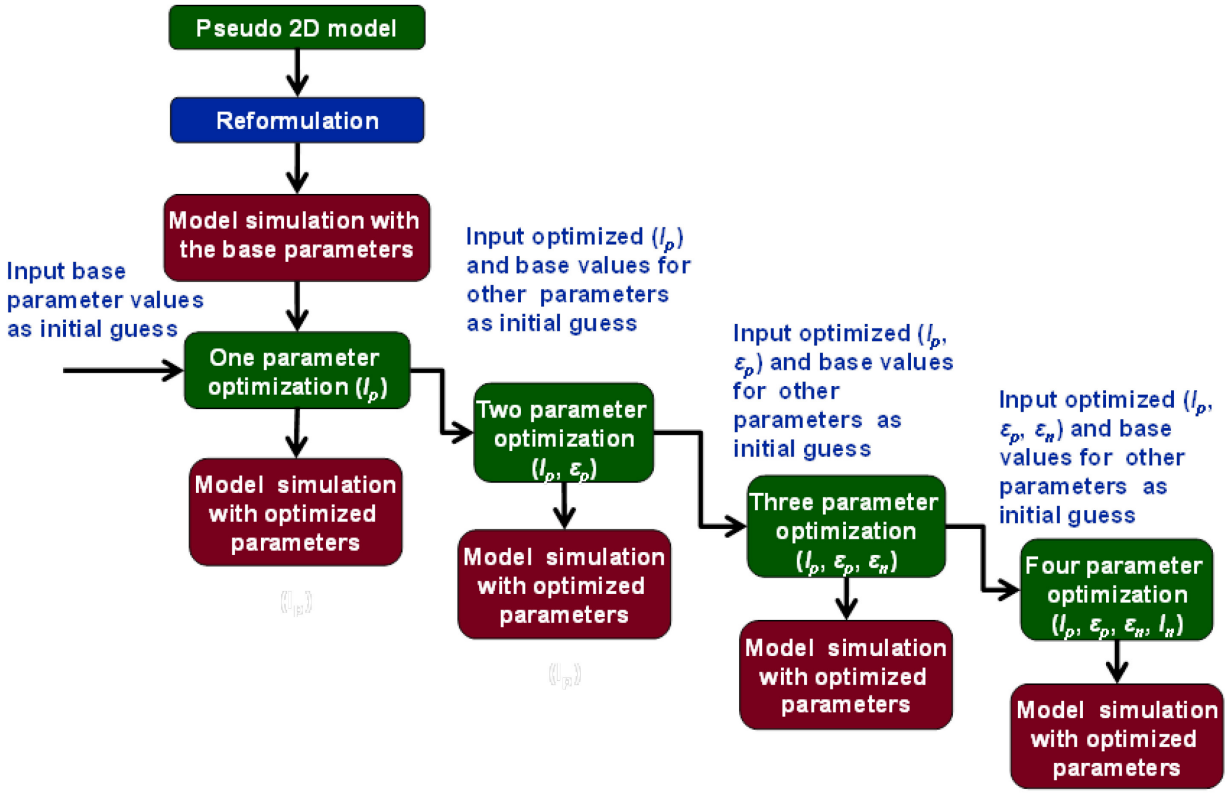

Figure 1-8: Sequential approach for robust optimization of battery models with multiple design parameters

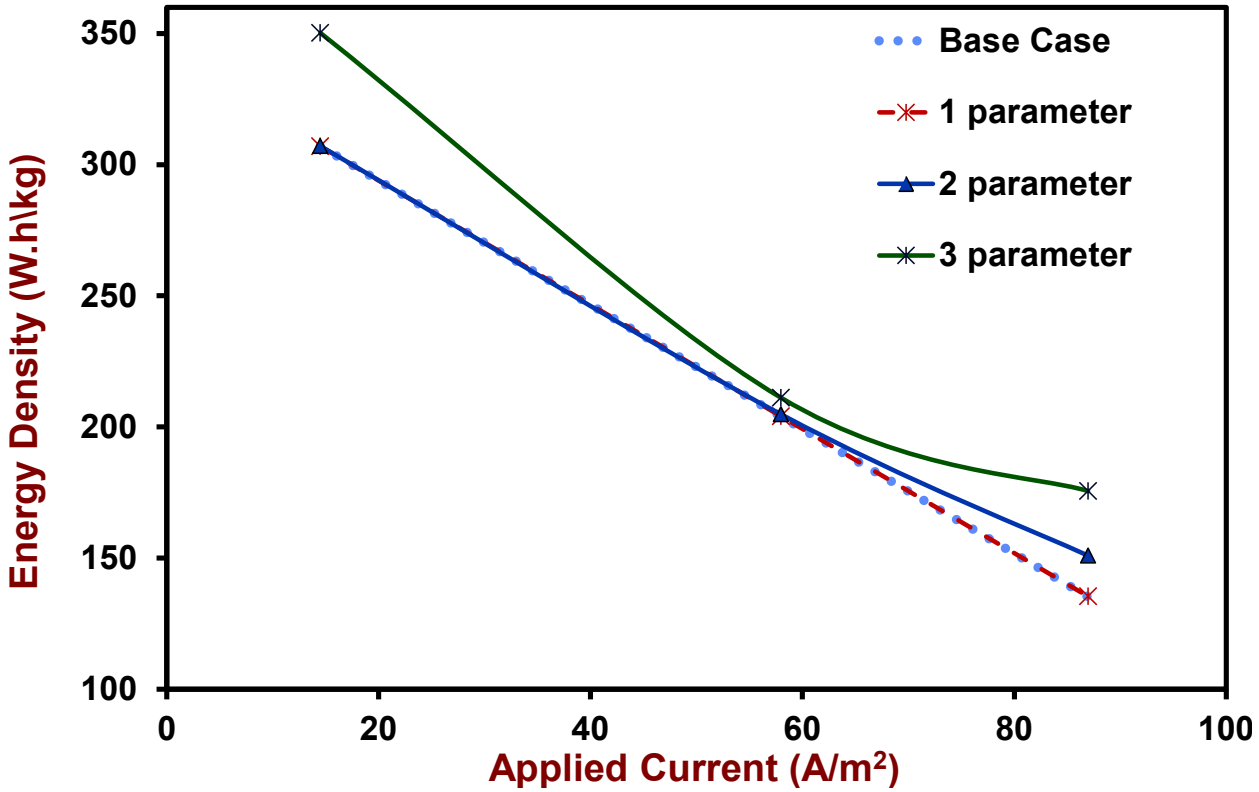

Figure 1-9: Optimization of the energy density for a lithium-ion battery, showing the effect of electrode thickness and porosities

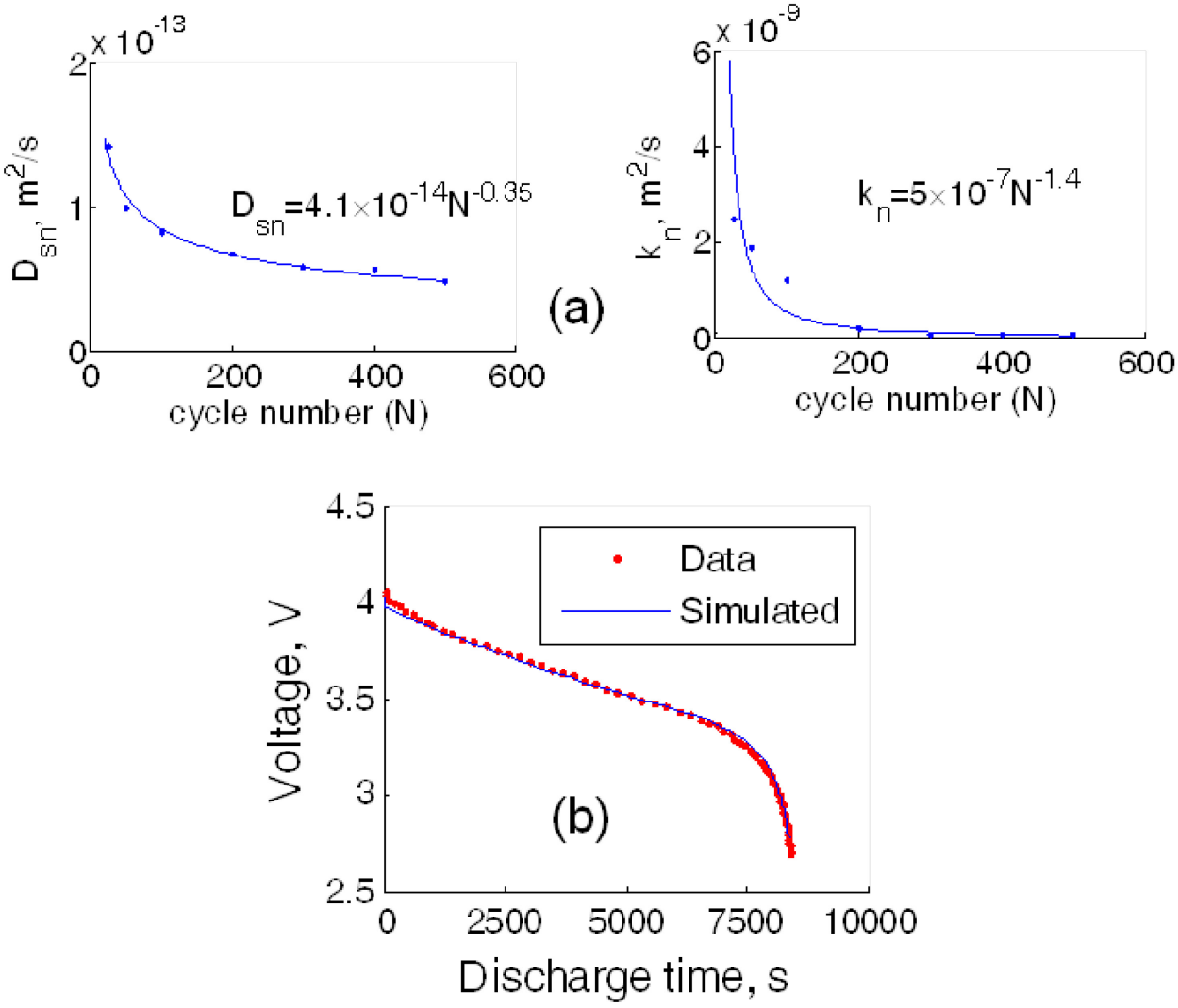

Figure 1-10: Parameter estimation, uncertainty analysis, and capacity fade prediction for a lithium-ion battery

Chapter 2 : Efficient Reformulation of Solid-Phase Diffusion in Physics-Based Lithium-ion Battery Models

This chapter is reproduced with permission from *J. Electrochem. Soc.*, **157** (7), A854 (2010). The author is grateful to the co-authors for their significant contributions under sections 2.3 and 2.5.

2.1. Introduction

Electrochemical power sources are expected to play a vital role in the future in automobiles, power storage, military, mobile, and space applications. Lithium-ion chemistry has been identified as a good candidate for high-power/high-energy secondary batteries. Significant progress has been made towards modeling and understanding of Lithium-ion batteries using physics based first principles models. First-principles based battery models typically solve electrolyte concentration, electrolyte potential, solid-state potential and solid-state concentration in the porous electrodes [1, 2] and electrolyte concentration and electrolyte potential in the separator. These models are based on transport phenomena, electrochemistry and thermodynamics. These models are represented by coupled nonlinear PDEs in 1-2 dimensions and are typically solved numerically and require few minutes to hours to simulate.

Even when one-dimensional transport in the macro-scale (x) is considered, the continuum models that are used to describe the electrochemical behavior of lithium-ion batteries, involve three coupled non-linear PDEs (in x, t) in the porous electrode and two coupled non-linear partial differential equations (PDEs) (in x, t) in the separator. For predicting the thermal behavior, one has to add an additional equation for temperature. In addition, solid-state diffusion should be solved in the pseudo-second-dimension (r) in the electrode. Li-ions diffuse (intercalate) in to

and out of the solid particles of porous electrodes in the pseudo-second-dimension. Hence, in addition to the equations in the *x*-direction, solid-state diffusion should be solved in the pseudo-dimension (*r*) in the porous electrodes. This diffusion in the micro-scale is typically modeled using Fick's law of diffusion. One of the major difficulties in the electrochemical engineering models is the inclusion of solid phase diffusion in a second dimension *r* which increases the complexity of the model as well as the computational time/cost to a great extent. Traditional simulation approaches toward solid phase diffusion leads to more difficulties, with the use of emerging cathode materials, which involve phase changes and thus moving boundaries. Concentration variations in the solid-phase is governed by Fick's law of diffusion and the same in spherical coordinates is given as

$$\frac{\partial c_s}{\partial t} = \frac{1}{r^2}\frac{\partial}{\partial r}\left(r^2 D_s \frac{\partial c_s}{\partial r} \right) \qquad [2.1]$$

$$at \;\; t = 0 \; for \; 0 \le r \le R_s \;\; c_s = c_{s0} \qquad [2.2]$$

$$\left.\frac{\partial c_s}{\partial r}\right|_{r=0} = 0 \qquad [2.3]$$

$$j(t) = -D_s \left.\frac{\partial c_s}{\partial r}\right|_{r=R_s} \qquad [2.4]$$

where $D_s = D_0 f(c)$. Equation[2.1] can be converted to dimensionless form using the following dimensionless variables and parameters:

$$\tau = \frac{D_0\, t}{R_s^{\,2}} \quad x = \frac{r}{R_s} \quad C = \frac{c_s}{c_0} \quad \delta(\tau) = \frac{j(t) R_s}{D_0 c_0} \qquad [2.5]$$

$$\frac{\partial C}{\partial \tau} = \frac{1}{x^2}\frac{\partial}{\partial x}\left(x^2 f(C) \frac{\partial C}{\partial x} \right) \qquad [2.6]$$

with the boundary conditions

$$at\ \tau\ =\ 0\ for\ 0\ \leq\ x\ \leq\ 1 \qquad C\ =\ 1 \tag{2.7}$$

$$\text{for } \tau > 0,\ \text{x} = 0\ \ \frac{\partial C}{\partial \text{x}} = 0 \tag{2.8}$$

$$\text{for}\ \ \tau > 0,\ \text{x} = 1\ \ f(C)\frac{\partial C}{\partial \text{x}}\ \ =\ -\ \delta(\tau) \tag{2.9}$$

This chapter presents two computationally efficient representations for the solid-phase diffusion. An efficient Eigen function based Galerkin Collocation method is introduced and discussed in this chapter. Further, a mixed order finite difference method with optimal node spacing is introduced that can be used to reduce the computational cost/time significantly even with varying diffusivities in the solid phase. The operating condition has a significant effect on the validity, accuracy and efficiency of various approximations for the solid-phase diffusion. It has been found that the discretization and solver scheme used in time is also a significant factor in deciding the best possible approximation for the solid-phase. This chapter also compares various methods[1-6] for approximating/representing solid-phase concentration variations within the active materials of porous electrodes for a full-order pseudo-2D model for lithium-ion batteries. A comparison among these available methods along with a brief mention about their merits and usability is made to identify the best possible method and incorporate in a full-order pseudo-2D model.[1]

2.2. Existing Approximations and the Need for Efficient Reformulation

Porous electrode models of Li-ion batteries often use approximations to eliminate the time consuming calculation in the second dimension *r* for the solid phase diffusion. These methods include the Duhamel's superposition method,[1] diffusion length method,[3] the polynomial approximation method,[4] the pseudo steady state (PSS) approach by Liu[5] and the penetration depth analysis and mixed order finite element approach.[6]

Each of the above listed methods has its own advantages and disadvantages when used in Li-ion battery models. The following section gives a brief summary about each of the methods and discusses their merits and usability.

2.2.1. Duhamel's Superposition method

The Duhamel's superposition method[1] is a robust method available for representing the solid phase diffusion for constant diffusivities. This method relates the solution of a boundary value problem with time dependent boundary conditions to the solution of a similar problem with time-independent boundary conditions by means of a simple relation. More information about the method and equations are presented elsewhere.[1, 2]

Duhamel's superposition method is a robust method and is valid for any kind of operating condition, like high rates of discharge, pulse power, etc. One of the major drawbacks of this method is that, it cannot be used in DASSL like solvers which do not accept equations discretized in time and might as well be time consuming for very stiff problems depending on the time steps taken. In addition, it cannot be used for nonlinear diffusivities.

2.2.2. Diffusion Length Method

The diffusion length method's approach[3] is based on a parabolic profile approximation for the solid phase. The diffusion length method predicts that the surface concentration and volume averaged concentration inside a particle are linearly dependent on each other, which should be valid only after the diffusion layer builds up to its steady state. Therefore, the method is inadequate at short times or under dynamic operations, such as pulse or current interrupt operations. The prediction based on the diffusion length method is inadequate at short times and very efficient at long times and low rates.

2.2.3. Polynomial Approximation

The polynomial approximation method by Subramanian et al.[4] is based on parabolic profile approximation and volume averaging of the solid phase diffusion equation. This high order polynomial method uses a different approach from the diffusion length method to improve the solution accuracy at short times. The diffusion length method uses the empirical exponential term in the equation and determines the multiplier value by matching surface concentration profiles to the exact solutions. The high order polynomial method uses a higher order polynomial for the concentration profile in the derivation, and one could derive new sets of equations with an even higher order polynomial model, if needed, following the same procedures discussed in the papers.[4, 7]

This method is very efficient at long time ranges, and for low/ medium rates, and is ideal for adaptive solvers for pseudo-2D models. However, it is inaccurate at short times and for high rates/pulses and hence would not be a suitable method for implementing in models for HEVs and other high rate applications.

2.2.4. Pseudo Steady State Method

The Pseudo Steady State (PSS) approach by Liu[5] is very robust and by having enough number of equations, this approach can cover the entire spectrum of high/low rates, pulses, *etc.* This is a form of a finite integral transform technique to eliminate the independent spatial variable r from the solid phase diffusion equation. For diffusion problems with a time dependent pore wall flux j_n appears in the boundary condition and in the calculation of coefficients.

However, this method involves terms/coefficients which blow up when the number of terms increases adding numerical difficulties for simulation. More details are given in the Results and

Discussion section when this method is compared with our proposed approach implemented in this work.

2.2.5. Penetration Depth Method

The penetration depth analysis approach was used earlier with empirically fits to numerical solution for penetration depth near the surface of the particle. The advantage of this method is that it is very accurate at short times/pulses and more accurate and efficient Penetration depth solutions can be directly obtained from the partial differential equation as discussed elsewhere.[6]

The drawback with this approach being the need to be reinitialized every time, and does not give a good match for varying δ . Though this method is very accurate and efficient at short times, it is not ideal for adaptive solvers in a pseudo-2D model (increases stiffness).

2.2.6. Finite Element Method

While the governing equation[1] describes solid phase concentration along the radius of each spherical particle of active material, the macroscopic model requires only the concentration at the surface, *cs (x, t)*, as a function of the time history of local reaction current density, *j(t)*. The PDE, is transformed from spherical to planar coordinates using and discretized in the *r*-direction with *N* suitably chosen linear elements. (They used five elements with node points placed at {0.7, 0.91, 0.97, 0.99, 1.0} × *Rs*.) Transformed back to spherical coordinates, the discretized system is represented as ODEs in state space form and then solved.[6]

The finite element node sizes were probably obtained using trial and error and perhaps may not be optimal at long times or different operating conditions. The following section describes two new methods that can be used for solid phase diffusion approximation and explains the derivation of the same.

2.3. Galerkin Reformulation of Solid Phase Diffusion

The reformulation discussed here is based on Eigen function based Galerkin collocation for constant diffusivity. In case of constant diffusivity *f(C)* in equations [2.6]and [2.9] will be 1. The following section describes the derivation for the eigenfunction based Galerkin collocation and the equations for approximation are given at the end. Expanding equation [2.6] can be written as

$$\frac{\partial}{\partial \tau} c(x,\tau) = \frac{2x\frac{\partial}{\partial x} c(x,\tau) + x^2 \frac{\partial^2}{\partial x^2} c(x,\tau)}{x^2} \qquad [2.10]$$

A general solution for the variable *c(x, τ)* can be written as a polynomial approximation given as

$$a(\tau) + b(\tau)x^2 + \sum_{n=1}^{\infty} \frac{d_n(\tau)\sin(\lambda_n x)}{x} \qquad [2.11]$$

where λ_n, *n=1…m* are the eigenvalues of the given problem (equation [2.22]). To get the value of *c(x, τ)* we need to evaluate the time dependent coefficients in the solution *a(τ)*, *b(τ)* and $d_n(\tau)$. This trial function is assumed to be the solution for *c(x, τ)* as the functions $\frac{\sin(\lambda_n x)}{x}$ are the eigen functions satisfying the given problem as given elsewhere.[5] In general, a polynomial form is assumed.[7] However, having the solution for constant boundary conditions as the trial function helps in simplifying the integrals. The choice is up to the researchers; however eigen functions for problems with constant boundary conditions and linear models are a good basis for nonlinear and time-varying boundary conditions. This idea follows from the Duhamel's superposition method[1] wherein models with time-varying boundary conditions are obtained from constant boundary condition models using the convolution theorem.

The coefficients are obtained by solving the final equation using the boundary conditions given above and solving for $c_{ave}(\tau)$. We introduce the average concentration as

$$c_{ave}(\tau) = \int_0^1 3c(x,\tau)x^2 dx \qquad [2.12]$$

The coefficients $a(\tau)$ and $b(\tau)$ are obtained in terms of $c_{ave}(\tau)$ and simplifying the expressions substituting $\sin(\lambda_n) = \lambda_n \cos(\lambda_n)$ we have

$$\begin{aligned} a(\tau) &= c_{ave}(\tau) + \frac{3\delta(\tau)}{10} \\ b(\tau) &= -\frac{1}{2}\delta(\tau) \end{aligned} \qquad [2.13]$$

Substitution in $c(x, \tau)$ yields

$$c_{ave}(\tau) + \frac{3\delta(\tau)}{10} - \frac{1}{2}\delta(\tau)x^2 + \sum_{n=1}^{\infty} \frac{d_n(\tau)\sin(\lambda_n x)}{x} \qquad [2.14]$$

Substitution of $c(x, \tau)$ in our original equation [2.6] yields

$$\begin{aligned} &\left(\frac{d}{d\tau}c_{ave}(\tau)\right) + \frac{3}{10}\frac{d}{d\tau}\delta(\tau) - \frac{1}{2}\left(\frac{d}{d\tau}\delta(\tau)\right)x^2 + \sum_{n=1}^{\infty}\frac{\left(\frac{d}{d\tau}d_n(\tau)\right)\sin(\lambda_n x)}{x} \\ &- \frac{\left(\begin{array}{l} 2x\left(-\delta(\tau)x + \sum_{n=1}^{\infty}\frac{d_n(\tau)\cos(\lambda_n x)\lambda_n}{x} - \sum_{n=1}^{\infty}\frac{d_n(\tau)\sin(\lambda_n x)}{x^2}\right) \\ +x^2\left(\begin{array}{l} -\delta(\tau) - \sum_{n=1}^{\infty}\frac{d_n(\tau)\sin(\lambda_n x)\lambda_n{}^2}{x} - 2\sum_{n=1}^{\infty}\frac{d_n(\tau)\cos(\lambda_n x)\lambda_n}{x^2} \\ +2\sum_{n=1}^{\infty}\frac{d_n(\tau)\sin(\lambda_n x)}{x^3} \end{array}\right) \end{array}\right)}{x^2} \end{aligned} \qquad [2.15]$$

Calculating $c_{ave}(\tau)$ from the above equation multiplying with differential volume $3x^2$, also multiplying by $\frac{\sin(\lambda_n x)}{x}$ and integrating to find $c_{ave}(\tau)$, after simplification we have

$$\frac{3}{2}\frac{d}{d\tau}d_n(\tau)-3\frac{\left(\frac{d}{d\tau}\delta(\tau)\right)\cos(\lambda_n)}{\lambda_n}+\frac{3}{2}\lambda_n{}^2 d_n(\tau)$$
$$-\frac{3}{2}\left(\frac{d}{d\tau}d_n(\tau)\right)\left(\cos(\lambda_n)\right)^2-\frac{3}{2}\lambda_n{}^2 d_n(\tau)\left(\cos(\lambda_n)\right)^2 \quad [2.16]$$

To solve the above equation efficiently, we introduce a variable Q_n such that

$$d_n(\tau)=\frac{d}{dt}Q_n(\tau) \quad [2.17]$$

Substituting the above relation, and integrating the above equation we have

$$\frac{3}{2}\frac{d}{d\tau}Q_n(\tau)-3\frac{\delta(\tau)\cos(\lambda_n)}{\lambda_n}+\frac{3}{2}\lambda_n{}^2 Q_n(\tau)-$$
$$\frac{3}{2}\left(\cos(\lambda_n)\right)^2\frac{d}{d\tau}Q_n(\tau)-\frac{3}{2}\lambda_n{}^2\left(\cos(\lambda_n)\right)^2 Q_n(\tau)+k_n \quad [2.18]$$

where k_n is a constant for integration.

Grouping like terms we may write equation [2.18] as

$$\frac{3}{2}\frac{d}{d\tau}Q_n(\tau)\left(1-\cos^2(\lambda_n)\right)-3\frac{\delta(\tau)\cos(\lambda_n)}{\lambda_n}$$
$$+\frac{3}{2}\lambda_n{}^2 Q_n(\tau)\left(1-\cos^2(\lambda_n)\right)+k_n \quad [2.19]$$

Simplifying and substituting $\lambda_n=\tan(\lambda_n)$, the above equation can be written as

$$\frac{dQ_n}{d\tau}+\lambda_n{}^2 Q_n=2\frac{\delta(\tau)}{\lambda_n{}^2\sin(\lambda_n)}+\lambda_n{}^2 k_n' \quad [2.20]$$

The above equation can be written as

$$\frac{dQ_n}{d\tau}+\lambda_n{}^2\left(Q_n-k_n'\right)=2\frac{\delta(\tau)}{\lambda_n{}^2\sin(\lambda_n)} \quad [2.21]$$

Substituting $Q_n'=Q_n-k_n'$ doesn't alter the value of *d(τ)* as $\frac{dQ_n}{d\tau}$ remains unchanged. Hence, the final set of equations is not affected by the value of integration constant k_n'.

The final set of equations can be written as:

$$\frac{d\overline{C}}{d\tau} = -3\delta(\tau) \qquad [2.22]$$

$$C_s = \overline{C} - \frac{\delta(\tau)}{5} + 2\delta(\tau)\sum_{n=1}^{m}\frac{1}{\lambda_n^{\,2}} - \sum_{n=1}^{m} Q_n \lambda_n^{\,2}\sin(\lambda_n) \qquad [2.23]$$

$$\frac{dQ_n}{d\tau} + \lambda_n^{\,2} Q_n = 2\frac{\delta(\tau)}{\lambda_n^{\,2}\sin(\lambda_n)} \qquad [2.24]$$

$$\lambda_n = \tan(\lambda_n) \qquad [2.25]$$

An important advantage of this approach is, this reformulation is very robust and by having enough number of *Q's,* in other words, enough number of equations[2.24], this approach can cover the entire spectrum of high/low rates, pulses, *etc.* like the PSS method by Liu. However, in Liu's PSS approach the *q's* vary as $q_1<q_2<q_3<q_4$ and the order of q_4 is as high as 10^{40} causing stiffness and numerical instability in the pseudo-2D models using this approach. The *q's* mentioned here are the *q's* in final set of equations obtained from the PSS method[5] as mentioned in equations 9(a) to 9(c) elsewhere.[2] The present reformulation overcomes this problem. In this method the *Q's* vary as $Q_1>Q_2>Q_3>Q_4$, in other words we have a converging series in Q_n which makes this approach equivalent to PSS model in accuracy, but highly efficient in pseudo-2D environment for computation avoiding stiffness and computational difficulties.

2.4. Finite Difference Approach with Unequal Node Spacing

Finite difference method is one of the most widely used numerical techniques to solve ordinary or partial differential equations. Use of finite difference method has been first choice for solving first principles based lithium-ion battery models. However, for a pseudo-2D model, when dealing with a second dimension *r* for discretization, the number of equations increases by

many folds and thereby making the simulation of system slower and complex. About 20 node points in the *r* direction will increase the number of equations by a great deal and hence, based on mixed order finite element approach discussed earlier, where the size of linear elements were unequal instead of fixed equal elements, we used a mixed order finite difference approach, wherein we use less number of node points with unequal node spacing. The derivation of finite difference notations for different approximation for the derivatives is given in the following section.

Taylor series expansion at $x = x+h_{i+1}$ and $x - h_i$ are written as

$$f\left(x+h_{i+1}\right)=f\left(x\right)+\left(\frac{d}{dx}f\left(x\right)\right)h_{i+1}+\frac{1}{2}\left(\frac{d^2}{dx^2}f\left(x\right)\right){h_{i+1}}^2 \qquad [2.26]$$

$$f\left(x-h_i\right)=f\left(x\right)-\left(\frac{d}{dx}f\left(x\right)\right)h_i+\frac{1}{2}\left(\frac{d^2}{dx^2}f\left(x\right)\right)h_i^2 \qquad [2.27]$$

where h_i is the unequal node spacing between at the i^{th} node in the domain.

Truncating the series expansion with the required amount of accuracy and solving for the first and second order derivatives, we can obtain formula for the central finite difference for the first and second order derivatives. We use an order of h^2 accuracy for all our approximations.

$$\left(\frac{dc}{dx}\right)_{central}=\frac{-c_{i+1}h_i^2+c_ih_i^2+{h_{i+1}}^2c_{i-1}-{h_{i+1}}^2c_i}{h_{i+1}\left(h_i+h_{i+1}\right)h_i} \qquad [2.28]$$

$$\left(\frac{d^2c}{dx^2}\right)_{central}=2\frac{c_{i+1}h_i-c_ih_i+h_{i+1}c_{i-1}-h_{i+1}c_i}{h_{i+1}\left(h_i+h_{i+1}\right)h_i} \qquad [2.29]$$

Similarly forward and backward finite differences relations for the derivatives can be obtained, and used in for boundary conditions.

$$\left(\frac{dc}{dx}\right)_{forward}=-\frac{c_{i+2}{h_{i+1}}^2-{h_{i+1}}^2c_{i+1}-2h_{i+1}h_{i+2}c_{i+1}+2h_{i+1}h_{i+2}c_i-{h_{i+2}}^2c_{i+1}+{h_{i+2}}^2c_i}{h_{i+2}\left(h_{i+1}+h_{i+2}\right)h_{i+1}} \qquad [2.30]$$

$$\left(\frac{dc}{dx}\right)_{backward} = \frac{c_{i-2}h_i^2 - h_i^2 c_{i-1} - 2h_i h_{i-1} c_{i-1} + 2h_i h_{i-1} c_i - h_{i-1}^2 c_{i-1} + h_{i-1}^2 c_i}{h_{i-1}\left(h_i + h_{i-1}\right)h_i} \quad [2.31]$$

Figure 2-1 presents a general methodology for obtaining efficient reformulation/representation for the solid-phase equation for nonlinear diffusivities. First, a mixed-finite difference representation is written, say with N = 5 node points. For the optimization, $h_i=1/(N+1)$ is the initial guess with $0.001<h_i<0.999$ as the constraint, the error between expected full-order numerical solution and the mixed-finite difference method is minimized to a set tolerance. Typically, Jacobian based methods are sufficient for convergence.[8] For difficult nonlinearities, global optimization including genetic algorithms might be needed for convergence and robustness[9, 10] though they are likely to be very slow compared to Jacobian methods.

For the solid phase diffusivity (D_s) varying as a function of concentration, the Galerkin approach cannot be used. We used finite difference (FD) with unequal node spacing in the r direction and discretized the diffusion equation[2.6]. The mixed finite difference form of this equation with constant D_s using the above derived finite difference stencil is given as

$$\frac{d}{d\tau}C_i = 2\frac{h_i C_{i+1} - h_i C_i + h_{i+1} C_{i-1} - h_{i+1} C_i}{h_i h_{i+1}\left(h_{i+1} + h_i\right)} - 2\frac{h_{i+1}^2 C_{i-1} - h_{i+1}^2 C_i - h_i^2 C_{i+1} + h_i^2 C_i}{\sum_{j=1}^{i} h_j h_i h_{i+1}\left(h_{i+1} + h_i\right)},\ i = 1..N \quad [2.32]$$

where N is the number of interior node points. A similar expression for varying D_s can be derived.

One of the advantages of this method is that, for our case the concentration gradient is more near the surface compared to the center and hence, strategically placing more node points near the surface and less node points at the center would give results with the same accuracy with lesser total number of node points compared to a large number of equally spaced node

points. Lesser number of node points in r leads to lesser number of equations and hence faster simulation for the whole battery model. The placement of these node points are important and to find the exact position of these node points we ran an optimization algorithm to find the best h_1, h_2, h_3, *etc.* and minimize N and the CPU time. This method is very accurate for short times/high rates/pulses; and is recommended for varying diffusion coefficients. Varying diffusivities are important and is likely to get more attention because of its requirement for addressing stress effects in the Li-ion batteries.[11] Note that though this approach is robust as an optimization algorithm proposed in this work will automatically detect instead of having to guess and arrive at the node spacing by trial and error.

2.5. Coupling Solid Phase Diffusion with Full-order Pseudo-2D Battery Models

In the traditional formulation of solid phase diffusion, equations [2.1]-[2.4] are coupled to the equations of a full-order pseudo-2D model for lithium-ion batteries, which is described elsewhere.[12, 13] For comparison, two efficient methods, the eigen function based Galerkin method and the mixed finite-difference (FD) method (with 5 internal nodes) are also coupled to the full-order pseudo-2D model.

Three pseudo-2D codes were written in FORTRAN and solved with the DASKR differential-algebraic equation solver, which is a root-finding version of DASPK.[14] They consisted of the traditional finite difference in r and x (with 50 node points in x direction and 35 in r direction) model, the Galerkin model, and the mixed finite difference model for intra-particle diffusion. For all cases in Figure 2-6, D_s is a constant.

2.6. Results and Discussion

Figure 2-2 shows the comparison of the Galerkin method, with traditional finite difference (full-order) numerical solution for varying $\delta(\tau)$, and a constant D_s along with the PSS method. From this figure it is clear that results obtained with the full-order numerical solution (50 node points in r) can be efficiently obtained at reduced computational time with no compromise in accuracy. Though this figure compares the results for a single PDE (solid state diffusion alone) the results obtained help in simulating a pseudo-2D model with efficient approximation/representation for the solid-phase.

Figure 2-3a shows the values of Q_i*'s* obtained when solving the above equation for the given sin function as input for the current. As described above, it can be seen that the values of Q_i decrease with increasing i as well as with time as opposed to the PSS method thus giving a converging solution and also making it easier for stiff equation solvers to converge faster and more efficiently. The q_i*'s* from Ref. [2] are plotted in Figure 2-3b and it is clearly observed that they are a diverging series at low precision computations and reach very high values which may cause the solvers to become unstable. Thus the Galerkin method provides a more efficient way of including the solid phase diffusion without compromising on accuracy for all possible operating conditions with constant diffusion coefficients.

Figure 2-4 shows the comparison of mixed finite difference method with 5 internal nodes for a constant value of $\delta(\tau)$, and constant D_s compared with the full-order numerical solution. It can be observed that the reformulation agrees accurately with the full-order numerical solution. Again, it is observed that both at short times and long times, the mixed finite difference representation matches with the full-order solution. The values of optimized node spacing

obtained in this case for different values of h_i's are [0.2183372643, 0.1779355824, 0.1228253438, 0.1698047152, 0.1499086011, 0 .1611884932].

Proton diffusion in to nickel hydroxide electrodes used in the Ni-MH batteries are strong function of solid-phase concentration and decreases approximately three orders of magnitude. This varying transport property was captured by using the complex faradaic impedance of the nickel hydroxide active material and reported as Eq. [5] elsewhere.[15] This work has been used for accounting variable diffusion coefficient[16] to determine a diffusion coefficient that is a function of the dimensionless flux rate of the material diffusing into the particle. Verbrugge et al.[17] expressed the intercalate diffusion coefficient as an indirect function of solid-phase concentration consisting of fraction occupancy of intercalating host material and activity coefficient. The significance of taking an account of this variation in intercalating electrodes was demonstrated by Botte and White.[18] Here, mathematical models are developed to simulate the potentiostatic charge/discharge of a partially graphitic carbon fiber and the galvanostatic discharge of a lithium foil cell under solid diffusion limitations. Evidence that shows the importance of accounting for nonlinear diffusion was shown by Karthikeyan et. al.[19] for the recently popular $LiNi_{0.8}Co_{0.15}Al_{0.05}O_2$ positive active material in lithium-ion batteries where the thermodynamic expressions along with the activity correction are incorporated into a single particle diffusion model for a Li-ion cell. Hence the use nonlinear diffusion, wherein the diffusion coefficient is a function of concentration, is becoming more and more popular in the battery modeling domain and the mixed order finite difference method is capable of giving accurate results with nonlinear diffusivities as well. To illustrate this fact, Figure 2-5 is presented with the comparison of mixed order finite difference method with 5 internal nodes for constant $\delta(\tau)$, and D_s varying as a simple function of C with the full-order numerical solution. For

varying D_s, $f(C) = 1 + 0.1\ C$, mixed FD approach was found to be efficient and accurate at short times.

Comparisons between the solid-phase diffusion models for the full-order pseudo-2D model and approximations developed show excellent agreement. The time history of cell voltage was monitored for several discharge rates. For very high discharge rates of 5C and 10 C, Figure 2-6 shows the comparison of the full-order, Galerkin (with 5 q's), and Mixed finite differrence (with 5 internal nodes) methods for constant D_s. The computations were terminated when the potential dropped to 2.5 V. Agreement is very good between the traditional Finite Difference and the mixed finite difference methods, indicating that this efficient method could substitute for the traditional method for any discharge rate (low or high). The mixed Finite Difference method is in remarkable agreement with the-full-order finite difference method and can also be used for nonlinear diffusivities and hence can increase the computational efficiency of the whole battery model. The Eigen function based Galerkin collocation approach included in a full pseudo-2D Li-ion battery model also shows excellent agreement at high rates of discharge indicating that this is a good alternative for cases with constant diffusivities.

Table 2-1shows the cpu time taken for performing the above mentioned simulations and it can clearly be seen that the two new proposed methods take lesser simulation time compared to the simulation time for a full order pseudo-2D model. We can also observe that the Eigen function based Galerkin method takes more time compared to mixed finite difference method. The solid phase reformulations are necessary for faster simulation of Li-ion battery models which help in faster estimation of parameters from these models from the experimental data.[20]

2.7. Conclusion

The different approximation schemes available for solid phase approximation for Li-ion batteries were reviewed and certain disadvantages pertaining to some of those methods were discussed. To overcome these small disadvantages an Eigen function based Galerkin-weighted residual approximation was presented that provides efficient reformulation for the solid-phase equation for constant diffusivities. The result from this method compares very well with the Pseudo steady state method and also facilitates easily converging solutions for the Q values. Mixed order finite difference based on finite volume equations can be derived for varying values of diffusion coefficient as a function of concentration (non-linear case), and are very efficient for short times and so far seem to be the only option for reformulating nonlinear diffusivities efficiently. The two methods presented here seem to be better compared to the existing solid phase approximations with absolutely no shortcomings as they are valid for any kind of operating conditions. For the case of linear diffusivity (D_s is constant) the eigen function based Galerkin collocation is the most efficient method, that does not compromise on accuracy, however providing excellent computational efficiency. For nonlinear diffusivities, the mixed order finite difference method can be used to obtain accurate solutions by using lesser number optimally spaced node points thereby reducing the total number of equations being solved for the full pseudo-2D Li-ion battery model. Future work involves efficient reformulation for moving boundary models for phase change materials and coupling the solid phase models with reformulated models at very high rates.

2.8. List of Symbols

C dimensionless concentration of lithium ions in the intercalation particle of electrode

c_0 reference concentration, mol/m^3

c_s concentration of lithium ions in the intercalation particle of electrode, mol/m^3

$\overline{c}$ average concentration of lithium ions in the intercalation particle of electrode, mol/m^3

C_i dimensionless concentration at i^{th} node point

$\overline{C}$ dimensionless average concentration of lithium ions

D_s Li-ion diffusion coefficient in the intercalation particle of electrode, m^2/s

D_0 diffusion coefficient at reference concentration c_0, m^2/s

h_i node spacing at i^{th} node point

$j(t)$ pore wall flux of Li ion the intercalation particle of electrode, mol/m^{2}s

q volume averaged concentration flux, mol cm^{-4}

R_s radius of the intercalation particle of electrode, m

λ_n positive eigen values

2.9. References

1. M. Doyle, T. F. Fuller and J. Newman, *J. Electrochem. Soc*., **140**, 1526 (1993).
2. Q. Zhang and R.E. White, *J. Power Sources*, **165**, 880 (2007).
3. C. Y. Wang, W. B. Gu and B. Y. Liaw, J. Electrochem. Soc., **145**, 3407 (1998).
4. V. R. Subramanian, V. D. Diwakar and D. Tapriyal, *J. Electrochem. Soc*., **152**, A2002 (2005).
5. S. Liu, *Solid State Ionics*, **177**, 53 (2006).
6. K. Smith and C. Y. Wang, *J. Power Sources*, **161**, 628 (2006).
7. V. R. Subramanian, V. Boovaragavan and V. D. Diwakar, *Electrochem. Solid-State Lt*., **10**, A225 (2007).
8. Y. Bard, Nonlinear Parameter Estimation. Academic Press, New York (1974).
9. W. R..Esposito and C.A. Floudas, *I & EC Research*, **39**, 5, 1291 (2000).
10. F. Tlacuahuac, A., S. Terrazas Moreno, and L. T. Biegler, *I & EC Research,* **47,** 8, 2643 - 2655 (2008).
11. J. Christensen and J. Newman, *J. Solid State Electrochem*., **10**, 293 (2006).
12. G. G. Botte, V. R. Subramanian and R. E. White, *Electrochim. Acta*, **45** (15-16), 2595 (2000)..
13. V. Boovaragavan, and V. R. Subramanian, *Electrochem. Comm.*, **9**, 1772 (2007).
14. P.N. Brown, A.C. Hindmarsh, and L.R. Petzold, SIAM J. Sci. Comp., **19**, 1495 (1998).
15. S. Motupally, C. C. Streinz, and J. W. Weidner, *J. Electrochem. Soc.*, **145** (1), 29 (1998).
16. G. G. Botte and R. E. White, *J. Electrochem. Soc.*, **148** (1), A54 (2001).
17. M. W. Verbrugge and B. J. Koch, *J. Electrochem. Soc.*, **143** (1), 24 (1996).
18. V. R. Subramanian, P. Yu, B. N. Popov and R. E. White, *J. Power Sources*, **96**(2), 396 (2001).
19. D. K. Karthikeyan, G. Sikha and R. E. White, *J. Power Sources*, **185**, 1398 (2008).
20. V. Ramadesigan, K. Chen, N. A. Burns, V. Boovaragavan, R. D. Braatz and V. R. Subramanian, *J. Electrochem. Soc*., **158** (9), A1048 (2011). [ECS Trans. **19**, 11-19 (2009)].

2.10. Tables

Table 2-1: Comparison of CPU times taken for full order pseudo-2D, Galerkin based and mixed FD methods for obtaining discharge curves in Figure 2-6 at 5C and 10C rates.

Method	CPU time for 5C rate (s)	CPU time for 10C rate (s)
Full order Pseudo-2D	19.2	20
Galerkin based	4.5	4.84
Mixed Finite Difference	1.438	1.297

2.11. Figures

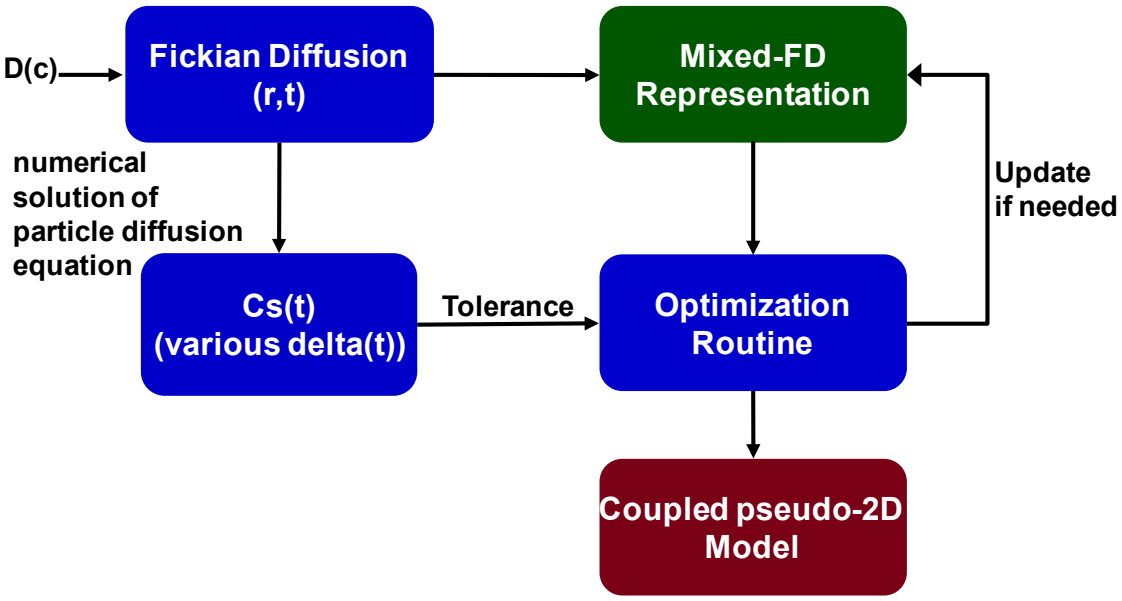

Figure 2-1: Schematic of steps involved in mixed FD method for optimized spacing and hence reformulation of solid phase diffusion.

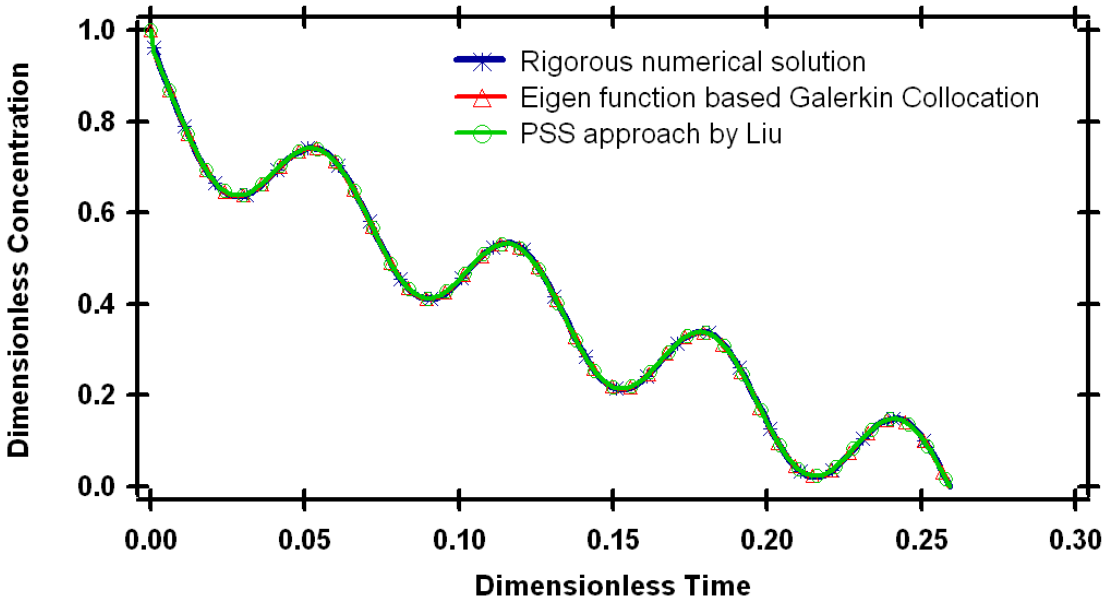

Figure 2-2: Comparison of Eigen function based Galerkin reformulation with full-order numerical solution and PSS by Liu for $\delta(\tau) = 1 + \sin(100)$ and $n = 5$.

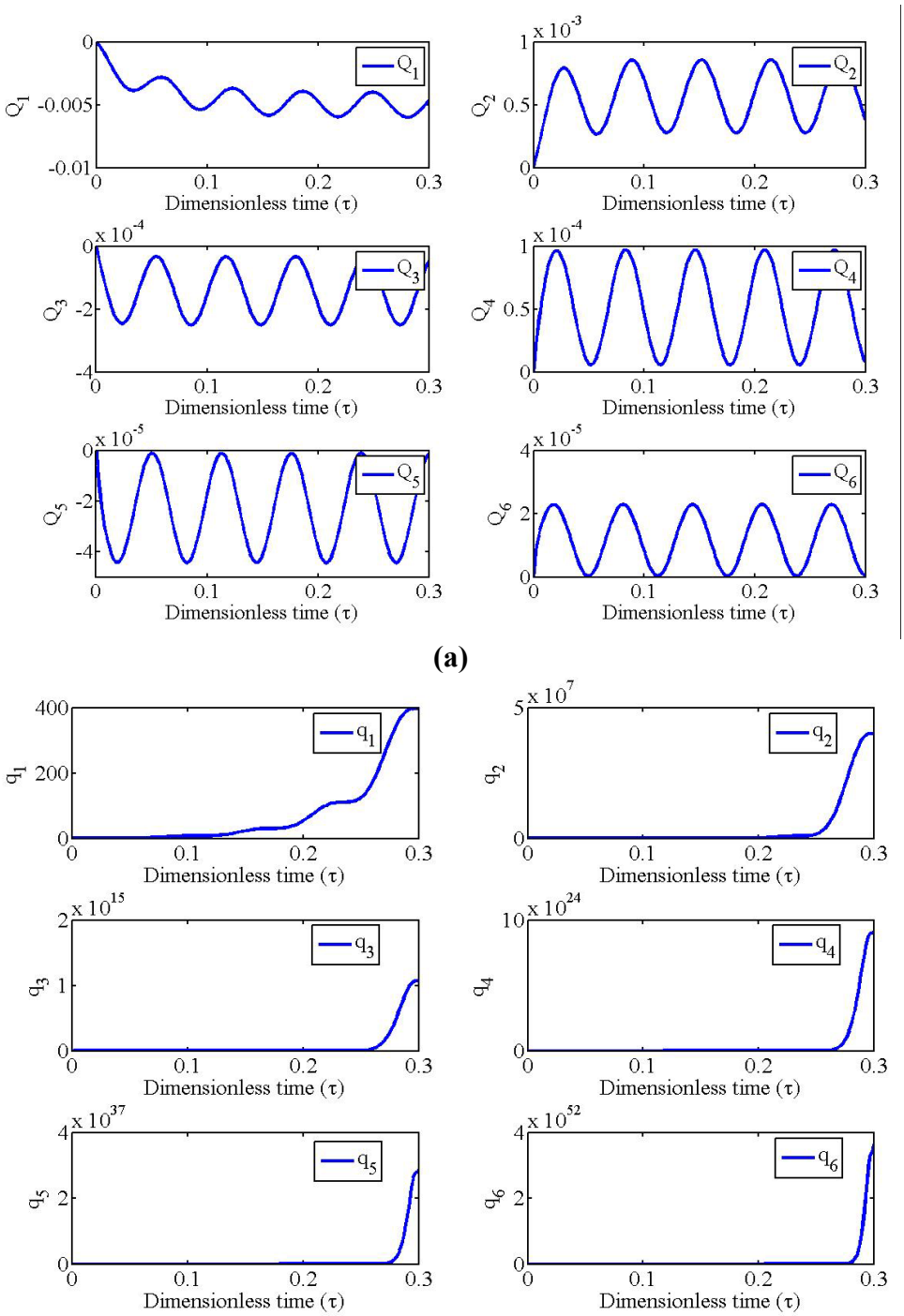

Figure 2-3: (a) Plot of Q_i's obtained during the simulation of Figure 2-2 showing the converging behavior for increasing i and with time. (b) Plot of q_i's from the PSS method obtained during the simulation of Figure 2-2 showing the diverging behavior for increasing i and with time

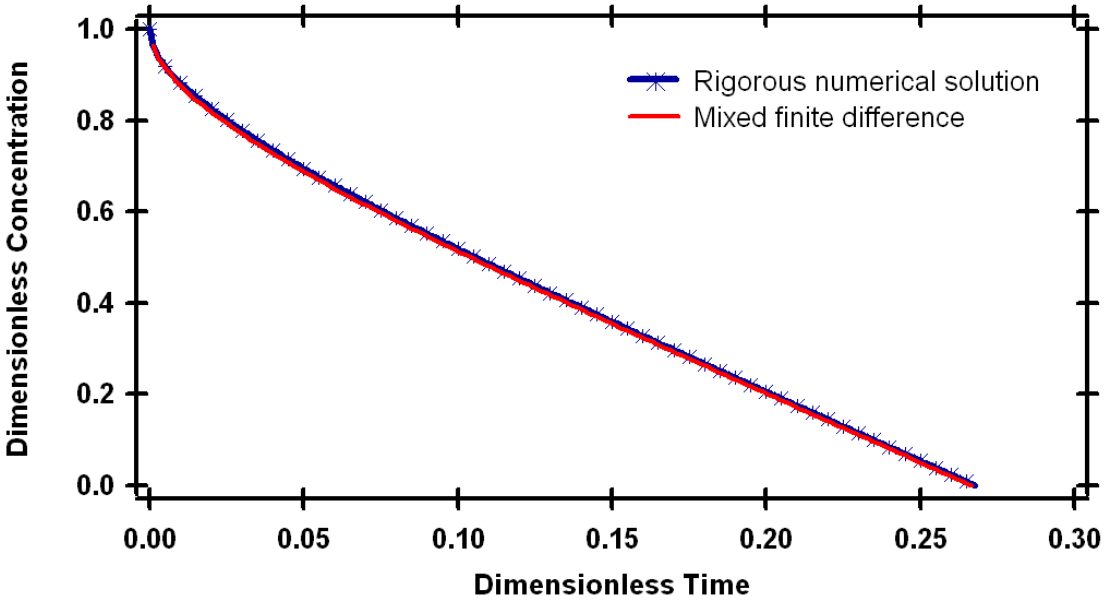

Figure 2-4: Comparison of mixed FD method with 5 interior nodes with full-order numerical solution for constant Ds and δ (τ) = 1, etc.

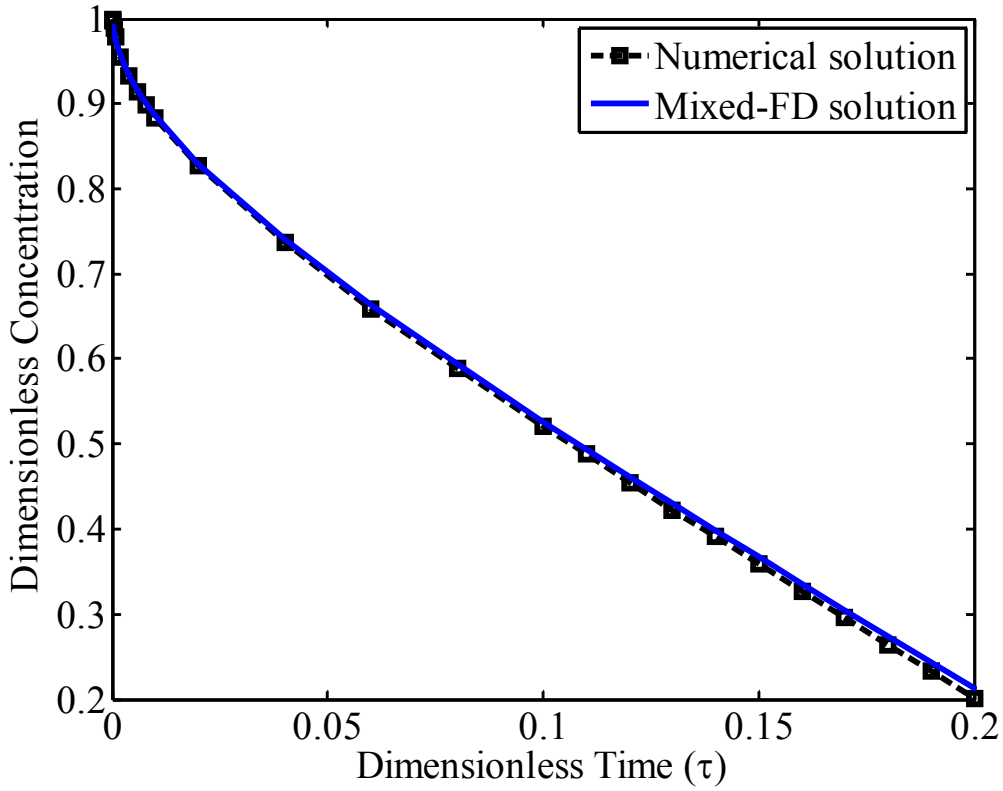

Figure 2-5: Comparison of mixed FD method with 5 interior nodes with full-order numerical solution for f(C) = 1 + 0.1C and δ (τ) = 1

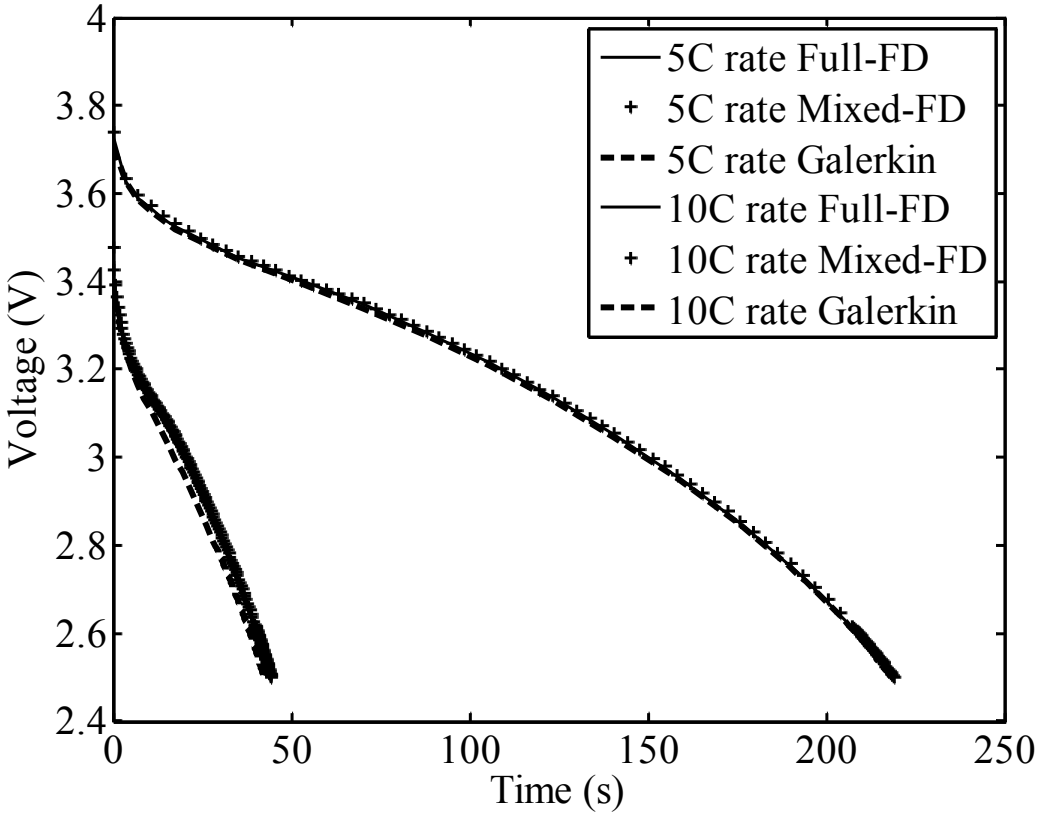

Figure 2-6: Discharge curves at 5C and 10C rate for a Pseudo-2D model for Li-ion battery: Comparison of full order pseudo-2D, Galerkin based, and mixed finite difference methods for solid phase diffusion.

Chapter 3 : Parameter Estimation and Capacity Fade Analysis of Lithium-ion Batteries Using Reformulated Models

This chapter is reproduced with permission from *J. Electrochem. Soc.*, **158** (9), A1048 (2011). The author is grateful to the co-authors for their significant contributions under sections 3.3.3, 3.4 and 3.5.

3.1. Introduction

Electrochemical power sources appear in applications in automobiles, power storage, military, mobile applications, and space. Lithium-ion chemistry has been identified as a preferred candidate for high-power/high-energy secondary batteries. Significant progress has been made in developing lithium-ion battery models that incorporate transport phenomena, electrochemical kinetics, and thermodynamics.[1-8] While these models have been used to produce reliable predictions for a small number of cycles, their ability to predict the reduction in capacity during cycling is limited. Different mechanisms causing capacity fade include (i) capacity fade during formation cycles, (ii) overcharging, which results in a decrease in capacity in both positive and negative electrodes and the electrolyte, (iii) decomposition of the electrolyte during the reduction process, (iv) self-discharge depending on the purity of materials used in manufacturing, and (v) formation of a passive film on the electrode that grows in thickness as the cycle number increases.[5,7] Figure 3-1 shows the region in which each phenomenon occurs within a battery. Table 3-1 lists some of the mechanisms causing capacity fade and the possible parameters that could be affected in a pseudo-2D porous-electrode-based model of a lithium-ion battery.

In some recent work, Safari *et al.*[9,10] assessed the possibility of using a mechanical-fatigue life-prognostic method for the life prediction of lithium-ion batteries. This method was

successfully demonstrated for predicting the capacity loss but is limited by the choice between the time frame of the aging experiments and the life-prediction accuracy. In addition, the method is an empirical tool, which has its own limitations. Yoshida[11] fabricated a lithium-ion cell with 5-Ah capacity, fitted experimental data on the thickness of the SEI layer growth, and demonstrated that their empirical fit predicted the life under certain conditions. Other recent efforts have developed more efficient simulation techniques for phenomenological models of capacity fade.[4,12] A complete phenomenological model for capacity fade has not been forthcoming due to (i) incomplete understanding of all of the capacity fade mechanisms, (ii) lack of knowledge for the values of the model parameters in these mechanisms, (iii) difficulties in obtaining these parameter values due to cumulative non-separable effects of individual mechanisms occurring simultaneously, and (iv) numerical inability and lack of efficient numerical solvers to be able to solve the complex models efficiently with proper state detections. Oftentimes in the quest for adding detailed mechanisms, researchers have neglected important electrochemical/transport phenomena typically in porous electrode-based battery models. For example, researchers have employed simpler single-particle models or empirical fits that neglect important electrochemical/transport phenomena to accommodate the increased complexity of capacity fade mechanisms. Today very few phenomenological models include mechanisms for capacity fade in Li-ion batteries[8,12] and no models include all of the postulated mechanisms.

This chapter proposes an alternative approach to the estimation of the life of a battery, which uses voltage-discharge curves measured during initial cycles to predict voltage-discharge curves during later cycles. A model reformulation[4] is employed to efficiently extract the effective kinetic and transport parameters from experimental data, with uncertainties in parameters and model predictions quantified using established analysis techniques. The next sections describe

the lithium-ion battery model used in this study, the numerical algorithms used to implement the discrete approach to capacity fade prediction, the results and discussion, and the conclusions.

3.2. Lithium-ion Battery Model and Simulation

Phenomenological battery models typically solve electrolyte concentration, electrolyte potential, solid-state potential, and solid-state concentration in the porous electrodes and electrolyte concentration and electrolyte potential in the separator regions.[1,2] These models are represented by coupled nonlinear partial differential equations in one, two, or three dimensions, are typically solved numerically, and require a few seconds to minutes to simulate. Simulation of lithium-ion battery models requires simultaneous evaluation of concentration and potential fields, both in the solid and electrolyte phases. The porous nature of the battery electrodes leads to highly nonlinear and heterogeneous electrochemical reaction kinetics. A pseudo-two-dimensional (P2D) model developed by Doyle *et al.*[6] is considered in this work. The governing equations in the full physics-based P2D model for the five variables Φ_1, Φ_2, c, c_s^{ave}, and j_p that vary with x are given in Table 3-2. Usually lithium-ion battery models are numerically simulated by finite-difference discretization of all the variables in the spatial coordinates. The discretization of the cathode, separator, and anode into 50 equally spaced node points would result in 600 Differential Algebraic Equations (DAEs) to be solved in the finite difference model, which is impractical for real-time simulation. Parameter estimation and optimization of lithium-ion battery, where the life and health of the battery is vital to the operation of the device, requires quick-solving models that can give an accurate account of the battery variables. A model reformulation[4] of the P2D model[6] was developed by exploiting the mathematical structure of the DAEs while conserving mass, charge, and current in each electrode and having much lower

memory requirements and computational costs compared to standard finite-difference methods. The details on the reformulation of the P2D model are provided elsewhere.[4]

The accuracy and simplicity of the reformulated model enables an easy computation of parameter sensitivities and even numerical jacobians are likely to be more accurate and stable compared to the direct finite-difference method applied to the original P2D model. These features of the model reformulation were utilized during the parameter estimation described in Section 3.3.2 to extract effective kinetic and transport parameters from experimentally measured voltage-discharge curves. The reformulated model also enabled the application of the Markov Chain Monte Carlo (MCMC) method, as described in Section 3.3.3, to quantify the magnitude of uncertainties in the model parameters.

3.3. Numerical Algorithms

This section describes the discrete approach to capacity fade prediction and the parameter estimation and uncertainty quantification methods used in the implementation of the discrete approach.

3.3.1. Discrete Approach to Capacity Fade Prediction

This chapter reports a discrete parameterized approach to predict capacity fade in Li-ion batteries. The variations in effective transport and kinetic parameters are tracked with discharge curves at different cycles as described in Section 3.3.2. The estimated parameters were the effective diffusion coefficient of lithium ion in the solution phase (D_1), effective diffusion coefficient of lithium in the solid phase for the negative and positive electrodes (D_{sn} and D_{sp}), and electrochemical reaction rate constants for the negative and positive electrodes (k_n and k_p). Note that the effective diffusion coefficient through porous media is a function of a species' molecular diffusion coefficient and the porosity, tortuosity, and constrictivity of the media,[13]

which change as a battery ages, so that the effective diffusion coefficient changes with cycle #. The electrochemical rate constants are also *effective*, in that they are a function of the true electrochemical rate constant and the surface area available for electrochemical reaction, which will decrease as alloys are formed on the electrode surface that block or hinder electrochemical reaction. In an application to a Quallion battery, Section 3.4 demonstrates that power-law extrapolation of the change in the effective transport and kinetic parameters predicted the future voltage-discharge curves and the life of the battery.

Uncertainty quantification methods are applied to avoid over-fitting of the model parameters to the experimental data. Uncertainties in the effective model parameters are quantified as described in Section 3.3.3, and used to reduce the set of estimated model parameters to include only those parameters that can be estimated with sufficient accuracy from the experimental data. Uncertainties in the model predictions are also quantified, with the 95% predictive intervals for future cycles compared with the experimental data in Section 3.4.

3.3.2. Parameter Estimation

The model parameter estimates were obtained by the solution of a nonlinear optimization that minimizes the sum-of-squared differences between the model outputs and their experimentally measured values for each cycle i:[14-16]

$$\min_{\theta_i} \sum_{j=1}^{n_i} \left[y_i(t_j) - y_{model,\,i}(t_j;\theta_i) \right]^2 \qquad [3.1]$$

where $y_i(t_j)$ is the measured voltage at time t_j for cycle i, $y_{model,i}(t_j;\theta_i)$ is the voltage computed from the reformulated model at time t_j for cycle i for the vector of model parameters θ_i (the 5 parameters being the effective solid-phase diffusion coefficient and reaction rate constant in each electrode and solution-phase diffusion coefficient of the electrolyte), and n_i is

the number of time points in cycle *i*. Solving the optimization [3.1] is known in the literature as *least-squares estimation*.[14-16] Many numerical algorithms are available for solving the nonlinear optimization [3.1], such as the steepest descent, Gauss-Newton, and Marquardt methods.[14] In this work, the Gauss-Newton method[14] was applied to estimate parameters using the reformulated model. For the least-squares estimation, this Jacobian-based method is an iterative process that reduces the sum-of-squared differences between the model outputs and the experimental data points until the error is no longer significantly reduced.

3.3.3. Uncertainty Quantification

Uncertainties in the model parameter estimates were quantified by three methods: (i) estimation of hyper-ellipsoidal 95% confidence regions by applying Chi-squared statistics to a Taylor series expansion between the model parameters and the model outputs,[15,16] (ii) estimation of 95% confidence regions by applying F-statistics to the parameter estimation objective function [3.1],[15,16] and (iii) estimation of probability distributions using the Markov Chain Monte Carlo (MCMC) method.[17,18] The first two methods, which are the most commonly applied in the literature, gave highly inaccurate confidence regions for this application, whereas the MCMC method is a very accurate method for uncertainty quantification for any application. The MCMC method employs a Monte Carlo sampling method to numerically construct the probability distribution for each model parameter and cycle *i* from the posterior distribution for the parameter estimates obtained using Bayes' rule:[17,18]

$$\Pr(\theta_i \mid Y_i) = \frac{\Pr(Y_i \mid \theta_i)\Pr(\theta_i)}{\Pr(Y_i)} \qquad [3.2]$$

where Y_i was the vector obtained by stacking the voltage measurements $y_i(t_j)$, $\Pr(\theta_i)$ is the prior distribution of θ_i which was specified as a uniform distribution with a width of 20%

centered at the parameters estimated using the least-squares method [3.1], $\Pr(Y_i \mid \theta_i)$ is the likelihood of obtaining the data Y_i given parameters θ_i, and $\Pr(Y_i)$ is a normalization constant so that the posterior distribution $\Pr(\theta_i \mid Y_i)$ integrates to unity. The term $\Pr(Y_i \mid \theta_i)$, which is known as the *likelihood function*, for this application is

$$\prod_{j=1}^{n_i} \frac{1}{\sqrt{2\pi}\sigma_\varepsilon} \exp\left(\frac{(y_i(t_j) - y_{model,\,i}(t_j;\theta_i))^2}{2\sigma_\varepsilon^2} \right) \qquad [3.3]$$

where $\sigma_\varepsilon = 0.01$ V was the standard deviation of the voltage measurement noise. The probability distribution for each model parameter is equal to integrals of the posterior distribution [3.2] over the other model parameters. Unlike the conventional Monte Carlo method for computing integrals,[19] the samples in the MCMC method are correlated; generating what is known as a *Markov chain*, whose probability distribution approaches the probability distribution for each parameter. More detailed descriptions are provided in the references.[17,18]

Other advantages of the MCMC method are its explicit consideration of constraints and arbitrary non-Gaussian distributions for prior knowledge on the parameters, and that it exactly handles the full nonlinearity in the model equations. For an accurate quantification of the uncertainties, the MCMC method requires many simulation runs, which was facilitated by use of the reformulated model.

The effect of the parameter uncertainties on the accuracy of the predictions of the lithium-ion battery model was also quantified. Although the reformulated model was computationally efficient enough for the standard Monte Carlo method to be applied to quantify the accuracy of the model predictions, the computational cost was further reduced by replacing the reformulated model with a polynomial series expansion[20,21] during the computation of the prediction intervals.

The application of this approach to electrochemical and materials systems is described in great detail in the literature.[22-25]

3.4. Results and Discussion

The experimental data for the analysis were obtained for Quallion BTE cells and chemistry.[26,27] Five effective transport and kinetic parameters were estimated by applying least-squares estimation to the Quallion BTE cells experimental voltage-discharge data. The standard finite-difference model and the reformulated model gave the same voltage-discharge curves at cycle 0 (see Figure 3-2). Using the model parameters at cycle 0 as an initial guess, Figure 3-2 compares the experimental voltage-discharge curve at cycle 25 with the reformulated model output obtained using five model parameters fit by least-squares estimation to that experimental data set. Similar parameter estimations and fits were obtained for later cycle numbers (50 and 100n where n = 1,...,10).

The expected monotonic reduction in capacity with cycle # is shown in the voltage-discharge curves obtained by fitting the five model parameters to experimental data (see Figure 3-3a). The mechanisms of capacity fade and its overall reduction in battery performance (see Figure 3-1) suggest that all five effective model parameters should decrease monotonically with cycle #. The effective negative-electrode solid-phase diffusion coefficient and reaction rate constant (D_{sn} and k_n) decrease monotonically with cycle #, whereas the other three parameters did not follow any particular trend (see Figure 3-3a). This suggested that the voltage-discharge curves may not contain sufficient information to accurately estimate the effective values of D_1, D_{sp}, and k_p, and that the change in the voltage-discharge curves with cycle # could be captured by estimation of only the effective solid-phase diffusion coefficient D_{sn} and reaction rate constant k_n for the negative electrode. The voltage-discharge curves could be fit using just the two model

parameters D_{sn} and k_n, which had to significantly change their values to be able to fit the voltage-discharge curves at higher cycle number (see Figure 3-3b).

An initially surprising observation was that, when only 2 model parameters were fit, the effective reaction rate constant k_n was not monotonically decreasing with cycle # between cycle 0 and cycle 25 (see Figure 3-3b). This observation motivated a more detailed analysis by application of sensitivity analysis and the MCMC method. The voltage-discharge curves were very sensitive to the value of the effective solid-phase diffusion coefficient D_{sn} but weakly sensitive to deviations in the model parameters D_1, D_{sp}, k_p, and k_n from their nominal values, resulting in large uncertainties in their values when fit to experimental voltage-discharge curves (see Table 3-3). The nominal estimate of the effective solid-phase diffusion coefficient D_{sn} monotonically decreases with increased cycle number (see Figure 3-3b), with the nominal estimates being highly accurate according to the probability density function (pdf) computed by the MCMC method (see Figure 3-4). The pdfs for D_{sn} at different cycle numbers have minimal overlap, providing very high confidence that the monotonic reduction of the effective solid-phase diffusion coefficient with increase cycle number is statistically significant. That the voltage-discharge curves were much sensitive to a negative-electrode parameter (D_{sn}) suggests that mechanisms for capacity fade in the negative electrode, rather than the electrolyte or positive electrode, were the most important for this battery under these operating conditions. The pdfs of the other model parameters are sufficiently broad (see Table 3-3) that an observed increase in a model parameter from one cycle to the next, as seen in Figure 3-3b, may not be statistically significant.

The overall trend in the variation of model parameters is more reliably assessed by plotting nominal estimates over many cycles. A discrete approach was adopted for the prediction of

capacity fade by tracking the change in effective transport and kinetic parameters with cycle number (N). Figure 3-5 shows the variation with cycle number of the effective diffusion coefficient D_{sn} and electrochemical reaction rate constant k_n for the negative electrode. Power laws are commonly used to fit the decay of a property,[28] which motivated the estimation of the model parameters and computation of the voltage-discharge curve at cycle 600 by extrapolation of power-law fits for the variations in each model parameter as a function of cycle number for 25, 50, 100, and 200. The mathematical model produces accurate predictions of the voltage-discharge curve at cycles 500 and 600 (see Figure 3-5 and Figure 3-6).

The model parameters D_{sn} and k_n fit to the experimental data for cycles 50, 100, 200, 300, 400, and 500 were used to predict the remaining battery life based on voltage-discharge curves measured in past cycles. To characterize the degradation in the model parameters, a power law was fit to the estimated parameter values from cycles 25 to 500 similar to what was done for least-squares estimation. Implicitly assuming that the changes in the parameter values are the result of the same mechanism in later cycles, the parameter values for the subsequent cycles were predicted using the power-law expressions. The voltage-discharge curve predicted by this model was in very good agreement with the experimental data at cycle 1000 (see Figure 3-7), indicating that the model was able to predict capacity fade.

3.5. Conclusions

The effective solid-phase diffusion coefficients and electrochemical reaction rate constants in positive and negative electrodes and the effective electrolyte diffusion coefficient were estimated and tracked as a function of cycle #. The mathematical analysis indicated that (i) nearly all of the variation in voltage-discharge curves could be explained by changes in only the two model parameters associated with transport and electrochemical kinetics in the negative electrode

(Figure 3-3b), and (ii) the monotonic reduction in the estimated effective solid-phase diffusion coefficient in the negative electrode due to capacity fade was due to actual changes in the model parameter rather than uncertainties in the parameter estimation resulting from limited parameter identifiability and limited data (Figure 3-4). After characterizing uncertainties in the parameters (Table 3-3), the effects of the parameter uncertainties on the voltage-discharge curve were quantified (Figure 3-6). Small prediction intervals, as well as comparisons of model predictions with experimental data (Figure 3-5 to Figure 3-7), provided confidence in the ability of the model to predict capacity fade. Tracking cycle-dependent variations in the effective values for transport and electrochemical kinetics is valid only for a particular protocol of galvanostatic charge and discharge, and is not appropriate for use in the design of lithium-ion batteries with reduced capacity fade.

The proposed approach is appropriate for estimating the lifetime of a lithium-ion battery from past measured voltage-discharge curves. This study considers a battery operating for a consistent set of conditions; it would be useful to assess whether the approach is useful for time-varying discharge conditions (within an allowable window of operations). The proposed approach is computationally efficient enough that it could be integrated into an inexpensive microprocessor for estimating the remaining battery lifetime, based on minimum requirements on the voltage-discharge curve for the battery to be useful in its application. The proposed approach can also provide guidance as to which battery components are likely the primary causes for capacity fade for a battery operating within a specified window of operating conditions. For example, in this study the voltage-discharge curves were sensitive to the negative-electrode parameters which suggested that the capacity fade mechanisms in the negative electrode have a more pronounced effect on the voltage-discharge curves. A designer working to improve the

battery designed for this operating condition would focus on modification of the negative-electrode parameters (e.g., geometries, porosity) to reduce the capacity fade.

3.6. List of Symbols

a_i specific surface area of electrode i ($i = p, n$), m^2/m^3

$brugg_i$ Bruggman coefficient of region i ($i = p, s, n$)

c electrolyte concentration, mol/m^3

c_0 initial electrolyte concentration, mol/m^3

$c_{s,i}$ concentration of lithium ions in the intercalation particle of electrode i ($i=p, n$), mol/m^3

$c_{s,i,0}$ initial concentration of lithium ions in the intercalation particle of electrode i ($i = p, n$), mol/m^3

$c_{s,max,i}$ maximum concentration of lithium ions in the intercalation particle of electrode i ($i = p, n$), mol/m^3

D_1 electrolyte diffusion coefficient, m^2/s

$D_{s,i}$ lithium ion diffusion coefficient in the intercalation particle of electrode i ($i = p, n$), m^2/s

F Faraday's constant, C/mol

I applied current density, A/cm^2

i_1 solid-phase current density, A/m^2

i_2 solution-phase current density, A/m^2

$i_{0,s}$ exchange current density for the solvent reduction reaction, A/m^2

j_s solvent reduction current density, mol/m^2s

j_i wall flux of Li^+ on the intercalation particle of electrode i ($i = n, p$), mol/m^2s

k_i intercalation/deintercalation reaction rate constant of electrode i ($i = p, n$), $mol/(mol/m^3)^{1.5}$

l_i thickness of region i ($i = p, s, n$), m

M_s molecular weight of the solvent reaction product, g/mol

n negative electrode

N cycle number (dimensionless)

p positive electrode

r radial coordinate, m

R universal gas constant, J/(mol·K)

R_{film} Initial SEI layer resistance at the negative electrode, $\Omega \cdot m^2$

R_i radius of the intercalation particle of electrode i ($i = p, n$), m

s separator

t_+ Li^+ transference number in the electrolyte

T absolute temperature, K

U_i open-circuit potential of electrode i ($i = p, n$), V

U_s standard potential of the solvent reduction reaction, V

x spatial coordinate, m

x_{i0} initial state of charge at the electrode

δ thickness of the solvent reduction product film, m

δ_0 initial thickness of the solvent reduction product film, m

ε_i porosity of region i ($i = p, s, n$)

$\varepsilon_{f,i}$ volume fraction of fillers of electrode i ($i = p, n$)

η_i overpotential driving a reaction, V

η_s overpotential driving the side reaction, V

κ ionic conductivity of the electrolyte, S/m

$\kappa_{eff,i}$ effective ionic conductivity of the electrolyte in region i ($i = p, s, n$), S/m

Φ_1 solid-phase potential, V

Φ_2 electrolyte-phase potential, V

ρ_s density of the solvent reduction product film, g/m^3

σ_i electronic conductivity of the solid phase of electrode i ($i = p, n$), S/m

$\sigma_{eff,i}$ effective electronic conductivity of the solid phase of electrode i ($i = p, n$), S/m

θ_i dimensionless concentration of lithium ions in the intercalation particle of electrode i ($\theta_i = c_{s,i}/c_{s,max,i}$)

3.7. References

1. G. G. Botte, V. R. Subramanian and R. E. White, *Electrochim Acta*, **45**, 2595 (2000).
2. T. F. Fuller, M. Doyle and J. Newman, *J Electrochem Soc*, **141**, 982 (1994).
3. V. R. Subramanian, V. Boovaragavan and V. D. Diwakar, *Electrochem Solid St*, **10**, A255 (2007).
4. V. R. Subramanian, V. Boovaragavan, V. Ramadesigan and M. Arabandi, *J Electrochem Soc*, **156**, A260 (2009).
5. Q. Zhang and R. E. White, *J Power Sources*, **179**, 793 (2008).
6. M. Doyle, T. F. Fuller and J. Newman, *J Electrochem Soc*, **140**, 1526 (1993).
7. P. Arora, R. E. White and M. Doyle, *J Electrochem Soc*, **145**, 3647 (1998).
8. P. Ramadass, B. Haran, P. M. Gomadam, R. White and B. N. Popov, *J Electrochem Soc*, **151**, A196 (2004).
9. M. Safari, M. Morcrette, A. Teyssot and C. Delacourt, *J Electrochem Soc*, **157**, A892 (2010).
10. M. Safari, M. Morcrette, A. Teyssot and C. Delacourt, *J Electrochem Soc*, **157**, A713 (2010).
11. T. Yoshida, M. Takahashi, S. Morikawa, C. Ihara, H. Katsukawa, T. Shiratsuchi and J. Yamaki, *J Electrochem Soc*, **153**, A576 (2006).
12. V. Ramadesigan, V. Boovaragavan, J. C. Pirkle and V. R. Subramanian, *J Electrochem Soc*, **157**, A854 (2010).
13. J. van Brakel and P. M. Heertjes, *Int J of Heat & Mass Transfer*, **17**, 1093 (1974).
14. A. Bjorck, *Numerical Methods for Least Squares Problems*, SIAM Press, Philadelphia (1996).
15. R. Gunawan, M. Y. L. Jung, E. G. Seebauer and R. D. Braatz, *AIChE J*, **49**, 2114 (2003).
16. J. V. Beck and K. J. Arnold, *Parameter Estimation in Engineering and Science*, Wiley, New York (1977).
17. M. W. Hermanto, N. C. Kee, R. B. H. Tan, M. S. Chiu and R. D. Braatz, *AIChE J*, **54**, 3248 (2008).
18. L. Tierney, *Ann Stat*, **22**, 1701 (1994).
19. R. E. Caflisch, *Acta Numerica*, **7**, 1 (1998).
20. Z. K. Nagy and R. D. Braatz, *J Process Contr*, **17**, 229 (2007).
21. N. Wiener, *Am J of Mathematics*, **60**, 897 (1938).
22. D. L. Ma and R. D. Braatz, *IEEE T Contr Syst T*, **9**, 766 (2001).
23. D. L. Ma, S. H. Chung and R. D. Braatz, *AIChE J*, **45**, 1469 (1999).
24. Z. K. Nagy and R. D. Braatz, *J Process Contr*, **14**, 411 (2004).
25. B. J. Debusschere, H. N. Najm, A. Matta, O. M. Knio, R. G. Ghanem, O. P. Le Maitre, *Physics of Fluids*, 15, 2238 (2003).
26. http://www.quallion.com (01/25/2011).
27. V. R. Subramanian, V. Boovaragavan, V. Ramadesigan, K. Chen and R. D. Braatz, in *Design for Energy and the Environment: Proceedings of the Seventh International Conference on the Foundations of Computer-Aided Process Design*, M. M. El-Halwagi and A. A. Linninger, Editors, CRC Press, Boca Raton, p. 987 (2009).
28. A. Coniglio, A. Fierro, H. J. Herrmann, M. Nicodemi and Ebooks Corporation., *Unifying Concepts in Granular Media and Glasses*: *From the Statistical Mechanics of Granular Media to the Theory of Jamming*, Elsevier, Burlington (2004).

3.8. Tables

Table 3-1: List of capacity fade mechanisms and possibly affected parameters in a pseudo-2D model

Mechanism of Capacity Fade	Possible Affected Parameters
Capacity fade during formation cycles	x_{p0}, x_{n0}, ε_p, ε_n, D_{sp}, D_{sn}, k_p, k_n
Overcharging that results in decrease in capacity in both positive and negative electrodes	D_{sp}, D_{sn}, k_p, k_n
Decomposition of the electrolyte during the reduction process	D_1, k_p, k_n
Self-discharge depending on the purity of materials used in manufacturing	D_{sp}, D_{sn}, k_p, k_n
Formation of a passive film on the electrode that grows in thickness as the cycle number increases	k_s, R_{film}
Loss of active material during cycling	x_{p0}, x_{n0}, ε_p, $\varepsilon_{n,}$, $\varepsilon_{f,p}$, $\varepsilon_{f,n}$

Table 3-2: Governing equations for a lithium-ion battery (published as Table 1 of Ref [4])

Region	Eq#	Governing equations	Boundary conditions
Positive electrode	T1	$\varepsilon_p \frac{\partial c}{\partial t} = D_{eff,p} \frac{\partial^2 c}{\partial x^2} + a_p (1-t_+) j_p \;\; ; \;\; c\big\|_{t=0} = c_0$	$-D_{eff,p} \frac{\partial c}{\partial x}\Big\|_0 = 0 \quad \& \quad -D_{eff,p} \frac{\partial c}{\partial x}\Big\|_{l_p,-} = -D_{eff,s} \frac{\partial c}{\partial x}\Big\|_{l_p,+}$
	T2	$-\sigma_{eff,p} \frac{\partial \Phi_1}{\partial x} - \kappa_{eff,p} \frac{\partial \Phi_2}{\partial x} + \frac{2\kappa_{eff,p} RT}{F}(1-t_+) \frac{\partial \ln c}{\partial x} = I$	$-\kappa_{eff,p} \frac{\partial \Phi_2}{\partial x}\Big\|_0 = 0 \quad \& \quad -\kappa_{eff,p} \frac{\partial \Phi_2}{\partial x}\Big\|_{l_p,-} = -\kappa_{eff,s} \frac{\partial \Phi_2}{\partial x}\Big\|_{l_p,+}$
	T3	$\sigma_{eff,p} \frac{\partial^2 \Phi_1}{\partial x^2} = a_p F j_p$	$\frac{\partial \Phi_1}{\partial x}\Big\|_0 = -\frac{I}{\sigma_{eff,p}} \quad \& \quad \Phi_1 = 4.2$
	T4	$\frac{d}{dt} c_s^{ave} + 3\frac{j_p}{R_p} = 0 \quad \& \quad \frac{D_{s,p}}{R_p}\left(c_s^{surf} - c_s^{ave}\right) = -\frac{j_p}{5}$	$c_s^{ave}\big\|_{t=0} = c_{s,max,p}$
Separator	T5	$\varepsilon_s \frac{\partial c}{\partial t} = D_{eff,s} \frac{\partial^2 c}{\partial x^2}$	$-D_{eff,p} \frac{\partial c}{\partial x}\Big\|_{l_p,-} = -D_{eff,s} \frac{\partial c}{\partial x}\Big\|_{l_p,+} \;\&\; -D_{eff,s} \frac{\partial c}{\partial x}\Big\|_{l_p+l_s,-} = -D_{eff,n} \frac{\partial c}{\partial x}\Big\|_{l_p+l_s,+}$
	T6	$I = -\kappa_{eff,s} \frac{\partial \Phi_2}{\partial x} + \frac{2\kappa_{eff,s} RT}{F}(1-t_+) \frac{\partial \ln c}{\partial x}$	$-\kappa_{eff,p} \frac{\partial \Phi_2}{\partial x}\Big\|_{l_p,-} = -\kappa_{eff,s} \frac{\partial \Phi_2}{\partial x}\Big\|_{l_p,+} \;\&\; -\kappa_{eff,s} \frac{\partial \Phi_2}{\partial x}\Big\|_{l_p+l_s,-} = -\kappa_{eff,n} \frac{\partial \Phi_2}{\partial x}\Big\|_{l_p+l_s,+}$
Negative electrode	T7	$\varepsilon_n \frac{\partial c}{\partial t} = D_{eff,n} \frac{\partial^2 c}{\partial x^2} + a_n (1-t_+) j_n \;\; \text{IC: } c\big\|_{t=0} = c_0$	$-D_{eff,s} \frac{\partial c}{\partial x}\Big\|_{l_p+l_s,-} = -D_{eff,n} \frac{\partial c}{\partial x}\Big\|_{l_p+l_s,+} \;\&\; -D_{eff,n} \frac{\partial c}{\partial x}\Big\|_{l_p+l_s+l_n} = 0$
	T8	$-\sigma_{eff,n} \frac{\partial \Phi_1}{\partial x} - \kappa_{eff,n} \frac{\partial \Phi_2}{\partial x} + \frac{2\kappa_{eff,n} RT}{F}(1-t_+) \frac{\partial \ln c}{\partial x} = I$	$-\kappa_{eff,s} \frac{\partial \Phi_2}{\partial x}\Big\|_{l_p+l_s,-} = -\kappa_{eff,n} \frac{\partial \Phi_2}{\partial x}\Big\|_{l_p+l_s,+} \quad \& \quad \frac{\partial \Phi_2}{\partial x}\Big\|_{l_p+l_s+l_n} = 0$
	T9	$\sigma_{eff,n} \frac{\partial^2 \Phi_1}{\partial x^2} = a_n F j_n$	$-\sigma_{eff,n} \frac{\partial \Phi_1}{\partial x}\Big\|_{l_p+l_s} = 0 \;\&\; \frac{\partial \Phi_1}{\partial x}\Big\|_{l_p+l_s+l_n} = -\frac{I}{\sigma_{eff,n}}$
	T10	$\frac{d}{dt} c_s^{ave} + 3\frac{j_n}{R_n} = 0 \quad \& \quad \frac{D_{s,n}}{R_n}\left(c_s^{surf} - c_s^{ave}\right) = -\frac{j_n}{5}$	$c_s^{ave}\big\|_{t=0} = c_{s,max,n}$

Table 3-3: Estimated uncertainty ranges for the four least-sensitive battery model parameters

Cycle #	D_{sp}	k_n	D_1	k_p
1	[-60%,+20%]	[-60%,+20%]	[-60%,+20%]	[-10%,+10%]
100	[-60%,+20%]	[-60%,+20%]	[-20%,+60%]	[-10%,+10%]
200	[-60%,+30%]	[-60%,+20%]	[-20%,+40%]	[-10%,+10%]
300	[-30%,+60%]	[-20%,+60%]	[-30%,+60%]	[-10%,+10%]
500	[-60%,+60%]	[-20%,+20%]	[-60%,+60%]	[-10%,+10%]
600	[-60%,+30%]	[-20%,+20%]	[-60%,+10%]	[-10%,+10%]
1000	[-20%,+60%]	[-10%,+60%]	[-20%,+60%]	[-5%,+5%]

3.9. Figures

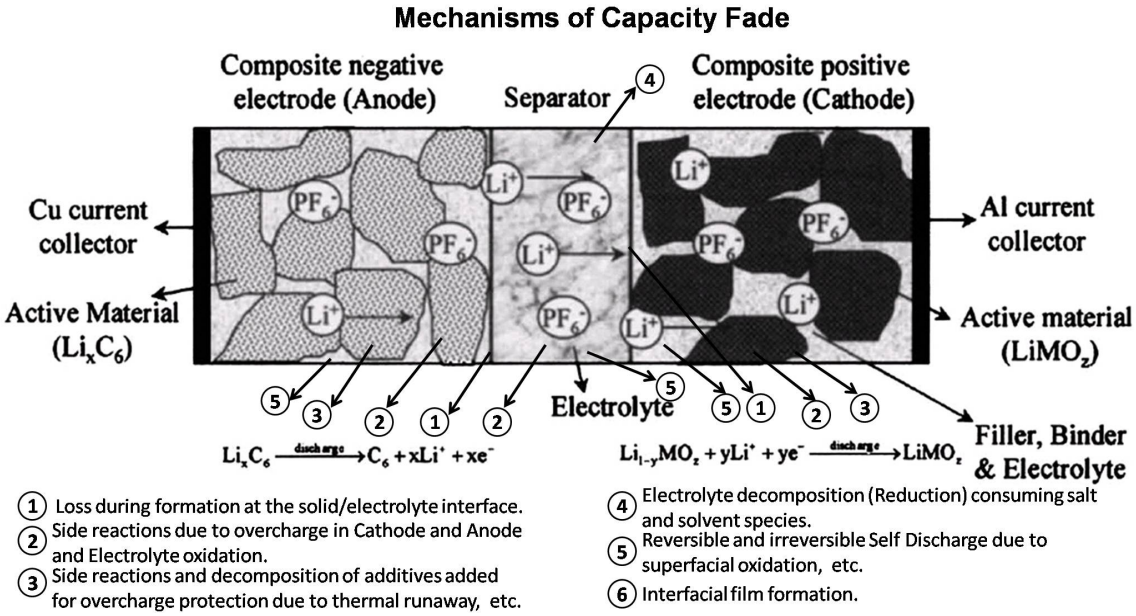

Figure 3-1: A schematic of some capacity fade mechanisms postulated in a Li-ion battery

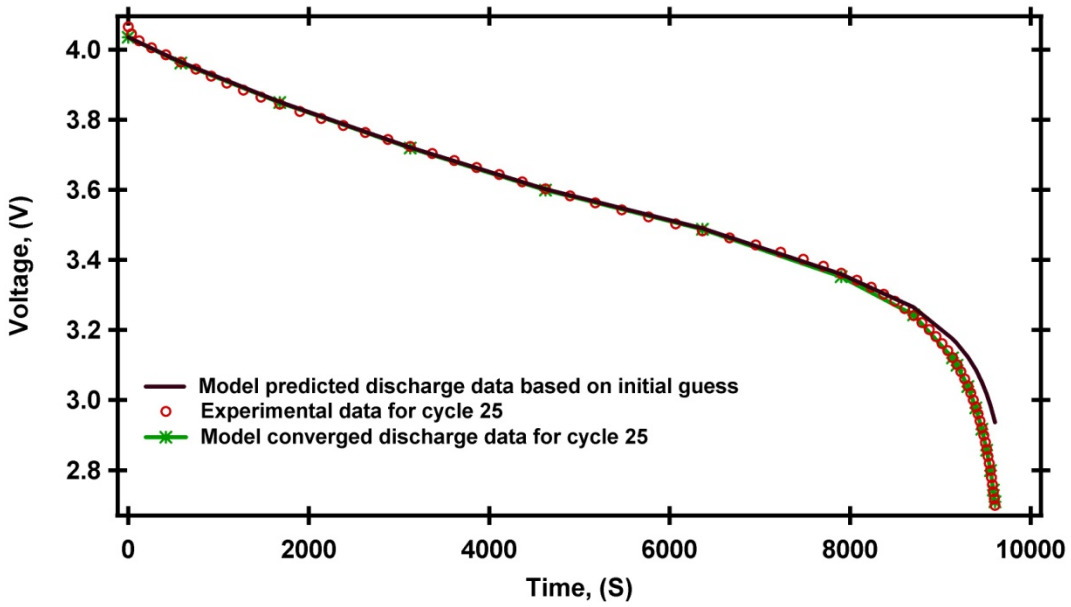

Figure 3-2: Comparison of voltage-discharge curves from the battery models with the experimental data, with five model parameters obtained from least-squares estimation applied to the experimental data for cycle 25. The voltage-discharge curve for cycle 0, which was the same for the finite-difference model and reformulated model, was used as the initial guess

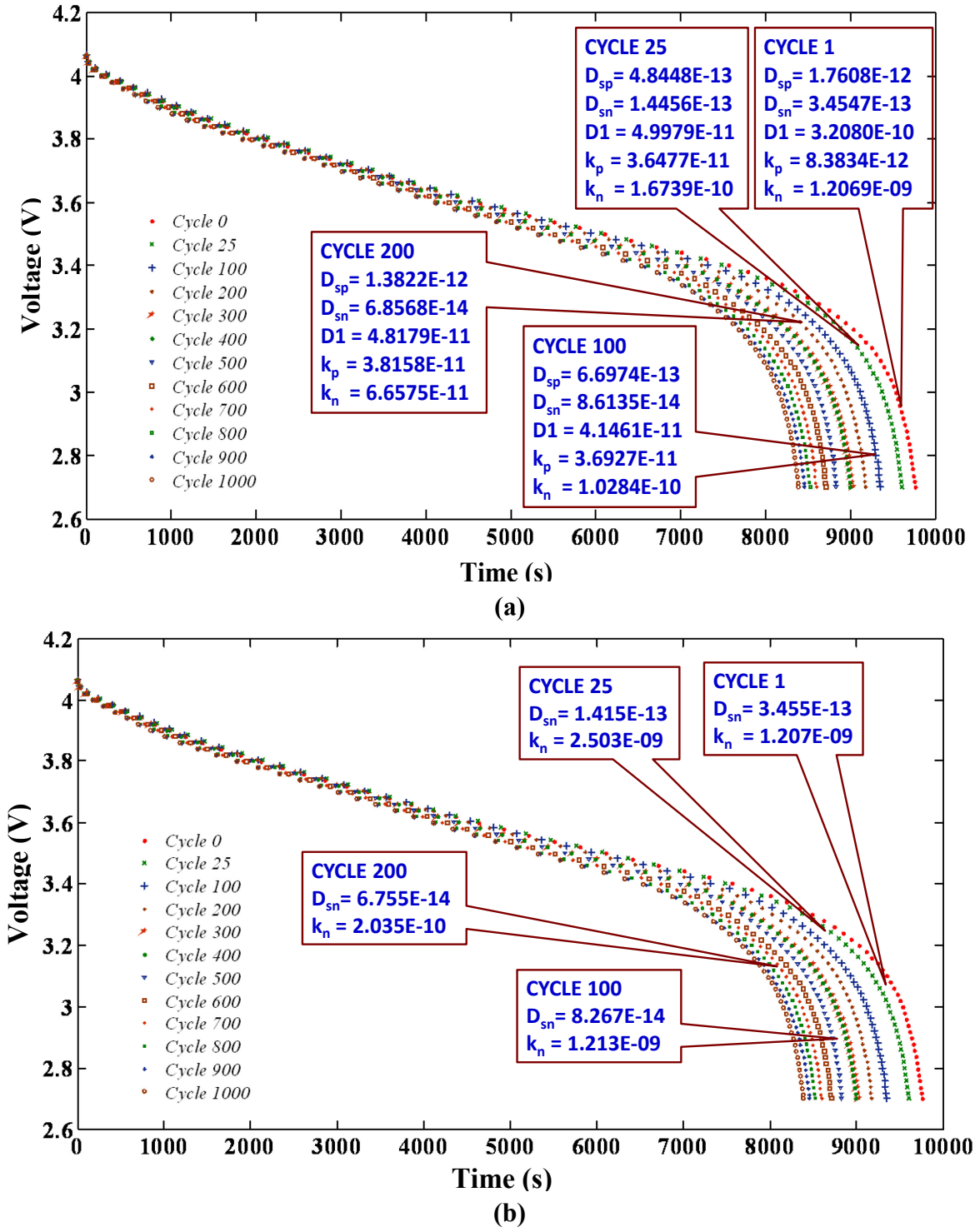

Figure 3-3: Voltage-discharge curves for the Quallion BTE cells with model parameters obtained from least-squares estimation applied to the experimental data for (a) five parameters, (b) two parameters. The voltage-discharge curves for the models fall on top of the experimental data so only one set of curves are plotted. The curves shift towards the left monotonically as the cycle # increases

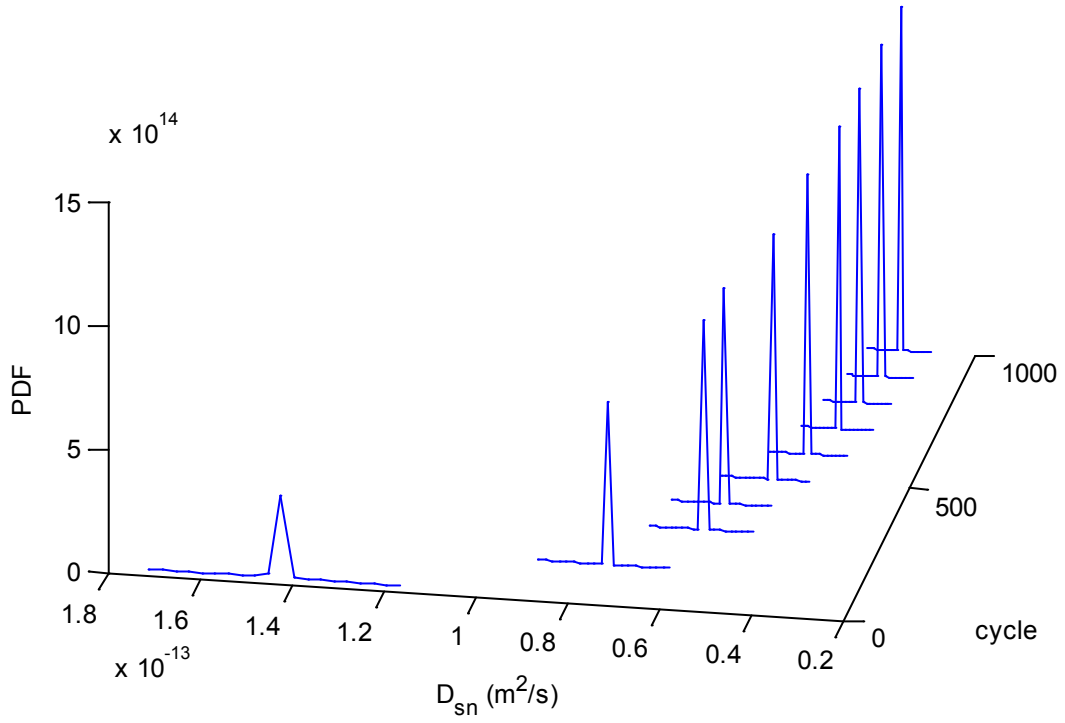

Figure 3-4: Probability density function (pdf) for the effective solid-phase diffusion coefficient Dsn at the negative electrode as a function of cycle number determined by the MCMC method

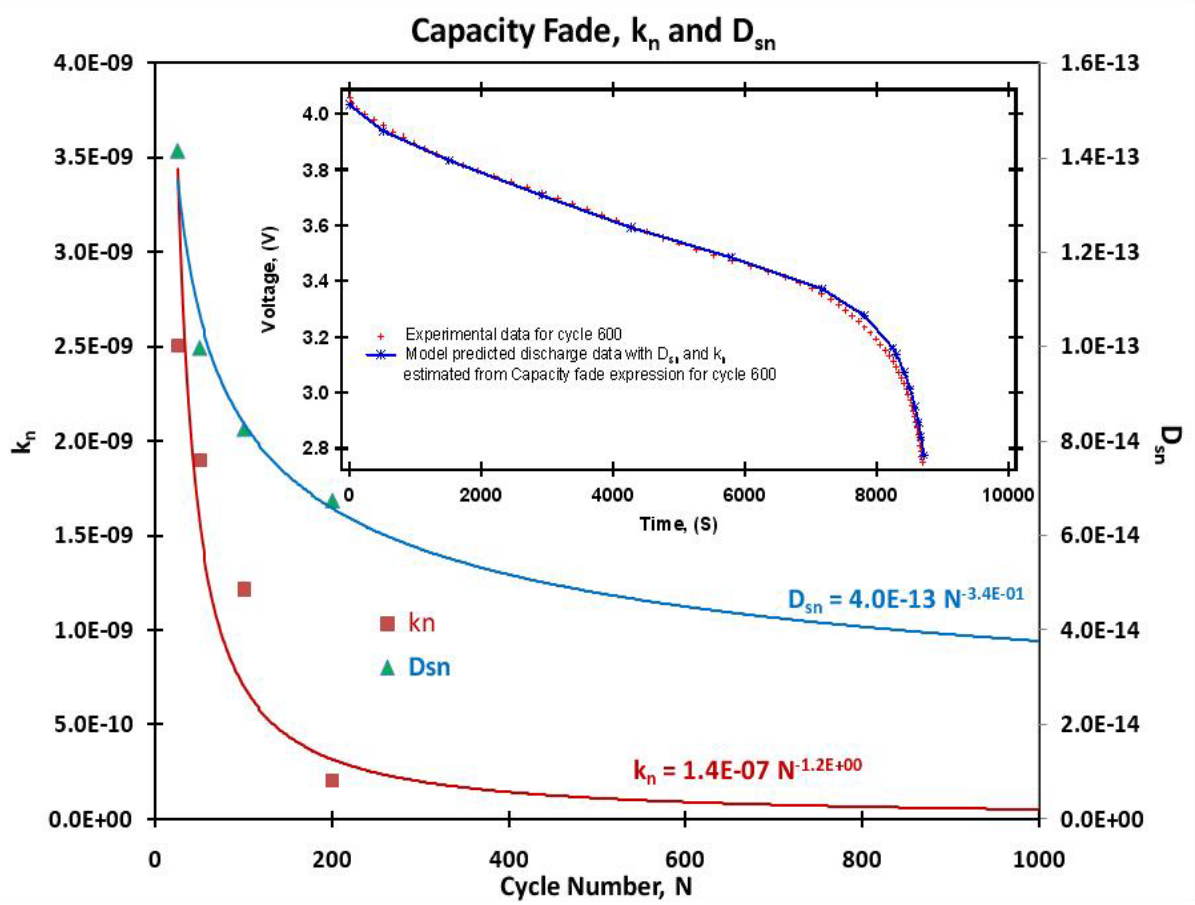

Figure 3-5: Variations in the effective solid-phase diffusion coefficient D_{sn} and electrochemical reaction rate constant k_n at the negative electrode. The inset plot compares the experimental data at cycle 600 with model prediction in which model parameters were extrapolated from power-law fits to model parameters estimated only up to cycle 200

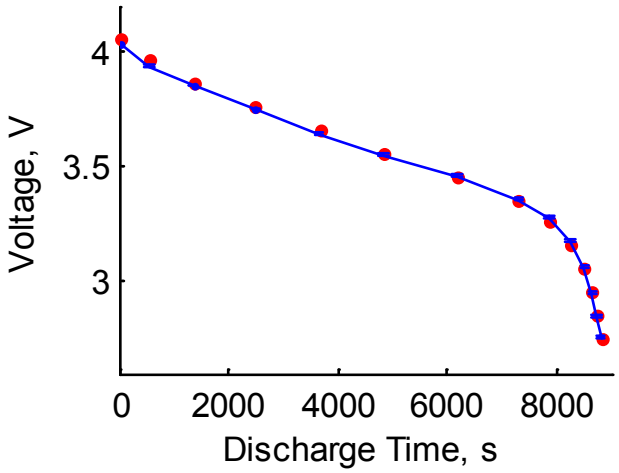

Figure 3-6: Comparison of the experimental voltage-discharge curve with the model prediction with estimated parameters for cycle 500. Each red dot is a data point, the blue line is the model prediction, and the 95% predictive intervals were computed based on the parametric uncertainties quantified by pdfs of the model parameters

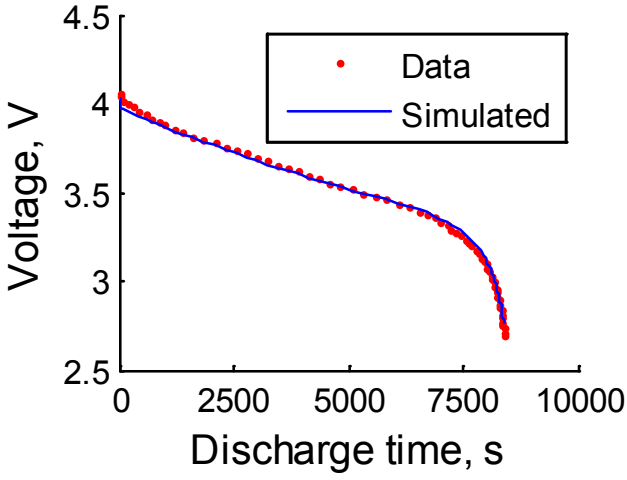

Figure 3-7: Comparison of the experimental voltage-discharge curve at cycle 1000 with the model prediction using parameter values calculated from the power law fits to model parameters fit to voltage-discharge curves for cycles 50 and 100n for n = 1,…,5. Each red dot is a data point, the blue line is the model prediction, and the 95% predictive intervals were computed based on the parametric uncertainties quantified by pdfs of the model parameters. Similar quality fits and prediction intervals occurred for the other cycles

Chapter 4 : Optimal Porosity Distribution for Minimized Ohmic Drop Across a Porous Electrode

This chapter is reproduced with permission from *J. Electrochem. Soc.*, **157** (12), A1328 (2010). The author is grateful to the co-authors for their significant contributions under sections 4.4, 4.5.1 and 4.6

4.1. Introduction

Electrochemical power sources have had significant improvements in design and operating range and are expected to play a vital role in the future in automobiles, power storage, military, and space applications. Lithium-ion chemistry has been identified as a preferred candidate for high-power/high-energy secondary batteries. Applications for batteries range from implantable cardiovascular defibrillators (ICDs) operating at 10 μA current to hybrid vehicles requiring pulses of up to 100 A. Today, the design of these systems have been primarily based on (i) matching the capacity of anode and cathode materials, (ii) trial-and-error investigation of thickness, porosity, active material, and additive loading, (iii) manufacturing convenience and cost, (iv) ideal expected thermal behavior at the system level to handle high currents, and (v) detailed microscopic models to understand, optimize, and design these systems by changing one or few parameters at a time.

Traditionally, macroscopic models have been used to optimize the electrode thickness or spatially uniform porosity in lithium-ion battery design. Many applications of mathematical modeling to design Li-ion batteries are available in the literature.[1-10] An approach to identify the optimal values of system parameters such as electrode thickness has been reported by Newman and coworkers.[2, 5-10] Simplified models based on porous-electrode theory can provide analytical

expressions to describe the discharge of rechargeable lithium-ion batteries in terms of the relevant system parameters. Newman and coworkers[2, 5-8] have utilized continuum electrochemical engineering models for design and optimization as a tool for the identification of system limitations from the experimental data. Equations were developed that describe the time dependence of potential as a function of electrode porosity and thickness, the electrolyte and solid-phase conductivities, specific ampere-hour capacity, separator conductivity and thickness, and current density. Analysis of these equations yields the values of electrode porosity and electrode thickness so as to maximize the capacity for discharge to a given cutoff potential.[2] Simplified models based on porous-electrode theory were used to describe the discharge of rechargeable lithium batteries and derive analytic expressions for the cell potential, specific energy, and average power in terms of the relevant system parameters. The resulting theoretical expressions were used for design and optimization purposes and for the identification of system limitations from experimental data.[5] Studies were performed by comparing the Ragone plots for a range of design parameters. A single curve in a Ragone plot involves hundreds of simulations wherein the applied current is varied over a wide range of magnitude. Ragone plots for different configurations are obtained by changing the design parameters (e.g., thickness) one at a time, and by keeping the other parameters at constant values. This process of generating a Ragone plot is quite tedious, and typically Ragone curves reported in the literature are not smooth due to computational constraints. Batteries are typically designed only to optimize the performance at the very first cycle of operation of the battery, whereas in practice most of the battery's operation occurs under significantly degraded conditions. Further, multivariable optimization is not computationally efficient using most first-principles models described in the literature. A reformulated model[11, 12] is sufficiently computationally efficient to enable the simultaneous

optimal design of multiple parameters over any number of cycles by including the mechanisms for capacity fade. Further, this model can be used to quantify the effects of model uncertainties and variations in the design parameters on the battery performance. Recently, such an application was reported in which the utilization averaged over 1000 cycles was maximized for a battery design obtained by simultaneous optimization of the applied current density (I) and thickness of the separator and the two electrodes (l_s, l_n, l_p) for cycle 1, and the effects of variations in these four design parameters due to imprecise manufacturing was investigated.[13] The battery design optimized for cycle 1 did not maximize the cycle-averaged utilization.

This chapter describes the method to design spatially-varying porosity profiles in porous electrodes based on simultaneous optimization applied to a porous electrode model. The next section describes the simple electrochemical porous-electrode model used in this study. Then different methods for the simultaneous optimization of model parameters are discussed. The optimization procedure used in this study is then described, followed by the results and discussion and conclusions.

4.2. Electrochemical Porous Electrode Model

Garcia et al.[14] provided a framework for modeling microstructural effects in electrochemical devices. That model can be extended to treat more complex microstructures and physical phenomena such as particle distributions, multiple electrode phase mixtures, phase transitions, complex particle shapes, and anisotropic solid-state diffusivities. As mentioned earlier, there are several treatments for dealing with the microstructure of the porous electrodes in Li-ion batteries. However, there is no mention in the literature of using these models in optimization algorithms to extract optimal values of design parameters and hence perform model-based design for porous electrodes. As an initial investigation into the potential of such an approach, we employ a simple

model for a porous electrode with parameters matched to that of a cathode of a Li-ion battery to verify the feasibility of simultaneous optimization of design parameters and to investigate whether employing more detailed models for optimization is worthwhile.

This chapter considers the optimization of a single porous positive electrode, where the electrode has the current collector at one end ($x = 0$) and electrolyte separator at the other end ($x = l_p$). The expressions for current in the solid phase (i_1) and electrolyte phase (i_2) are given by[1]

$$i_1 = -\sigma(x)\frac{d\Phi_1}{dx} \quad [4.1]$$

$$i_2 = -\kappa(x)\frac{d\Phi_2}{dx} \quad [4.2]$$

where σ is the electrical conductivity, κ is the ionic conductivity, and Φ_1 and Φ_2 are the solid-phase and electrolyte-phase potentials, respectively. The total applied current density across the cross-section of the electrode is equal to the sum of the solid-phase and liquid-phase current densities:

$$i_{app} = i_1 + i_2 \quad [4.3]$$

The electrochemical reaction occurs at the solid-liquid interface with the solid-phase current (i_1), which is assumed to be related to the distance across the electrode (x) by linear kinetics:

$$\frac{di_1}{dx} = a(x)i_0\frac{F}{RT}(\Phi_1 - \Phi_2) \quad [4.4]$$

with the active surface area given by

$$a(x) = \frac{3\left(1-\varepsilon(x)\right)}{R_p} \quad [4.5]$$

R_p is the particle radius of active materials in the porous electrode, and $\varepsilon(x)$ is the spatially-varying porosity in the electrode. The electrical and ionic conductivities are related to the spatially-varying porosity by

$$\sigma(x) = \sigma_0 \left(1 - \varepsilon(x)\right)^{brugg} \quad [4.6]$$

$$\kappa(x) = \kappa_0 \varepsilon(x)^{brugg} \quad [4.7]$$

where *brugg* is the Bruggeman coefficient to account for the tortuous path in the porous electrode. The boundary conditions for solution of these equations are

$$\begin{aligned} \Phi_1\big|_{x=0} &= 1 \\ \Phi_2\big|_{x=l_p} &= 0 \\ i_1\big|_{x=l_p} &= 0 \end{aligned} \quad [4.8]$$

The ohmic resistance of this electrode is obtained by

$$\psi = \frac{\Phi_1\big|_{x=0} - \Phi_2\big|_{x=l_p}}{i_{app}} \quad [4.9]$$

$$i_{app} = -\sigma(x) \frac{d\Phi_1}{dx}\bigg|_{x=0} \quad [4.10]$$

The above equations apply for any continuous or discontinuous functional form for $\varepsilon(x)$ and can be extended to more detailed micro-scale models for the conductivities and transport parameters as a function of porosity. Garcia et al.[14] considered detailed microstructure while modeling and identifying porosity or particle size variations in the electrodes to maximize performance. Previous efforts have considered atomistic simulations of batteries,[15] microstructural simulations,[16] and modeling the relationships between the properties and microstructure of the materials within packed multiphase electrodes. In this manuscript the robustness of its optimal design results to the use of a simple model in the optimization of the

porous electrode is taken into account by analyzing the effects of variations in the model parameters.

The electrochemical modeling equations are usually solved by setting the applied current and computing the voltage, or vice versa. Many practical devices operate at constant current or constant power mode. It is important to realize that the capacity of each device is limited by the state variables and theoretical capacity of the material. To solve the mathematical model for a practical electrochemical device, it is necessary to obtain the physically realizable current value to be applied to or drawn from the electrode.

4.2.1. Constant-Current Method

For solving this model for constant current, the constant current i_{app} would be set and the modeling equations simulated for the variables like Φ_1, Φ_2, and i_1 as given in equations [4.1] to [4.7]. Equation [4.8] gives the boundary conditions for the constant current method. Then the resistance (ψ) is computed using the output equation [4.9]. This procedure is easy to implement and the model equations are straightforward to simulate. However, the applied fixed current may not be commensurate with the capacity of the given battery and there is a chance of obtaining physically inconsistent results such as a predicted potential of −100 or +1000 V. To avoid this potential error, the constant-potential method has been used as described in next subsection.

4.2.2. Constant-Potential Method

To avoid the shortcoming of the constant-current method, the constant-potential method was used in this study. In this method, the potential (Φ_1, Φ_2) is set and the current is treated as the output. This is done by solving i_{app} as the unknown variable in the model equations [4.1] to [4.7]. Then the resistance (ψ) is computed using the output equation [4.9]. The new boundary conditions are

$$\Phi_1\big|_{x=0} = 1$$
$$\Phi_2\big|_{x=l_p} = 0$$
$$i_1\big|_{x=l_p} = 0 \qquad [4.11]$$
$$i_{app} = -\sigma(x)\frac{d\Phi_1}{dx}\bigg|_{x=0}$$

This approach incorporates one additional boundary condition for describing the relationship of the applied current with the state variables. The advantage of this procedure is that the current has been determined using the state variables of the battery instead of being fixed to a preset number by the modeler. This computationally robust approach ensures that the voltage and current are at physically consistent values.

4.3. Optimization Procedure

A general formulation for the model-based optimal design of a system is[22]

$$\min_{\mathbf{z}(x),\mathbf{u}(x),\mathbf{p}} \Psi \qquad [4.12]$$

$$\text{such that } \frac{d}{dx}\mathbf{z} = \mathbf{f}(\mathbf{z}(x),\mathbf{y}(x),\mathbf{u}(x),\mathbf{p}), \qquad \mathbf{f}(\mathbf{z}(0)) = 0, \qquad \mathbf{g}(\mathbf{z}(1)) = 0, \qquad [4.13]$$

$$\mathbf{g}(\mathbf{z}(x),\mathbf{y}(x),\mathbf{u}(x),\mathbf{p}) = 0, \qquad [4.14]$$

$$\mathbf{u}_L \le \mathbf{u}(x) \le \mathbf{u}_U, \qquad \mathbf{y}_L \le \mathbf{y}(x) \le \mathbf{y}_U, \qquad \mathbf{z}_L \le \mathbf{z}(x) \le \mathbf{z}_U, \qquad [4.15]$$

where Ψ is the battery design objective to be minimized,[17] $\mathbf{z}(x)$ is the vector of differential state variables, $\mathbf{y}(x)$ is the vector of algebraic variables, $\mathbf{u}(x)$ is the vector of control variables, and $\mathbf{p}$ is the vector of design parameters. Different methods are available for solving constrained optimization problems, which include (i) variational calculus, (ii) Pontryagin's maximum principle, (iii) control vector iteration (CVI), (iv) control vector parameterization (CVP), and (v) simultaneous nonlinear programming.[18]

4.3.1. Complexities of Optimization for Battery Models

For a pseudo-2D battery model with 12 PDEs, assume that the cathode, separator, and anode are discretized into 50 equally-spaced node points in x and 20 nodes in r for each x. For the three regions (cathode, separator, and anode) the model will have 2400 DAEs, which includes 50×20 = 1000 equations each for the cathode and anode for the solid phase, 50 differential equations for the electrolyte concentration, 50 algebraic equations for the electrolyte potential (potential in the electrolyte phase), and 50 algebraic equations for the solid-phase potential each for the cathode and anode. For the same number of node points in x, the separator has 50 differential equations for the electrolyte concentration and 50 algebraic equations for the electrolyte potential. In total, the number of DAEs to solve becomes 2×1000 + 2×150 + 100 = 2400. Simultaneous optimization of many design valuables for a highly stiff system with 2400 DAEs is computationally expensive.

Indirect dynamic optimization methods such as variational calculus and Pontryagin's maximum principle method result in boundary value problems that are very difficult to solve for large systems of highly stiff nonlinear DAEs.[19] Direct methods for the solution of dynamic optimizations have gained prominence in the past few decades, in which the optimal solution is achieved by converting the optimization problem into nonlinear program using such methods as CVI, CVP, and simultaneous nonlinear programming.[20] Control vector parameterization is one of the commonly used methods and is the easiest method to implement. In the context of this particular application, the control variable $\mathbf{u}(x)$ is parameterized by a finite number of parameters, typically as a polynomial or piecewise-linear function or by partitioning its values over space, and the resulting nonlinear program is solved numerically. Most numerical optimization algorithms utilize an analytically or numerically determined gradient of the optimization objective and constraints to march towards improved values for the optimization variables in the

search space. While advances in simultaneous discretization have been made in the field of global dynamic optimization,[21] today's algorithms are still too computationally expensive to be used in electrochemical processes, which are usually highly stiff with highly nonlinear kinetics and requires adaptive time-stepping, stiff solvers, etc. The simultaneous simulation-optimization approach,[18] which fixes the time or independent variable discretization *a priori*, is not computationally efficient for highly stiff DAEs such as arise in electrochemical processes. For example, for battery models with 2400 DAEs, the simultaneous simulation-optimization approach may result in millions of equations in the resulting nonlinear program. Based on our experience, battery models may not converge easily with direct discretization schemes in time.

In CVP, as the number of intervals increases, the number of equations increases tremendously and makes optimization computationally very expensive. Hence the fastest and most efficient model and code is recommended for CVP or any of the optimization methods. In this chapter, as a first step, a simple model used that represents the essential dynamics of a porous electrode used in a lithium-ion battery. This model along with CVP makes the optimization computationally efficient and enables the implement of additional runs to evaluate the global optimality of the computed design variables.

4.4. Optimization using CVP

In this chapter, CVP is used to simultaneously optimize multiple parameters describing a spatial profile of porosity of an electrode in a lithium-ion battery. The numerical optimization was carried out using Marquardt's method,[22] in which new parameter values for the next iteration are related to the gradient multiplied by the old values of the design parameters. The numerical algorithm was repeated until a pre-specified tolerance on the change in the design parameters was met.

In this formulation, the control variable (i.e., porosity) is partitioned across the electrode length. In each partition, the modeling equations [4.1] to [4.11] are solved as a function of porosity. The boundary conditions at each partition are matched using the flux balance of the species. The number of equations is directly proportional to the number of partitions. The number of boundary conditions will also increase with the number of equations and partitions. The optimization objective was to minimize the ohmic resistance (ψ) across the electrode thickness in Eq. (1) for the control variable $u(x) = \varepsilon(x)$ subject to the constraints

a) $0 < \varepsilon(x) < 1$

b) Average $\{\varepsilon_i\} < 0.4$, where $i = 1, \ldots, N$ (when a specific amount of active material is desired)

c) Eqs. (1) to (11), where $\mathbf{y}(i) = [\Phi_{(1,i)}, \Phi_{(2,i)}, i_{(1,i)}]$ and $0 \le x \le l_p$

$$i_{(1,i)} = -\sigma_i \frac{\partial \Phi_{(1,i)}}{\partial x}$$

$$i_{(2,i)} = -\kappa_i \frac{\partial \Phi_{(2,i)}}{\partial x}$$

$$\frac{\partial i_{(1,i)}}{\partial x} = a_i i_0 \frac{F}{RT}(\Phi_{(1,i)} - \Phi_{(2,i)})$$

$$a_i = \frac{3(1-\varepsilon_i)}{R_p}$$

d) Boundary conditions for accommodating the partitions across the electrode are

$$\Phi_{(1,i)}\Big|_{x=l_p/N} = \Phi_{(1,i+1)}\Big|_{x=0}$$

$$\Phi_{(2,i)}\Big|_{x=l_p/N} = \Phi_{(2,i+1)}\Big|_{x=0}$$

$$i_{(1,i)}\Big|_{x=l_p/N} = i_{(1,i+1)}\Big|_{x=0}$$

where i indicates the i^{th} partition and $x = 0$ and $x = l_p/N$ indicate the starting and ending spatial boundaries of the i^{th} partition. The non-negativity constraint is imposed on the porosity and the average-value constraint is imposed when a specific amount of active material is desired in the electrode. The ohmic resistance is calculated as a function of the porosity from the modeling equations. The model equations along with fixed boundary conditions and boundary conditions arising from CVP were solved using a Boundary Value Problem (BVP) solver. Table 1 shows the base set of parameters used for the simulation of the model equations [4.1] to [4.11] at various conditions. All simulations are performed using Maple® 13's BVP solver using a personal computer with a 3 GHz Intel® Core 2 Duo processor and 3.25 GB of RAM.

4.5. Results and Discussion

4.5.1. Optimization Results for Uniform Porosity

Figure 4-1 shows the variation in the total resistance across the porous electrode as a function of spatially-uniform porosity obtained by brute-force gridding of the porosity, which shows a clearly identifiable optimal porosity of ~0.2. The same results for the $N = 1$ stage can be obtained using an analytical solution commonly used for porous electrodes and as discussed in the appendix. Operating with the porous electrode at this optimum porosity should provide the best performance for a system described by the model [4.1] - [4.11]. Figure 4-2a shows the convergence of the numerical optimization to the globally optimal value of the spatially-uniform electrode porosity. This plot was constructed by optimizing the electrochemical model described in Section 4.2 starting at three different initial guesses (the third guess being the optimal value obtained in Figure 4-1) for the electrode porosity. The final converged value for the electrode porosity was the same for many different initial guesses (two of which are shown in Figure 4-2a). Figure 4-2b shows the convergence of the ohmic resistance across the electrode to the same

single optimal value. A very low resistance was achieved by using the globally optimal value for the porosity of the electrode. Significant improvements in terms of performance were achieved by numerical optimization; the optimal design is about 15% more efficient in comparison with an average value of 0.4 used in practice for the electrode porosity for this chemistry.

4.5.2. Optimization Results for Graded Porosity

Numerical optimization was performed for a porous electrode with a graded porosity, that is, porosity that varies as a function of distance across the electrode. A recent patent (US patent 7553584) proposed the use of graded porosity described by a functional form for betterment of the performance of the porous electrode. Functional forms of porosity may be implemented for theoretical studies but to practically fabricate porous electrodes with smoothly varying porosity as a function of distance is difficult. A more practical way of representing graded porosity was applied here. The porosity profile was divided into N optimization zones, with constant porosity within each zone (see Figure 4-3). For $N = 5$, the resistance across the electrode is minimized when the porosity is higher towards the electrode-separator interface (see Figure 4-4), to have more electrolyte solution in the porous matrix. The optimal profile shows a significant decrease in pore volume at the other end, at the electrode-current collector interface. This optimization procedure shows improvement in electrode performance of 17.2% compared to the base-case spatially-uniform porosity of 0.4. The spatially-varying optimized electrode porosity has 4% better performance than the optimal spatially-uniform porosity ($\varepsilon \sim 0.2$, see Figure 4-1) for the same chemistry. Porous electrodes with more complicated chemistry models or different chemistry models, and optimization with additional physical constraints on the design, can have different performance improvements when using spatially-varying porosity. Increasing the value of the number of zones N above 5, while being more difficult to fabricate, does not show much

improvement in the performance. For instance, an improvement of 0.1% was obtained for $N = 12$ compared to $N = 5$. The choice of $N = 5$ provides a good tradeoff between optimality and manufacturability.

Now consider the same optimal design problem but with the additional constraint of having a specified amount of active material in the electrode, which is equivalent to having a fixed value for the porosity averaged across the electrode. For a fixed average porosity $\bar{\varepsilon} = 0.3$, the performance improvement is 15% compared to the base case, while having an optimal porosity profile that is qualitatively similar to that without the average porosity constraint (compare Figure 4-4a and Figure 4-5a). A qualitatively similar optimal porosity profile is obtained for a fixed average porosity $\bar{\varepsilon} = 0.5$, while providing a performance improvement of 33% over the base case.

Figure 4-6 shows the applied current profile across the electrode for the optimized and base-case design. The optimized current at the electrode-current collector interface is higher in magnitude due to lower resistance. The spatial variation in the electrolyte-phase potentials follow a similar qualitative trend but are very different quantitatively (see Figure 4-7). The solid-phase potential in both cases does not show much variation across the electrode (see Figure 4-8). The net potential drop ($\Phi_1 - \Phi_2$) at the electrode-current collector interface is greater in the base case compared to the optimized case, indicative of the lower resistance inside the cell with optimized porosity profile.

Due to limited manufacturing precision and capacity fade, model parameters will vary somewhat from one electrode to the next. The importance of quantifying the effects of such uncertainties on the performance of nano- and micro-structured materials is well established[23] it has been shown for many materials systems that most to all of the benefits of optimization can be

lost when uncertainties are ignored.[24,25] The uncertainties in the model parameters were described by Gaussian distributions with standard deviations that are 10% of the nominal parameter values. The probability distribution functions (pdfs) for the ohmic resistance for spatially-uniform electrode porosities indicate that the optimized design is more robust to uncertainties in comparison to a non-optimized porosity, with a reduction in variance for the optimal design of ~40% (see Figure 4-9). The design with the optimized spatially-varying porosity is slightly more robust, with a reduction of variance of ~43% compared to a non-optimized porosity (see Figure 4-10). The robustness could be further enhanced by explicitly including uncertainty quantification into the optimization formulation.[26]

4.6. Conclusions

Model-based optimization was applied to the design of a spatially-varying porosity profile in a next-generation porous electrode to minimize its ohmic resistance. The implementation of control vector parameterization is demonstrated for a simple porous electrode model. The parameters used for the electrode were based on the cobalt oxide chemistry, generally used in commercial lithium-ion batteries. The solid-phase intercalation phenomenon is not included in this work at this stage and is typically an important limiting factor for cobalt oxide and other intercalation electrodes. The optimal design of graded porosity was found to reduce the ohmic resistance by 15%-33% without increasing the amount of active material. The optimal porosity grading was predicted to have 40% lower variation in the ohmic resistance to variations in model parameters due to manufacturing imprecision or capacity fade. The results suggest the potential for the simultaneous model-based design of electrode material properties that employ more detailed physics-based first-principles electrochemical engineering models to determine optimal design values to manufacture and evaluate experimentally. Further investigations into a whole-

cell battery model may lead to engineering design alternatives that better satisfy energy and power requirements for emerging applications for batteries in vehicles, satellites, and in the military.

4.7. Appendix

For a porous electrode with linear kinetics, Eqs. [4.1]-[4.11] can be integrated analytically as

$$\begin{aligned} i_1 &= a\cosh\left(\nu\frac{x}{l_p}\right)+b\sinh\left(\nu\frac{x}{l_p}\right)+\frac{\sigma i_{app}}{\sigma+\kappa} \\ \Phi_1 &= a_1\cosh\left(\nu\frac{x}{l_p}\right)+b_1\sinh\left(\nu\frac{x}{l_p}\right)+c+\frac{i_{app}x}{\sigma+\kappa} \\ \Phi_2 &= a_2\cosh\left(\nu\frac{x}{l_p}\right)+b_2\sinh\left(\nu\frac{x}{l_p}\right)+c+\frac{i_{app}x}{\sigma+\kappa} \end{aligned} \tag{A.1}$$

There are only 3 constants of integration (a, b, c). The coefficients a_1, b_1, a_2, b_2 depend on these three constants and other model parameters. With the boundary conditions, the resistance can be obtained as

$$Z=\frac{l_p\left(1+\dfrac{2+\left(\dfrac{\kappa}{\sigma}+\dfrac{\sigma}{\kappa}\right)\cosh(\nu)}{\nu\sinh(\nu)}\right)}{\kappa+\sigma} \tag{A.2}$$

where $\nu=l_p\sqrt{\dfrac{(\kappa+\sigma)ai_0F(\alpha_1+\alpha_2)}{\kappa\sigma RT}}$

This analytical solution has been previously used in the literature.[2] Similar equations for Φ_1, Φ_2, and i_2 can be obtained for any number of stages, but the constants are too messy to be reported here in closed form. The constants are found by matching the dependent variables at the interfaces. The numerical solution of the original BVPs is used for the results reported in the chapter, as the constants for the analytical solutions cannot be conveniently used for optimization

purposes. In addition, the results obtained for the numerical solution can be conveniently used for nonlinear kinetics as a starting point or initial guess.

4.8. References

1. M. Doyle, T. F. Fuller and J. Newman, *J Electrochem Soc*, **140**, 1526 (1993).
2. W. Tiedemann and J. Newman, *J Electrochem Soc*, **122**, 1482 (1975).
3. T. F. Fuller, M. Doyle and J. Newman, *J Electrochem Soc*, **141**, 1 (1994).
4. T. F. Fuller, M. Doyle and J. Newman, *J Electrochem Soc*, **141**, 982 (1994).
5. M. Doyle and J. Newman, *J Power Sources*, **54**, 46 (1995).
6. M. Doyle and J. Newman, *Electrochim Acta*, **40**, 2191 (1995).
7. J. Newman, *J Electrochem Soc*, **142**, 97 (1995).
8. V. Srinivasan and J. Newman, *J Electrochem Soc*, **151**, A1530 (2004).
9. J. Christensen, V. Srinivasan and J. Newman, *J Electrochem Soc*, **153**, A560 (2006).
10. S. Stewart, P. Albertus, V. Srinivasan, I. Plitz, N. Pereira, G. Amatucci and J. Newman, *J Electrochem Soc*, **155**, A253 (2008).
11. V. R. Subramanian, V. Boovaragavan and V. D. Diwakar, *Electrochemical and Solid-State Letters*, 255 (2007).
12. V. R. Subramanian, V. Boovaragavan, V. Ramadesigan and M. Arabandi, *J Electrochem Soc*, **156**, A260 (2009).
13. V. R. Subramanian, V. Boovaragavan, V. Ramadesigan, K. Chen and R. D. Braatz, in *Design for energy and the environment : proceedings of the Seventh International Conference on the Foundations of Computer-Aided Process Design*, M. M. El-Halwagi and A. A. Linninger Editors, p. 987 CRC Press, Boca Raton (2009).
14. R. E. Garcia, Y. M. Chiang, W. C. Carter, P. Limthongkul and C. M. Bishop, *J Electrochem Soc*, **152**, A255 (2005).
15. G. Ceder, M. K. Aydinol and A. F. Kohan, *Comp Mater Sci*, **8**, 161 (1997).
16. N. Akaiwa, K. Thornton and P. W. Voorhees, *J Comput Phys*, **173**, 61 (2001).
17. Any maximization can be written as a minimization by multiplication of the objective by minus one.
18. S. Kameswaran and L. T. Biegler, *Comput Chem Eng*, **30**, 1560 (2006).
19. O. von Stryk and R. Bulirsch, *Annals of Operations Research*, **37**, 357 (1992).
20. M. Schlegel, K. Stockmann, T. Binder and W. Marquardt, *Comput Chem Eng*, **29**, 1731 (2005).
21. A. B. Singer and P. I. Barton, *J Global Optim*, **34**, 159 (2006).
22. D. W. Marquardt, *SIAM Journal on Applied Mathematics*, **11**, 431 (1963).
23. R. D. Braatz, R. C. Alkire, E. Seebauer, E. Rusli, R. Gunawan, T. O. Drews, X. Li and Y. He, *J Process Contr*, **16**, 193 (2006).
24. Z. K. Nagy and R. D. Braatz. *IEEE Trans Contr Syst Tech*, **11**, 494 (2003).
25. Z. K. Nagy and R. D. Braatz, *J. Process Contr*, **17**, 229 (2007).
26. Z. K. Nagy and R. D. Braatz, *J Process Contr*, **14**, 411 (2004).

4.9. Tables

Table 4-1: List of parameters used for the simulation ($LiCoO_2$ chemistry).

Parameter	Symbol	Parameter values
Electrical conductivity	σ_0	100 S/m
Bruggeman Coefficient	*brugg*	1.5
Ionic conductivity	κ_0	20 S/m
Particle radius of the active materials	R_p	5.0×10^{-6} m
Length of the electrode	l_p	8×10^{-5} m
Faraday constant	F	96,487 C/mol
Ideal gas constant	R	8.314 J/(mol·K)
Temperature	T	298.15 K
Exchange current density	i_0	1×10^{-3} A/m^2

4.10. Figures

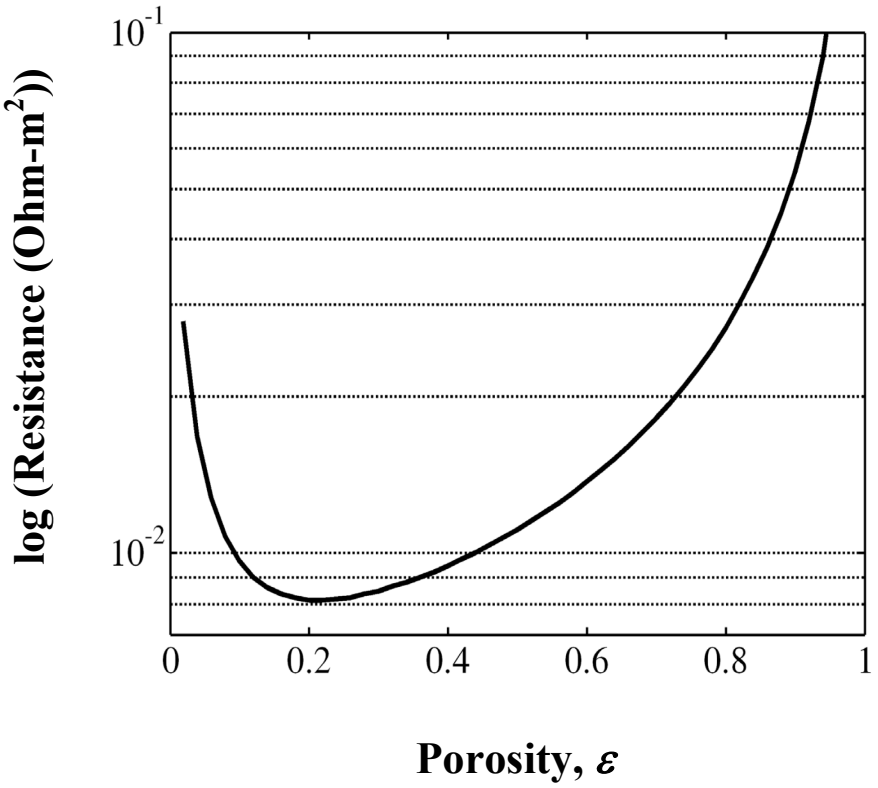

Figure 4-1: Resistance versus porosity, ε. The plot was constructed by computing the resistance from the model equations [4.5]-[4.11] *for each value of spatially-uniform porosity between 0 and 1. Note that the unit of resistance reported is Ohm-m^2 and can be converted to Ohm-m (typically reported in the literature), by dividing with the thickness of the electrode. The choice of the unit does not affect the optimization results*

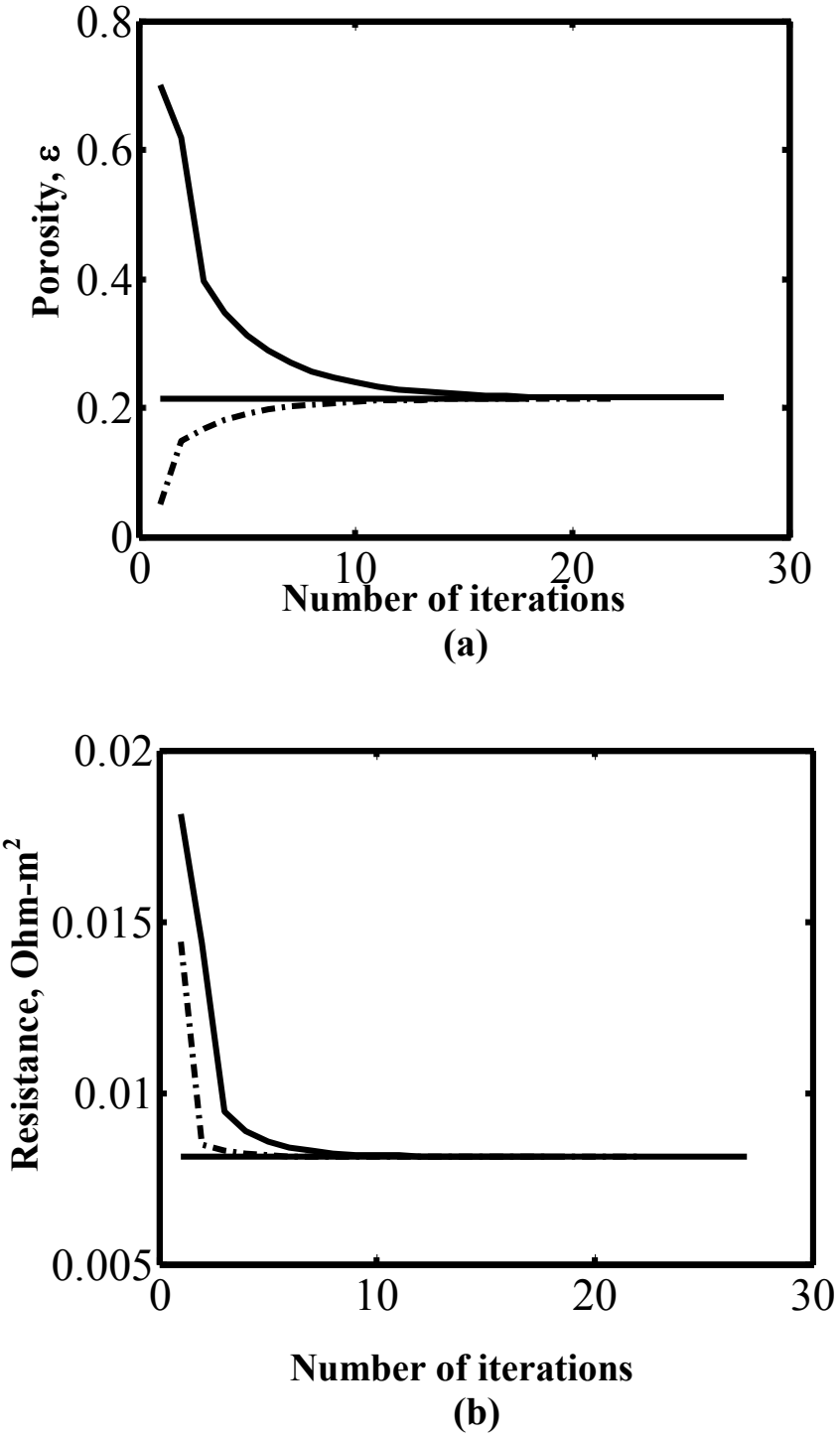

Figure 4-2: (a) Convergence to the optimal spatially-uniform porosity ε starting from different initial guesses for the porosity; (b) corresponding convergence of the ohmic resistance

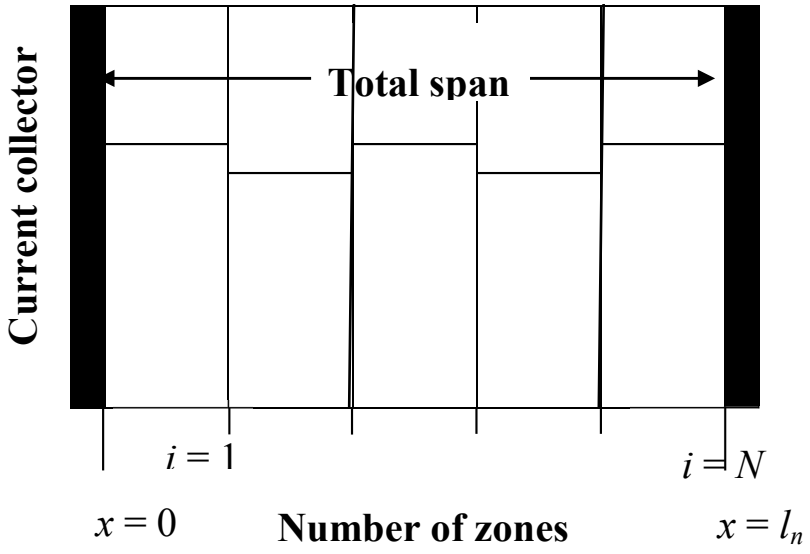

Figure 4-3: Schematic of an electrode of a lithium-ion battery divided into N optimization zones

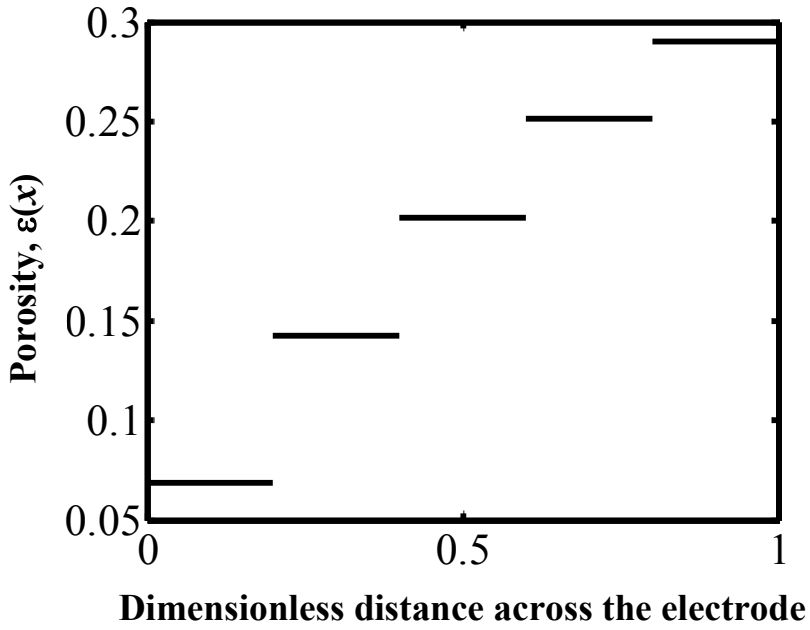

Figure 4-4: Optimal porosity profile for N = 5 optimization zones

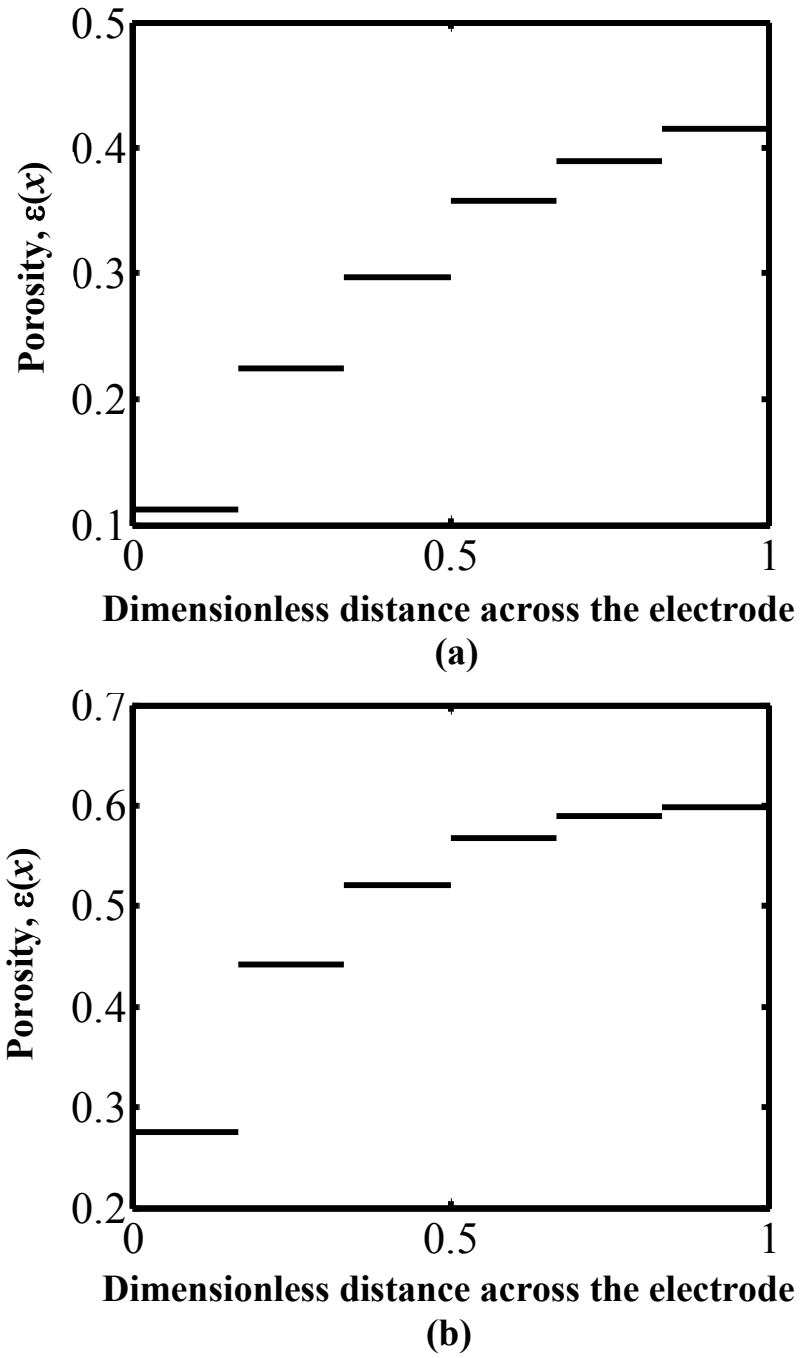

Figure 4-5: Optimum porosity profile for N = 6 optimization zones for a fixed average porosity of (a) 0.3 and (b) 0.5

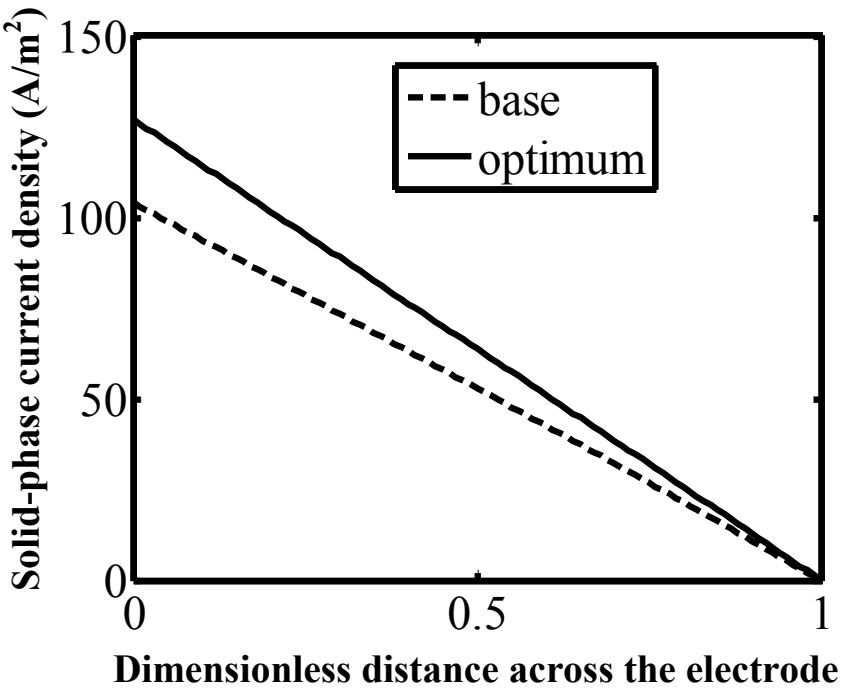

Figure 4-6: Solid phase current profile across the electrode in base-case and optimized designs

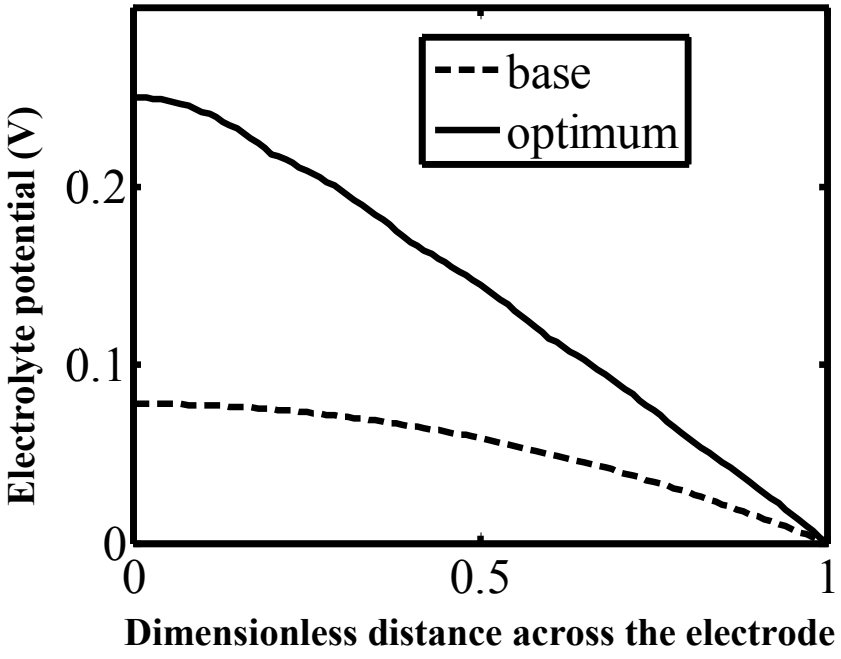

Figure 4-7: Electrolyte-phase potential profile in base-case and optimized designs

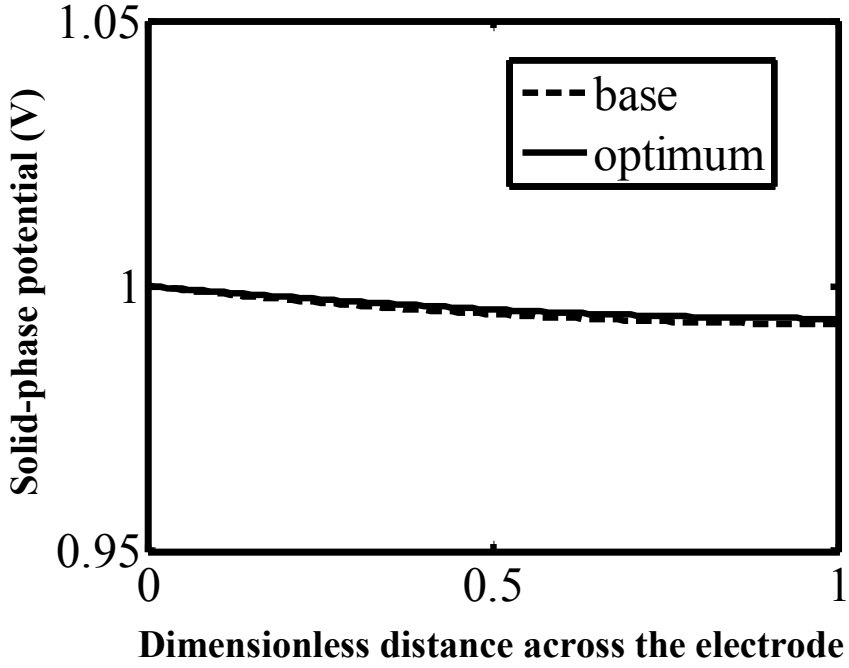

Figure 4-8: Solid-phase potential profile in base-case and optimized designs

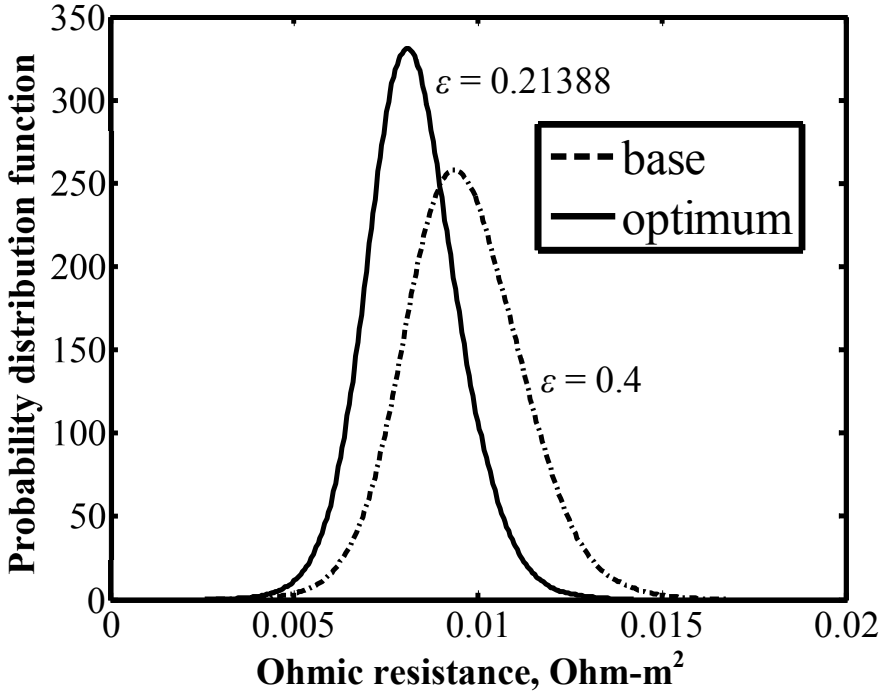

Figure 4-9: Probability distribution function for the ohmic resistance for electrodes with spatially-uniform porosities of ε = 0.4 (base) and obtained by optimization (ε = 0.21388)

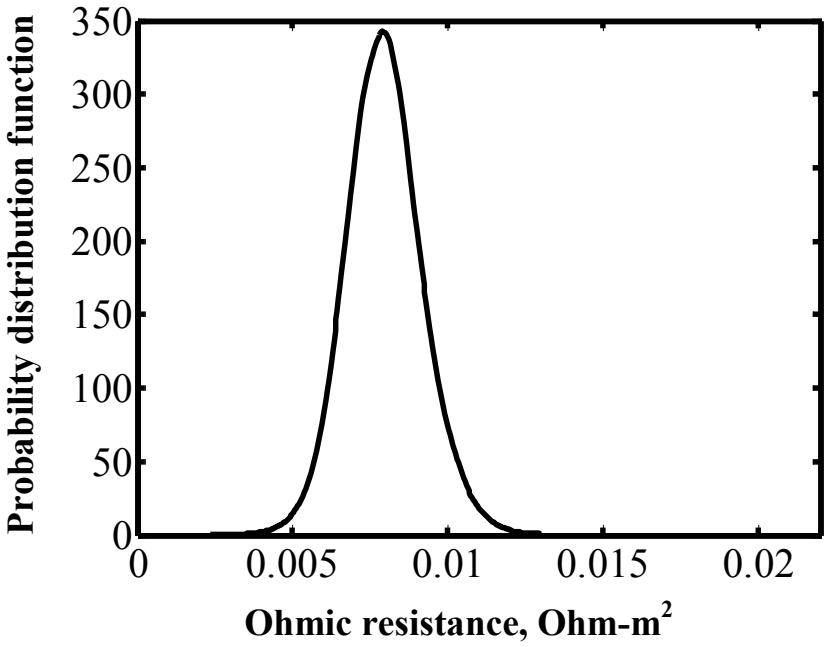

Figure 4-10: Probability distribution function for the ohmic resistance for an electrode with optimal spatially-varying porosity

Chapter 5 : Optimal Charging Profile for Lithium-ion Batteries to Maximize Energy Storage in Limited Time

5.1. Introduction

Electrochemical power sources such as lithium-ion batteries have had significant improvements in design, modeling, and operating range and are expected to play a vital role in the future in automotive, power storage, military, and space applications. Lithium-ion chemistry has been identified as a preferred candidate for high-power/high-energy secondary batteries. Applications for batteries range from implantable cardiovascular defibrillators (ICDs) operating at 10 μA current to hybrid vehicles requiring pulses of up to 100 A. Problems that persist with lithium-ion batteries include underutilization, capacity fade, and thermal runaway caused by operation outside the safe window.[1] The capability of a battery to store energy reduces with number of cycles due to formation of undesirable side reaction products during the discharging and charging process. To optimally use resources, an important problem is to maximize the stored energy in the battery.

In many applications, the ability to recharge quickly and efficiently is a critical requirement for a storage battery. In a Li-ion battery, during charging, the lithium ions first diffuse out of the lithium-metal oxide in the positive electrode, migrate through the electrolyte, and then diffuse into the carbon matrix in the negative electrode. Various processes occur simultaneously, which reduces the efficiency of the charging process and results in reducing the capacity to store energy in these secondary batteries.

The processes inside the battery are highly nonlinear and interactive in nature, and depend on various processes such as kinetics of the reactions, temperature of the reactions, rate of the diffusion of lithium ions, etc. A valuable objective is to characterize these nonlinearities and to

regulate the various micro-scale processes in an optimal way to enhance the energy-storing capacity of the battery. Achieving this objective is challenging due to the meager knowledge on these processes at the microscale level. On the positive side, significant amounts of details on these processes at the continuum level are available.[1-7] The capability to accurately predict the values of internal state variables such as state of charge would also be useful. Predicting and understanding the behavior accurately will expect to help in extending the life of the battery and improve the capability to store more energy. In lithium ion battery charging three most popular charging modes are given as constant current charging, constant potential charging, slower rate constant current followed by constant potential charging, which are discussed next.

5.2. Modes of Charging

Batteries are discharged according to the energy and power needs of a particular application. The batteries are typically charged at low rates to enable full storage of energy. However, often times there are a need to charge the batteries quickly, resulting in an inefficient storage of energy. Inefficient storing of energy results in underutilization of battery and decreases the efficiency. Batteries are typically charged using the following ways.

5.2.1. Constant Current Charging

In this charging protocol, batteries are charged at a constant current rate. If there are no time limits, a very low charging rate is generally employed to store more amount of energy. In fact, many researchers use the capacity obtained at very low rates of charge (c/50) as the maximum possible capacity. However, automobile applications require charging of battery within a specified time limit. Charging process of a battery is a exothermic process and while charging the battery its temperature increases. In addition, if the battery is charged at very fast rate, cut off potential will reach very fast (4.1V) and energy stored will not be maximum energy. On the

other hand charging at slower rate, leads to maximum energy stored with large amount of time required for charging.

5.2.2. Constant Potential Charging

In this charging protocol, batteries are charged with constant potential rate. This method is not typically used because, constant potential charging leads to very high currents at short times leading to thermal runaway and material degradation. If charged at very low potential difference, very minimal energy will stored. On the other hand if charged at very high potential difference, high currents and side reactions evolve.

5.2.3. Typical Experimental Method

In this charging protocol, the battery gets charged with slower rate constant current charging followed by constant potential charging. Slower rate of charging enables battery to store more energy and minimize the possibility of thermal runaway. However, slower rate current charging followed by constant potential charging will take large time for charging and may not be a feasible option for charging the lithium ion battery in automobile applications.

In above mentioned protocols, there exist slower rates of charging as well as faster rates of charging. These two charging rates, enables minimum to maximum energy storing in a lithium ion battery and hence there exist an optimum rate of charging, in which maximum energy storing in a lithium ion battery is possible. Figure 5-1 and Figure 5-2 show the energy stored in the given lithium ion battery with applied current as well as applied Voltage respectively. It is observed that there exists a maximum value of energy stored with respect to applied current as well as voltage.

In this work, a dynamic optimization framework for storing maximum energy in the lithium-ion battery is presented. Particularly, the estimation of the optimum profile of charging using

current as well as voltage has been carried out. Irrespective of the current or potential mode, the results obtained justify the need for dynamically varying control of input variables.

During optimized charging, various processes such as charge transfer, kinetics of the reactions, and rates of diffusion differ compared to un-optimized charging. This chapter explores the changing dynamics of the system by using an optimal current profile for charging. Dynamic behaviors are compared for various non-measurable internal variables including solid-phase and electrolyte concentrations and potentials under different scenarios of battery charging. Different types of charging processes are investigated:

- Conventional constant current charging with 1C rate: defined as constant current charging of the battery with current equivalent to 1C rate until the cut-off potential or the time limit,
- Constant current charging with optimized C rate: defined as constant current charging of the battery with an optimized C rate (value of current) until the cut-off potential or the time limit,
- (Dynamically) optimized charging profile: defined as charging with an optimal profile of current and voltage estimated using the dynamic optimization technique.

5.3. Dynamic Optimization Framework

An optimal control problem formulation is considered:

$$\min_{\mathbf{z}(t),\mathbf{u}(t),\mathbf{p}} \Phi \qquad [5.1]$$

such that

$$\frac{d}{dt}\mathbf{z} = \mathbf{f}(\mathbf{z}(t),\mathbf{y}(t),\mathbf{u}(t),\mathbf{p}),\ \ f(\mathbf{z}(0)) = 0,\ g(\mathbf{z}(1)) = 0, \qquad [5.2]$$

$$\mathbf{g}(\mathbf{z}(t),\mathbf{y}(t),\mathbf{u}(t),\mathbf{p}) = 0, \qquad [5.3]$$

$$\mathbf{u}_L \le \mathbf{u}(t) \le \mathbf{u}_U,\ \mathbf{y}_L \le \mathbf{y}(t) \le \mathbf{y}_U,\ \mathbf{z}_L \le \mathbf{z}(t) \le \mathbf{z}_U \qquad [5.4]$$

In this formulation, $\mathbf{z}(t)$ is the vector of differential state variables, $\mathbf{y}(t)$ is the vector of algebraic variables, $\mathbf{u}(t)$ is the vector of control variables, and $\mathbf{p}$ is the vector of parameters. The objective function Φ is formulated as maximum energy stored in the lithium-ion battery using reformulated model.[8] Numerous methods are available for solving constrained optimization problems. Typical methods for dynamic optimization include (1) the application of variational calculus, (2) Pontryagin's maximum principle, (3) control vector iteration, (4) control vector parameterization, and (5) simultaneous nonlinear programming.[9-11] Control vector parameterization (CVP) is the most commonly use in industrial applications and is used in this chapter.

The objective function of the energy stored in single cell is to store a maximum energy inside the cell with constraints on the operation time of the battery. In this work, the one hour charging of the battery was considered and the critical voltage limit is fixed at 4.1 V. as the constraints for the optimization and dynamic optimization. The objective function in charging of the battery is given as

$$\begin{aligned} &\frac{dE}{dt} = Vi_{applied} \\ &\max_{i_{applied}} E = \int Vi_{applied}\, dt \\ &s.t.\ V \le 4.05 \\ &\quad t \le 70\,(\text{dimensionless}) \\ &(\text{dimensionless time of 70 is equivalent to one hour}) \end{aligned} \qquad [5.5]$$

whereas E is the total energy stored in the cell, V is the voltage obtained from the cell, and $i_{applied}$ is applied current to the cell.

In dynamic optimization, the span for charging operation is divided into *n* local intervals. Applied current is optimized in each local interval by maximizing the energy stored at the end of operation. Each interval is subjected to same constraints as in the simple optimization. In general, number of intervals in control vector parameterization is optimally estimated using the optimization technique. However, in this work, we first divided total interval into two equal intervals, and the optimized value of decision variable(s) is given as initial guess for both intervals. Then total interval is divided into four intervals, the optimized value of decision variables from the previous two intervals optimization is given as the guesses for the four intervals optimization. Proceeding in this manner, until no further significant improvements achieved in the objective function will circumvent the estimation of number of optimal intervals in the control vector parameterization methodologies.

The dynamic optimization can take large number of simulation iterations for estimating the optimum value of an objective function, so a computationally expensive model would result in very long time to obtain optimization results. The computation of the objective function Φ for a single charging profile using a first-principles porous electrode-based electrochemical engineering model could take up to minutes depending on the solver, operating system, and computer. Due to the expensive computations, dynamic optimization of batteries using first-principles-based models has not been attempted or reported in the literature to our knowledge. This situation is not ideal for emerging applications like hybrid power systems or for on-line control, optimization, and monitoring of batteries and other electrochemical power sources. Our implementation of dynamic optimization was facilitated by the use of a reformulated model[8] to compute the objective function Φ.

Reformulated model used in this work is derived from the first-principles porous electrode-based electrochemical engineering model. We have worked extensively in model reformulation and have published the details on the reformulation of the lithium-ion battery model.[8] Dynamic optimization solves the system several times and then estimates the optimum for the given objective function. A Fortran implementation of the reformulated model takes only 15-50 ms to predict a discharge curve whereas the original model can take up to a few seconds to minutes depending on the solver, environment, and the computer. In addition, the memory requirement is far less as compared to finite-difference models. The dynamic optimization requires many individual simulation runs, so a computationally expensive model would result in very long time to obtain optimization results.

5.4. Simulation Results and Discussion

The reformulated model was solved using our own robust DAE solver, which is somewhat less efficient than some existing DAE solvers (e.g., DASSL/DASPK/Jacobian).[12-13] The optimization was carried out using Matlab's optimization toolbox on a 3 GHz Intel Core 2 Duo CPU with 3.25 GB of RAM. The reformulated model is solved for one hour of operation with 4.05 V cut off voltage as the constraint on the model solution. It is assumed in the battery literature[14] that, the battery will be safe if operated below 4.05 V. The system was solved for three different operating scenarios of charging *viz.*: (1) Constant current 1C rate charging; (2) constant current charging with optimized C rate and (3) (dynamically) optimized charging profile estimated using dynamic optimization procedure.

Figure 5-3 illustrates the current time profile used under three different types of charging. The charging at 1C rate corresponds to a current of 30 A/m^2 and the optimized C rate gives a current of 17.207 A/m^2 to the battery. When charging with the dynamically optimized current

profile, the optimum current profile decreases with time similar to that of a first-order process with negative gain. The optimal profile initially supplies more current and then decreases the current slowly over the time of charging. The stored energy is higher in dynamically optimized charging as compared with other two types of charging at a constant rate.

Figure 5-4 shows the voltage time profile for the lithium-ion battery during three different scenarios of charging. All three types of charging have initial rapid increases in the voltage and end operations at the same voltage, with widely different profiles at intermediate times. The dynamically optimized charging results in much faster charging rate than the other two types of charging. The rate of conventional charging using the 1C rate is higher than the constant current charging with optimized C rate charging and hence, cut off potential is quickly reached. The rate of the dynamically optimum charging is nearly linear after the dimensionless time is equal to 25.

Figure 5-5 shows the amount of the energy stored in the lithium-ion battery during the three different charging scenarios. Unlike the constant current charging scenario, in dynamically optimized current charging, energy increases nonlinearly with time after certain initial charging time. The final energy stored using the dynamically optimized current charging is more as compared with constant current charging. Although the rate of energy storage for conventional constant charging is higher than the constant current charging with optimized C rate, the amount of energy stored in the latter case is much more than the conventional charging at 1C rate. This happens due to the cut-off potential being encountered early in the conventional charging as compared to the conventional charging with optimized C rate (Figure 5-4). The dynamically optimized charging protocol yields (29.38%) better storage compared to constant charging at the optimized C rate.

Figure 5-6 shows the time profile for the electrolyte concentration at the cathode/current collector interface for the three different charging scenarios. This electrolyte concentration has a higher peak value during dynamically optimized charging followed by the conventional charging at 1C rate and then conventional charging with optimized C rate. This is due to the higher initial supply of current during dynamically optimized charging as compared to the other two types of charging (Figure 5-2). For the chosen chemistry, mass transfer limitations in the electrolyte occur at higher currents. This protocol indicates that, to increase the energy density, store more energy at shorter time albeit causing mass transfer limitations in the electrolyte and let the concentration equilibrate at longer times to ensure longer operability of the battery (70 dimensionless times). In the latter part of charging, the electrolyte concentration at the positive electrode decreases during dynamically optimized charging, whereas it almost remains constant during conventional charging with optimized C rate. During dynamically optimized charging, the electrolyte concentration decreases over time and the lithium-ion transfer process slows down while more lithium ions are packed into the carbon matrix in the negative electrode.

The solid-phase surface concentration at the current collector interfaces for the positive and negative electrodes at each time is different by as much as 50% for the three charging scenarios (see Figure 5-7). Each time profile for a solid-phase surface concentration varies monotonically, regardless of the electrode or the charging scenario. The spatially averaged concentration in the anode and cathode $\int c_{s,ave} dx$ also vary monotonically with time (see Figure 5-8). We see that % change is more in the anode than the cathode as this battery was inherently limited by diffusion in the anode and the optimum profile helps in overcoming this limitation. However, still the value obtained is far off from the theoretical maximum suggesting that one hour (70 dimensionless times) operation will always mean compromise for charging; however, it can be

significantly improved. The theoretical maximum is estimated by charging the Li-ion battery at a very low rate (approx. C/100) without time limitation to the same cut off potential.

Figure 5-9 and Figure 5-10 show the dynamic optimization results for two cells in series in a battery pack with different initial SOC (cell 1 at 0% SOC and cell 2 at 50% SOC) and a performance improvement of 23.64 % was observed compared to optimum constant current charging. Figure 5-9 shows convergence of energy stored with the number of intervals of the independent variable (time). It has been observed that energy stored is converged with 4 numbers of intervals of the independent variable. Figure 5-10 shows the current profile over the dimensionless time equivalent to 1 hour of charging operation. The optimization method can be used to improve the performance of battery packs that use combinations of cells in series and parallel to obtain longer life and higher efficiency.

Figure 5-11 and Figure 5-12 show time profiles for the current and voltage for optimized as well as dynamically optimized voltage charging. In optimized charging mode of voltage the amount of energy stored is equal to 3792.9 J were as in dynamically optimized charging it is 5977.3 J. The optimized voltages is estimated to be 3.818 V throughout the charging time, were as dynamically optimized voltage maintained at 3.815 V for first 4.1 dimensionless time and then increases to the upper bound (4.1 V). Figure 5-11 shows corresponding current profiles, in which for dynamically optimized voltage charging, a peak behavior is observed, when voltage increases from the low initial value to the upper bound.

5.5. Implications, current and future work

This work is an attempt to show the usefulness of systems engineering approach to improve the operating conditions for lithium-ion batteries using optimization. The benefit obtained is significant and relies on the validity, utility and limitation of the model used. If the model has

capability to predict capacity fade, thermal behavior then optimization can be used for minimization of capacity fade as well as thermal runaway. In general, an optimization frame work that can be used for lithium-ion batteries as of today is given in Figure 5-13. This approach can enable safer, cheaper and long-lasting batteries for the next generation.

5.6. Conclusion

The method in which a lithium-ion battery is charged can significantly alter the efficiency, safety, and lifetime of the battery. Various phenomena take place at the electrode/electrolyte level during charging. A continuum reformulated model for the lithium-ion battery is used in this work to perform dynamic optimization to store the maximum energy in the given battery during charging. The analysis shows a 100% improvement for dynamically optimized charging over the conventional charging at 1C rate and 29.38% improvement with constant current charging at optimized C rate. Time profiles for internal variables were used to explain some of the physics associated with charging for maximum energy storage. Dynamic analysis of all possible intrinsic variables along with optimization for storing the maximum energy in a lithium-ion battery pack is currently being investigated. In addition, optimal profiles for different specific objectives (reduced capacity fade, reduced SEI layer growth, enhanced life, uniform current distribution, ideal temperature behavior with temperature constraints) are being studied. This work will be further undertaken to perform optimal control so as to include this technique inside a battery management system to enable better control, safer operation and longer life of batteries for the future.

5.7. References

1. J. Newman, K. E. Thomas, H. Hafezi, D. R. Wheeler, *J. Electrochem. Soc.*, **150**, A176 (2003)
2. G. L. Plett, *J. Power Sources*, **134**, 252 (2004)
3. M. Doyle, T. F. Fuller, J. Newman, *J. Electrochem. Soc.,* **140**, 1526 (1993)
4. R. Darling, J. Newman, *J. Electrochem. Soc.*, **146**, 3765 (1999)
5. D. Zhang, B. N. Popov, R. E. White, *J. Electrochem. Soc.*, **147** 831(2000)
6. G. G. Botte, V. R. Subramanian, R. E. White, *Electrochima Acta.*, **45**, 2595(2000)
7. G. G. Botte, R. E. White, *J. Electrochem. Soc.*, **148**, A54 (2001)
8. V. R. Subramanian, V. Boovaragavan, V. Ramadesigan, M. Arabandi, *J. Electrochem. Soc.*, **156**(4), A260- (2009)
9. M. D. Canon, C. D. Cullum, E. Polak, McGraw-Hill, New York (1970)
10. L. T. Biegler, *Comp. Chem. Eng.*, **8**(3), 243 (1984)
11. S. Strand, PhD thesis, University of Trondheim, Norway (1991)
12. http://www.numericatech.com/jacobian.htm as on 11/30/2009
13. L. R. Petzold, *Scientific Computing*, eds. R.S. Stepleman et al., North- Holland, Amsterdam 68. (1983)
14. K. Kumaresan, G. Sikha, R. E. White, *J. Electrochem. Soc.*, **155**(2), A164 (2008)

5.8. Figures

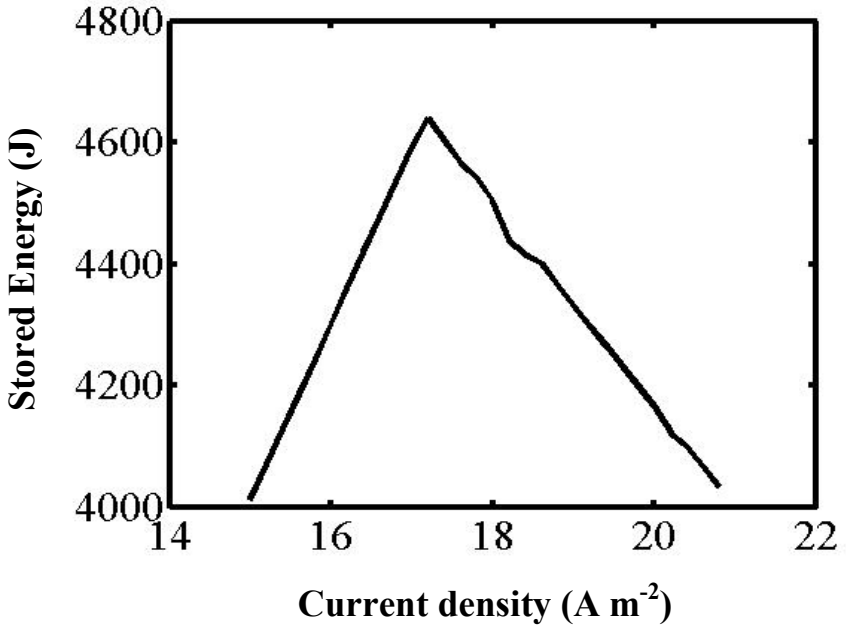

Figure 5-1: Energy stored in given lithium ion battery with applied current with maximum energy storage

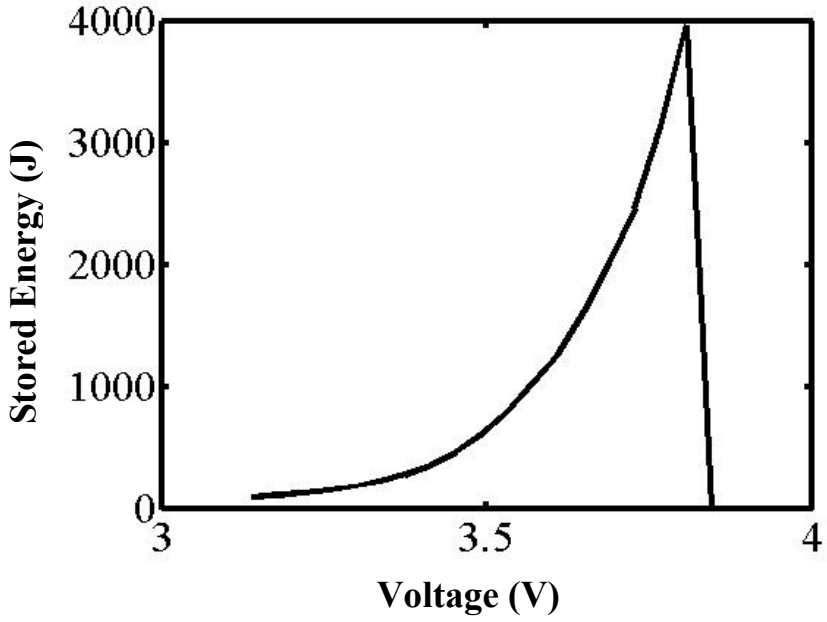

Figure 5-2: Energy stored in given lithium ion battery with applied voltage maximum

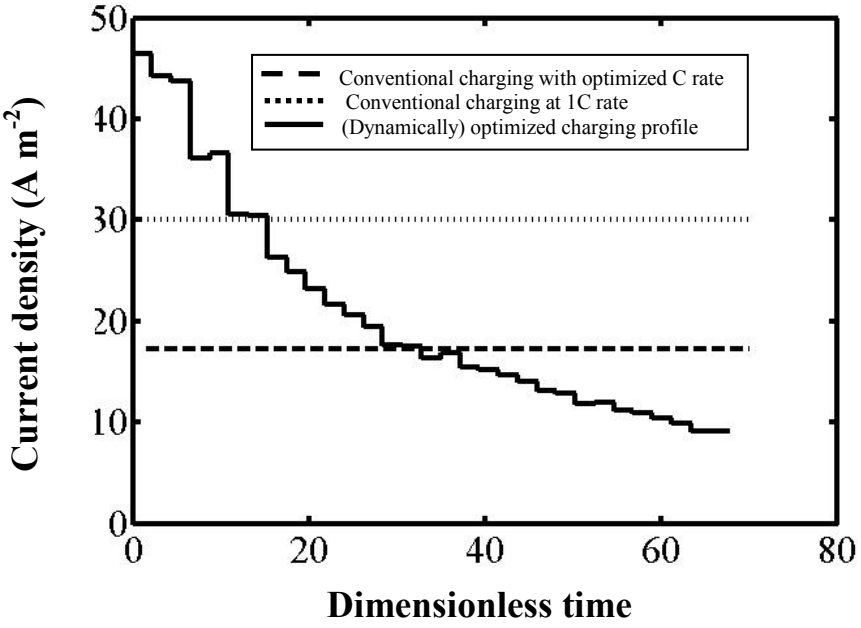

Figure 5-3: Comparison of current used for charging of lithium ion battery for three different types of charging protocol

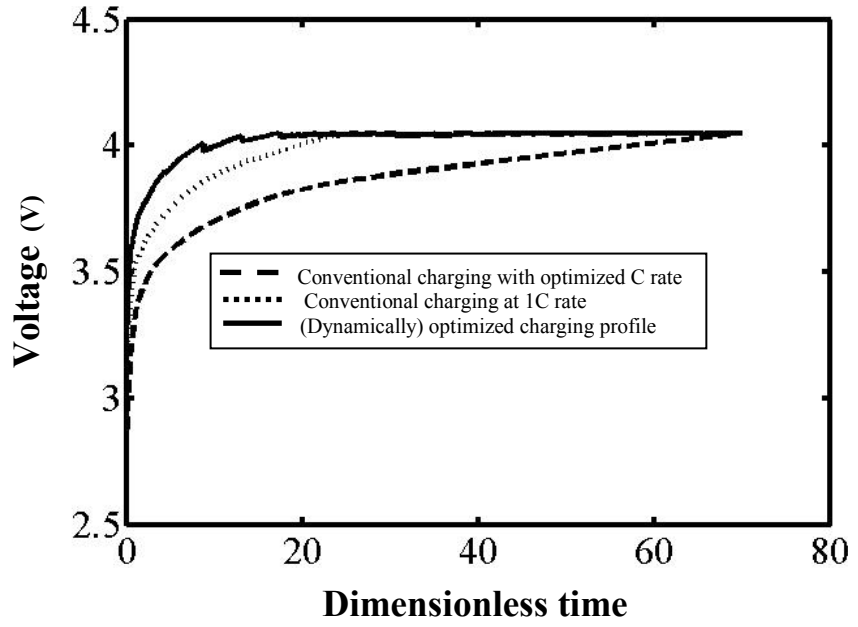

Figure 5-4: Comparison of voltage of lithium ion battery for three different types of charging protocol

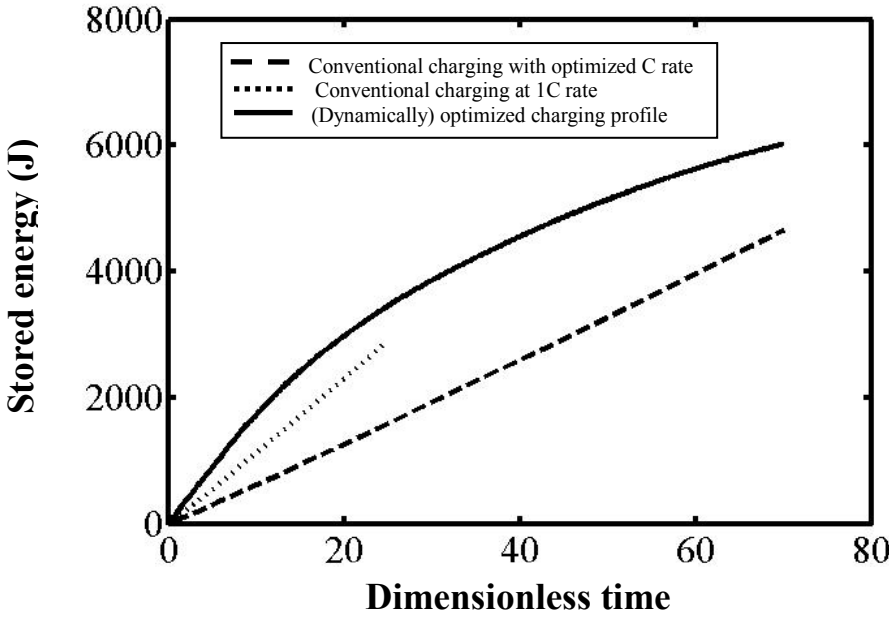

Figure 5-5: Comparison of energy stored in lithium ion battery for three different types of charging protocol

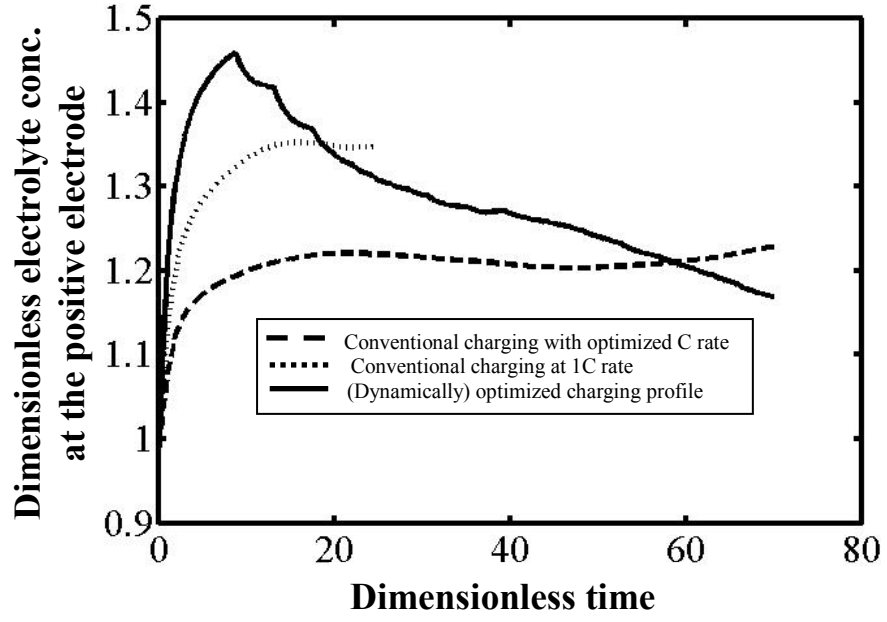

Figure 5-6: Dynamic analysis of electrolyte concentration at the positive electrode for the three different types of charging protocol

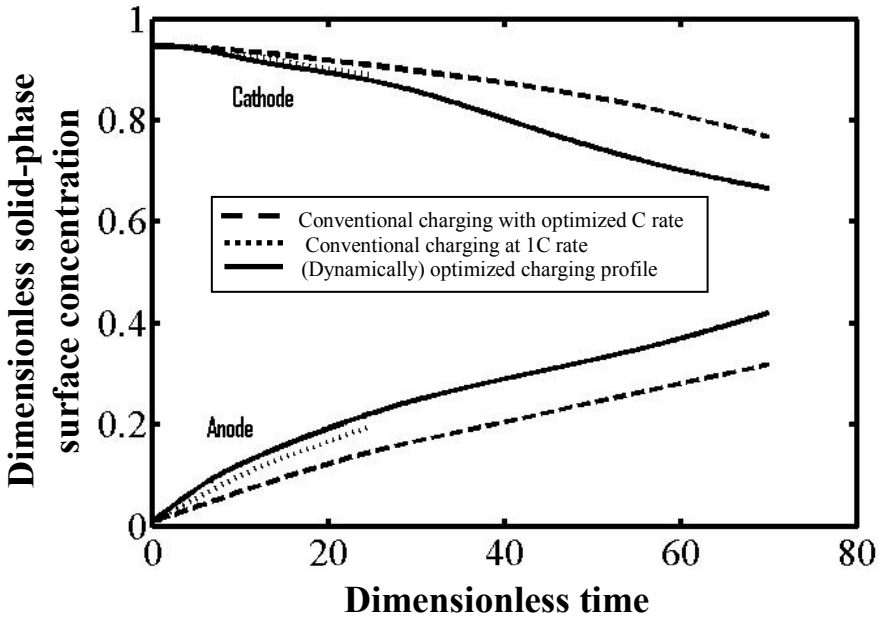

Figure 5-7: Solid-phase surface concentration at the current collector interfaces for the positive and negative electrodes for the three different types of charging protocol

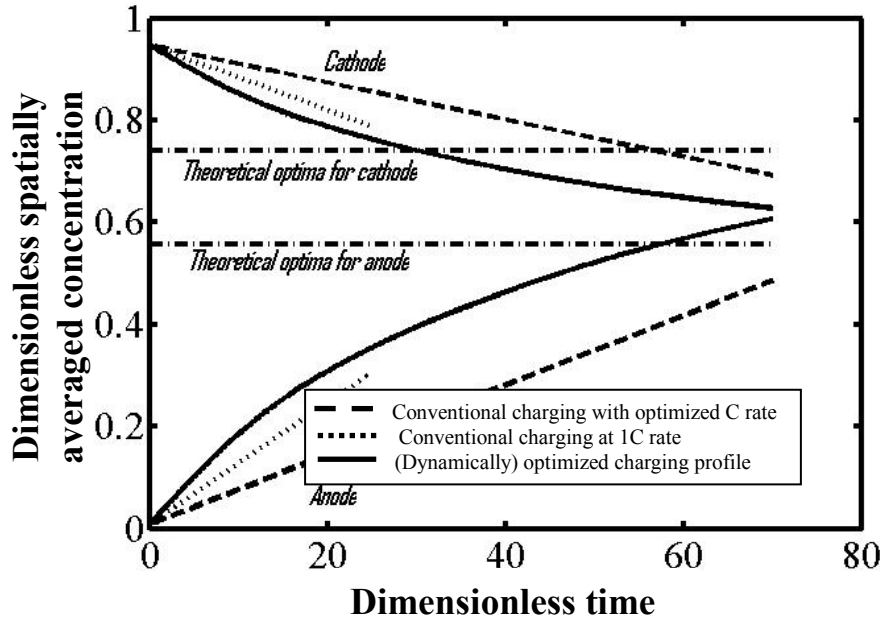

Figure 5-8: Spatially averaged concentration in the anode and cathode. (The theoretical maximum is estimated by charging the Li-ion battery at a very low rate (approx. C/100) without time limitation) for the three different types of charging protocol

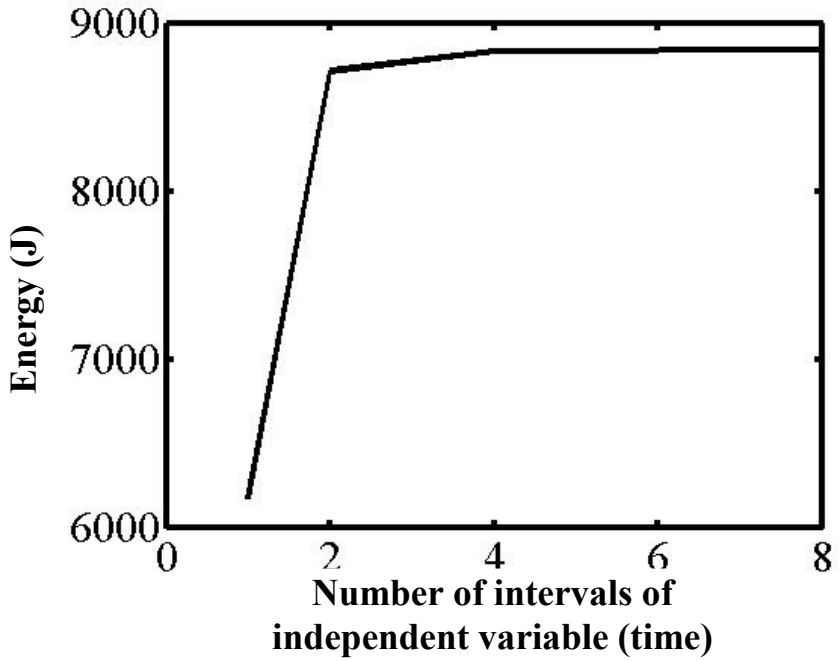

Figure 5-9: Convergence of energy stored with number of iteration in dynamic optimization of the battery using applied current as the manipulated variable

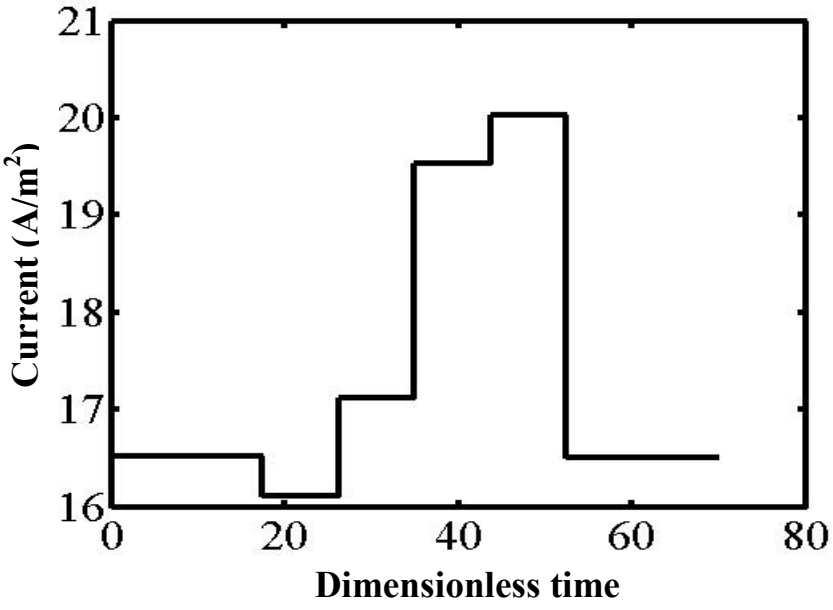

Figure 5-10: Convergence of energy stored with number of iteration in dynamic optimization of the battery using applied current as the manipulated variable

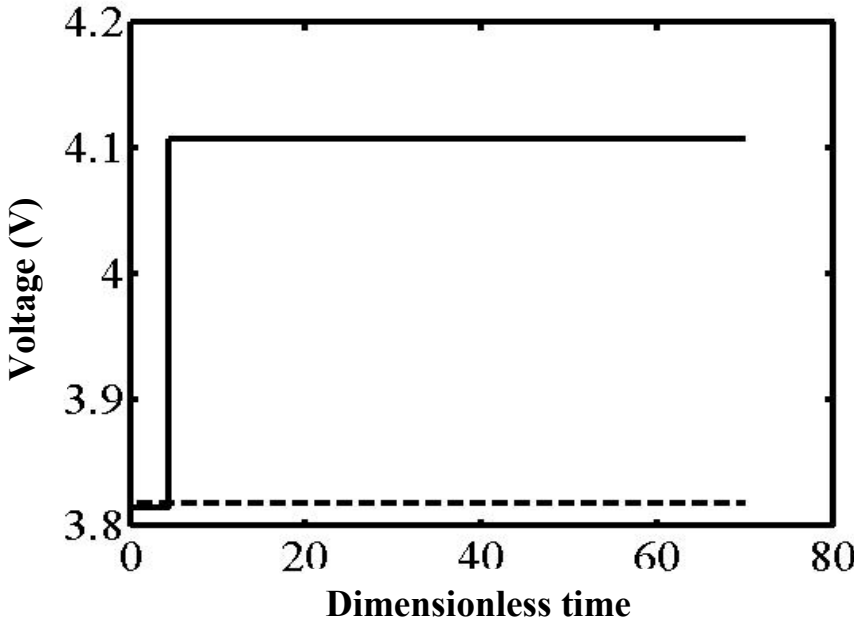

Figure 5-11: Time profile of voltage in optimum voltage charging and dynamically optimized voltage charging

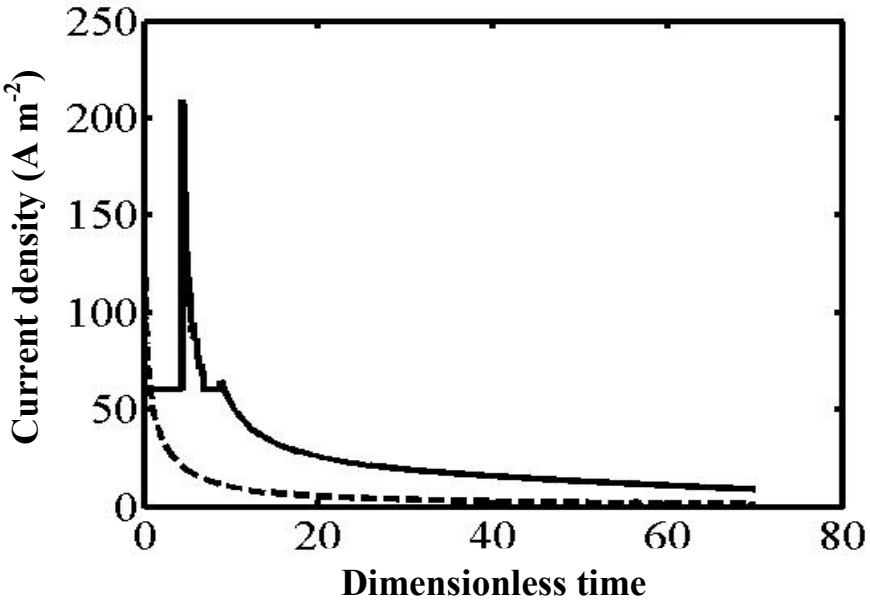

Figure 5-12: Time profile of current in optimum voltage charging and dynamically optimized voltage charging

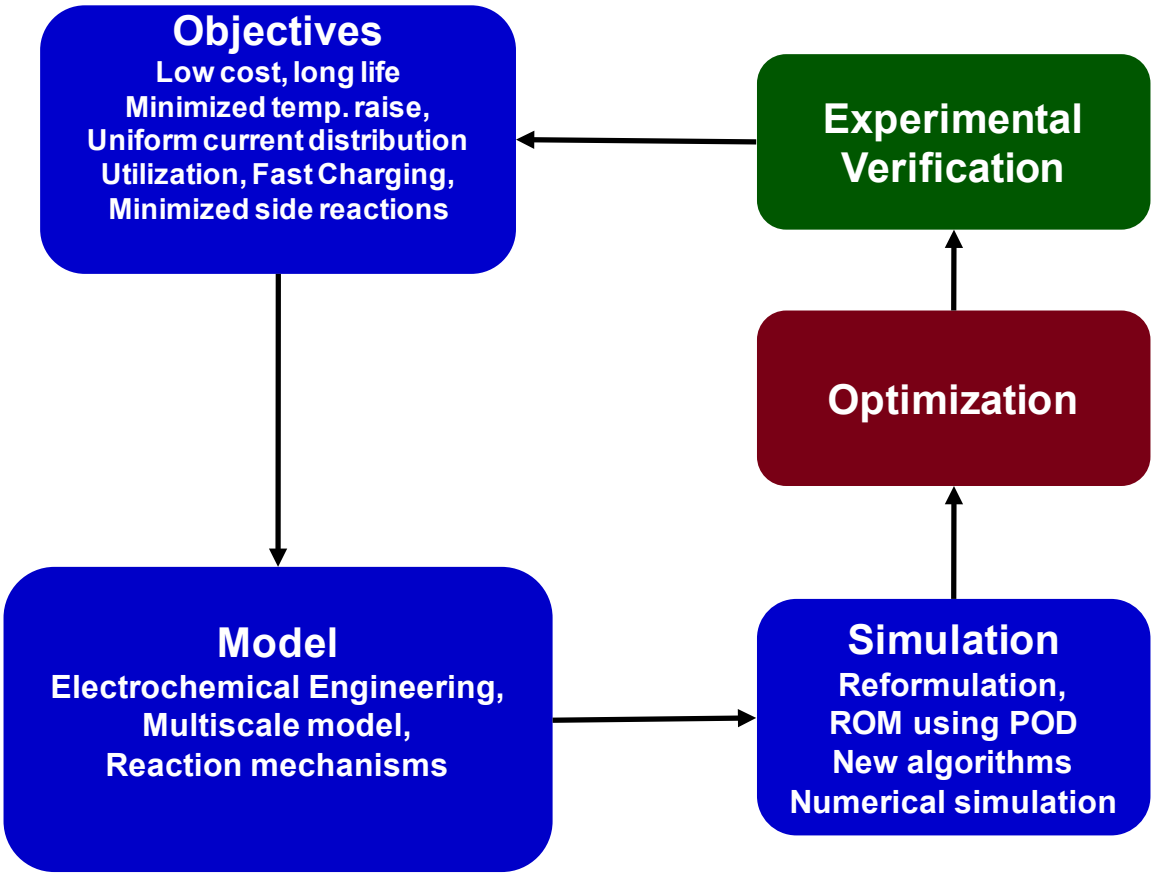

Figure 5-13: General optimization frame work for lithium-ion battery

Chapter 6 : Conclusions and Future Directives

6.1. Conclusions from Solid Phase Reformulation

Model reformulation allows an efficient battery model simulation for use in control and optimization routines, as well as for parameter estimation. Efficient simulation is essential for optimization and parameter estimation because of the large number of simulations that must be run to converge to an appropriate solution. As a first step, in order to simplify the model, the radial dependence of the solid phase concentration can be eliminated by using various approximations as mentioned in Chapter 2.

This work provides two robust methods to approximate the solid phase diffusion, so as to eliminate the radial dependence or decrease the number of node points. The mixed finite difference approach uses 6 optimally spaced node points (with 6 corresponding governing equations) to describe the behavior of the lithium ion concentration in the radial direction within the solid phase particles. This is in contrast to the other approximations, which relies on 2 governing equations to describe the solid phase concentration. This allows the mixed finite difference approach to better capture the dynamics within the electrode at high rates, though at the cost of additional computation time. As this work reformulated the radial dependence, it enabled the future work on model reformulation using orthogonal collocation and other techniques in the spatial co-ordinates.[1]

6.2. Conclusions from Capacity Fade Analysis

One of the prime objectives of this thesis was to understand and perform capacity fade analysis with the help of modeling. This fundamental objective is achieved as illustrated in the previous chapters that explain the underlying concepts that were utilized for better understanding

of capacity fade of Li-ion batteries and also will enable us to predict the capacity fade in Li-ion batteries better. The efficient reformulated models were used for this purpose to enable efficient simulation.

It is likely that when more detailed multiscale models become available and simulated efficiently, there will not be a need to perform fitting and tracking of transport and kinetic parameters with cycles. Instead a continuous approach may be adopted where a suitable model that includes capacity fade mechanisms can be cycled continuously for charge and discharge based on the specific operating protocol and can be used to predict the capacity fade and hence the life of the battery. Researchers have modeled different capacity fade mechanisms at different scales ranging from molecular dynamics models, Kinetic Monte Carlo simulations predicting surface heterogeneity of the SEI layer formation, to the models at the continuum level. Researchers are trying to understand multiple phenomena that could cause the capacity fade including advances in stress/strain models, including population balance models for modeling shape and size changes. Other commonly used hypotheses for failure include (1) capacity fade caused by change in porosity alone, (2) capacity fade caused by growth of a resistive film, (3) capacity fade caused by side reactions, and (4) a combination of multiple mechanisms.

As many researchers have reported, this kind of modeling efforts using a single mechanism was tried with the experimental data, however, since the capacity fade can be due a combination of multiple mechanisms, including just one of many mechanisms did not fit the experimental data well. For the current set of data used in this work, we believe, the discrete approach methods is the best way of analyzing capacity fade and predicting the life of Li-ion batteries used for applications with similar protocols.

6.3. Conclusions from Model Based Optimal Design

Model-based optimization was applied to the design of a spatially-varying porosity profile in a porous electrode to minimize its ohmic resistance. The results suggest the potential for the simultaneous model-based design of electrode material properties that employ more detailed physics-based first-principles electrochemical engineering models to determine optimal design values to manufacture and evaluate experimentally. The advantage of using a physics based model is that, it is possible to study the effect of material properties with the variation of intrinsic variables, such as electrolyte concentration, that are non-measurable and come up with a physically meaningful design that would enhance the performance of the batteries. A model based optimal design framework was developed with a porous electrode as a proof of concept. This enabled simultaneous optimization of multiple design parameters for better design the results of which are published elsewhere.[2]

6.4. Conclusions from Dynamic Optimization

The major objective of this work to perform dynamic optimization or optimal control was to demonstrate the applicability of a reformulated model[1] for deriving control action in real time. In chapter 5, the objective of improved charging performance in a limited time in a lithium-ion battery was addressed while providing insight into the dynamics of the battery with competing transport and reaction phenomena at various locations inside the battery. A better understanding of the internal variables and insight into the battery variables during non-optimal and optimal charging process was studied and presented. This creates a very huge potential for this model to be used for various control oriented purposes some of which are discussed in the following section under future directives.

6.5. Future Directives

It is worth noting that the one of the intents of this contribution is to use the pseudo-2D model to obtain profiles that can be fed as inputs to detailed microscale, multiscale models that include stress relationships, molecular models, etc. to obtain meaningful material design characteristics. Some of the future directives include: development and implementation of models for varying porosity and for porosity varying with an unknown distribution function, limiting cases of porosity variation models (ohmically-limited batteries, solid-phase diffusion-limited batteries, solution-phase diffusion batteries, etc). The validation and implementation of robust model-based design into user-friendly and commercial software for lithium-ion battery simulation and analysis would revolutionize a rapidly growing and science and technology-intensive segment of the U.S. economy. The ability to robustly optimize chemistries, geometries, and materials to achieve specific performance objectives would increase battery safety, reliability, energy-efficiency, and profitability. The creation of efficient multiscale multiphysics battery simulations would have a transformative effect on the way that academic and industrial researchers interact with models and material design, and would tighten the coupling between product performance at the system level and advances in science at the small length scales.

The advantages offered by the reformulated model are significant since it restricts the number of internal states to a manageable level without compromising on the accuracy while being solvable in real-time (on the order of tens of milliseconds for an entire discharge curve). These qualities make the reformulated model a suitable candidate for embedded applications and in Battery Management Systems (BMS). The reformulated model can be used for real-time implementation in receding-horizon approaches for control and estimation (aka model predictive control and moving-horizon estimation). For control evaluation, the reformulated model can be

used to compute optimal protocols for battery operations, which would be the computation carried out at each time instance in a model predictive control implementation. As a first step towards model predictive control using physics-based reformulated models for lithium-ion batteries, open-loop optimal control has been performed with a computation time of less than a minute. Further, state estimation using a moving horizon technique and performing MPC and closed-loop control using this model is feasible.[3]

A new battery management system that will be based on very fast models capable of predicting the state inside battery cells accurately and quickly enough for the model results to be used in making control decisions. These models will be able to predict temperature, remaining energy capacity, and progress of unwanted reactions that reduce the battery lifetime. By providing this extra, difficult to measure or predict, information to the battery management software, we can demonstrate improvements in safety, charging rate and useful capacity, and battery lifetime.

6.6. References

1. P. W. C. Northrop, V. Ramadesigan, S. De, and V. R. Subramanian, J. Electrochem. Soc., **158** (12), A1461 (2011).
2. S. De, P.W.C. Northrop, V. Ramadesigan and V. R. Subramanian, *J. Power Sources,* **221**, 161 (2013).
3. B. Suthar, V. Ramadesigan, P. W. C. Northrop, R. D. Braatz, and V. R. Subramanian, "Optimal Control and State Estimation of Lithium-ion Batteries Using Reformulated Models," *American Control Conference (ACC) 2013*, accepted.